NASA Technical Paper 1206

Longitudinal Aerodynamic Characteristics of a Fighter Model With a Close-Coupled Canard at Mach Numbers From 0.40 to 1.20

Richard J. Re and Francis J. Capone
Langley Research Center
Hampton, Virginia

National Aeronautics
and Space Administration

**Scientific and Technical
Information Office**

1978

SUMMARY

An investigation of the longitudinal aerodynamic characteristics of a fighter model with a close-coupled canard mounted above the wing chord plane has been conducted. Model angle of attack was varied from -4° to 15°; canard incidence was varied from -5° to 18°; and selected canard and wing flap deflections were investigated.

The model could be trimmed by changing canard incidence for lift coefficients up to 0.80 at subsonic free-stream Mach numbers. By using the canard incidence for trim (with canard and wing flaps at 0°), maximum trimmed lift-drag ratios of about 8.8, 7.7, and 4.7 were obtained at free-stream Mach numbers of 0.40, 0.90, and 1.20, respectively. At a lift coefficient of 0.60, model trim angle of attack could be varied over an incremental range (nose-pointing capability) between 3.0° and 3.8°, depending on Mach number, by different combinations of control settings. At high lift coefficients, larger trimmed lift-drag ratios were obtained by using the deflection capability of the canard leading- and trailing-edge flaps before increasing canard incidence angle.

INTRODUCTION

The potential benefits of the canard-wing configuration for maneuvering aircraft have been investigated in generalized lift interference studies of various canard-wing arrangements. (See refs. 1 to 7.) Canards, when positioned appropriately, offer attractive features such as increased trimmed lift capability and the potential for reduced trimmed drag. When the canard-wing configuration, with its advantages, is coupled with control configured vehicle concepts, that is, vehicles with relaxed or negative stability margins, improved maneuver potential results. The generation of trimmed direct lift and side force with a close-coupled canard-wing combination expands the capability for nonconventional flight modes such as vertical or lateral translation (without aerodynamic cross-coupling) and the ability to point the nose of the vehicle away from the flight path (gun pointing). Discussions of the military applications of nonconventional flight modes in control-configured vehicles are contained in references 8 to 11.

The present investigation was conducted to determine the longitudinal aerodynamic characteristics of a configuration whose planform was more typical of a fighter than the close-coupled canard configurations of references 1 to 6. The wing had an aspect ratio of 2.759, a taper ratio of 0.200, 50° leading-edge sweep, and full-span leading- and trailing-edge flaps. The canard which was positioned above the wing plane had an aspect

ratio of 2.506, a taper ratio of 0.376, 45° leading-edge sweep, and full-span leading- and trailing-edge flaps.

The investigation was conducted in the Langley 16-foot transonic tunnel at free-stream Mach numbers from 0.40 to 1.20 and at angles of attack from -4° to 15°. Canard incidence angles were varied from -5° to 18° with selected configurations having canard leading- and trailing-edge flaps deflected up to 15°. Model configurations were tested with wing leading-edge flaps deflected up to 15° and with trailing-edge flaps deflected up to 10°.

The results of a wind-tunnel investigation of this model with the canard panels deflected incrementally or differentially as direct side-force generators are reported in reference 12.

SYMBOLS

All aerodynamic coefficients are referenced to the wind-axis system except the fuselage base axial-force coefficient, which is referenced to the body-axis system. The moment reference center, which represented an airplane center of gravity, was located at a point 98.22 cm rearward of the fuselage nose and in the plane of the uncambered wing. (See fig. 1.) All dimensions presented are in the International System of Units (SI).

A_B fuselage base area, 91.44 cm^2

$C_{A,B}$ fuselage base axial-force coefficient, $-\frac{p_B - p}{q}\left(\frac{A_B}{S}\right)$

C_D drag coefficient, $\frac{\text{Drag}}{qS}$

$C_{D,0}$ drag coefficient at $C_L = 0$

C_L lift coefficient, $\frac{\text{Lift}}{qS}$

C_{L_α} lift-curve slope at $\alpha = 0^\circ$, per deg

$C_{L_{\delta_{c,trim}}}$ rate of change of trimmed lift coefficient with canard incidence angle (measured at $\delta_{c,trim} = 0^\circ$), per deg

$C_{L_{\delta_{w,te}}}$ rate of change of lift coefficient for $\alpha = 0^\circ$ with wing trailing-edge flap deflection angle (measured at $\delta_{w,te} = 0^\circ$), per deg

$C_{L,0}$ lift coefficient at $\alpha = 0^\circ$

C_m pitching-moment coefficient, $\frac{\text{Pitching moment}}{qS\bar{c}}$

$C_{m_{C_L}}$ longitudinal stability parameter at $C_L = 0$

$C_{m_{\delta_{w,te}}}$ rate of change of pitching-moment coefficient with wing trailing-edge flap deflection (measured at $\delta_{w,te} = 0^o$ for $\alpha = 0^o$), per deg

$C_{m,0}$ pitching-moment coefficient at $C_L = 0$

$\bar{c}$ wing mean geometric chord, 42.654 cm

$\bar{c}_c$ canard mean geometric chord based on total planform to fuselage center-line plane, 21.852 cm

c_r root chord of exposed aerodynamic surface, measured streamwise, cm

c_t tip chord, measured streamwise, cm

L/D lift-drag ratio

M free-stream Mach number

p free-stream static pressure

p_B static pressure in fuselage base

q free-stream dynamic pressure

S reference wing area (total), 0.3808 m^2

α angle of attack, deg

Δ increment in coefficient or deflection angle

δ_c canard incidence angle (positive leading edge up), deg

$\delta_{c,le}$ canard leading-edge flap deflection angle (positive leading edge down), deg

$\delta_{c,te}$ canard trailing-edge flap deflection angle (positive trailing edge down), deg

$\delta_{w,le}$ wing leading-edge flap deflection angle (positive leading edge down), $0^o/0^o$ indicates inboard flap segment deflection angle/ outboard flap segment deflection angle, deg

$\delta_{w,te}$ wing trailing-edge flap deflection angle (positive trailing edge down), $0^o/0^o$ indicates inboard flap segment deflection angle/ outboard flap segment deflection angle, deg

Subscripts:

max maximum

trim trimmed

DESCRIPTION OF MODEL

The geometry of the model and the external contours of the fuselage are shown in figures 1 and 2, respectively. A photograph showing the sting-mounted model in the wind-tunnel test section is presented in figure 3.

The uncambered wing had an NACA 65A005 airfoil section at the wing-body juncture and varied linearly in thickness to an NACA 65A004 airfoil section at the wing tip. The wing had a leading-edge sweep of 50^o, an aspect ratio of 2.759, a taper ratio of 0.200, and 0^o dihedral. Each wing panel had two leading- and trailing-edge flap segments as shown in figures 1(a) and 1(b). The flap deflection brackets, which were located on the wing upper surface, were interchangeable continuous spanwise strips smoothed on the upper surface to remove the sharp corner along the hinge line. The gaps between the flaps and main wing structure were sealed by the brackets and filler material.

The uncambered canard had an NACA 65A005 airfoil section at the canard-body juncture and varied linearly in thickness to an NACA 65A003 airfoil section at the tip. The canard had a leading-edge sweep of 45^o, an aspect ratio of 2.506, a taper ratio of 0.376, and 5^o dihedral when mounted on the model. The canard-panel axis of rotation was in a plane 66.68 cm rearward of the nose. The surface of the fuselage in the vicinity of the canard root was basically flat in the plane perpendicular to the canard-panel axis of rotation (fig. 4), so that as the canard rotated, only a small gap occurred between the canard leading edge and the fuselage side. The ratio of exposed canard area to wing reference area was 0.1943. Each canard panel had a full-span leading- and trailing-edge flap as shown in figures 1(a) and 1(c). Flap deflections were achieved in the same manner as previously described for the wing.

The twin vertical tails were perpendicular to the wing chord plane and were canted outboard 3^{o} about the point of intersection between the tail-root trailing edge and the wing trailing edge. The vertical tails had NACA 65A004 airfoil sections at the root varying linearly in thickness to NACA 65A003 airfoil sections at the tip. The twin ventral fins on the wing lower surface were perpendicular to the wing chord plane and were canted inboard 3^{o} about the point of intersection between the ventral root trailing edge and the wing trailing edge. The ventral fins had NACA 65A003 airfoil sections.

The fuselage represents that of a single-engine fighter aircraft with a chin inlet (faired over, see fig. 1) and an external nozzle geometry representing an afterburning power setting. The inlet was faired over because the model was originally designed for high-pressure air propulsion-simulation testing with a support-strut mounting system beneath the nose. For the present investigation, the model was sting supported in the tunnel. The sting diameter was 6.35 cm at the model base.

TESTS AND CORRECTIONS

The investigation was conducted in the Langley 16-foot transonic tunnel, a single-return atmospheric wind tunnel with continuous air exchange. The slotted test section is octagonal in shape and measures 4.724 m between opposite walls (an area equivalent to a circle 4.85 m in diameter). The tunnel sting-support system pivots in such a manner that the model remains on or near the test-section center line throughout the angle-of-attack range.

The model was tested at free-stream Mach numbers from 0.40 to 1.20, at angles of attack from -4^{o} to 15^{o}, and at a sideslip angle of 0^{o}. Reynolds number, based on wing mean geometric chord, varied from 3.4×10^{6} at $M = 0.40$ to 5.6×10^{6} at $M = 1.20$.

Aerodynamic forces and moments were measured by an internal six-component strain-gage balance. Model angle of attack was obtained by correcting the angle of the model support system for deflection of the sting and balance under aerodynamic loads and for test-section stream angularity. The force data are adjusted to the conditions of free-stream static pressure at the fuselage base. Some examples of the magnitude of the fuselage base pressure adjustment are shown in figure 5 in base axial-force coefficient form.

All configurations were tested with fixed boundary-layer transition on the model surfaces. The transition-fixing strips consisted of 0.25-cm-wide straight-line strips of No. 120 silicon carbide grit connecting points $0.05c_r$ and $0.10c_t$ aft of the leading edges of the wing, canard, and vertical tails. The transition strips on the ventral fins were located at a constant distance ($0.05c_r$) from the leading edge. A transition band on the fuselage nose was located 2.54 cm rearward of the tip of the nose.

PRESENTATION OF RESULTS

The data obtained in this investigation are presented graphically in figures 6 to 20. The model geometric variables included in the basic data comparisons (figs. 6 to 14) are listed in the following table:

Figure	Canard			Wing		Vertical tails and ventrals
	δ_c, deg	$\delta_{c,le}$, deg	$\delta_{c,te}$, deg	$\delta_{w,le}$, deg	$\delta_{w,te}$, deg	
6	Off	---	---	0/0	0/0	On
	-5	0	0	↓	↓	↓
	0	↓	↓	↓	↓	↓
	5	↓	↓	↓	↓	↓
	10	↓	↓	↓	↓	↓
	15	↓	↓	↓	↓	↓
	18	↓	↓	↓	↓	↓
7	0	0	0	0/0	0/0	On
	0	5	15	↓	↓	↓
	10	0	0	↓	↓	↓
	10	10	10	↓	↓	↓
8	Off	---	---	0/0	0/0	On
	↓	↓	↓	↓	5/5	↓
	↓	↓	↓	↓	10/10	↓
9	0	0	0	0/0	0/0	On
	↓	↓	↓	↓	5/5	↓
	↓	↓	↓	↓	10/10	↓
10	0	0	0	10/10	0/0	On
	0	0	0	10/10	10/10	On
11	18	15	15	0/5	0/0	On
	↓	↓	↓	↓	5/5	↓
	↓	↓	↓	↓	10/10	↓
12	0	0	0	0/0	0/0	On
	↓	↓	↓	10/10	↓	↓
	↓	↓	↓	15/15	↓	↓
13	Off	---	---	0/0	0/0	On
	↓	↓	↓	0/5	↓	On
	↓	↓	↓	↓	↓	Off
	↓	↓	↓	↓	0/5	On
	↓	↓	↓	↓	0/5	Off
14	0	0	0	15/15	0/0	On
	↓	↓	↓	15/15	5/5	↓
	↓	↓	↓	10/15	5/5	↓

An outline of the aerodynamic parameter and summary data figures follows:

DISCUSSION OF RESULTS

The effects of canard, canard incidence, and various wing and canard control deflections on the basic longitudinal aerodynamics of the model are shown in figures 6 to 14. Wing and canard flaps were deflected throughout the subsonic Mach number range so that their effectiveness at maneuver speeds and attitudes could be determined. Pertinent control effectiveness summary data and aerodynamic parameters are contained in figures 15 to 20.

Effect of Canard ($\delta_c = 0^o$)

The effect of the canard (at $\delta_c = 0^o$) on the model with the canard and wing flaps undeflected is shown in the basic data of figure 6. At angles of attack up to about 5^o, addition of the canard had no significant effect on lift. This effect indicates, as do earlier studies, that the additional lift associated with a close-coupled canard mounted on or above the wing plane is counteracted by a comparable loss in wing lift due to the canard downwash flow field. At angles of attack above 5^o the model with the canard on produced more lift, and the lift curve remained more nearly linear with increasing angle of attack. This effect is probably caused by favorable interference between the wing and canard flow fields which results in a delay in the breakdown of the vortices on the wing as discussed in reference 5.

Effect of Canard Incidence

The effects of canard incidence (with wing and canard flaps undeflected) on the basic longitudinal aerodynamic characteristics of the model are shown in figure 6 and in summary form in figure 15. At low angles of attack, deflecting the canard from 0° to 18° incidence increased the lift coefficient by about 0.05 for $M = 0.40$ to 0.90 (fig. 15(a)). At $M = 0.40$ and high incidence angles, the canard loses much of its pitch effectiveness at lift coefficients of 0.40 and above (fig. 6(a)). Canard pitch effectiveness, in general, decreased with increasing lift coefficient and/or canard incidence angle, although this trend diminished with increasing Mach number.

As canard incidence was increased, drag coefficient increased at most positive lift coefficients. The increase in drag was especially large for canard incidences above 5° as can be seen by comparisons of minimum drag (fig. 6) and drag at zero lift (fig. 15(b)). The increase in drag due to increased canard incidence angle for a given lift shifted the drag polars (fig. 6) so that large decreases in maximum lift-drag ratio occurred (fig. 15(b)). For example, at $M = 0.40$, maximum lift-drag ratios of 10.0 and 4.0 were obtained with canard incidences of -5° and 18°, respectively.

Trimming With Canard Incidence

The basic model with the wing and canard flaps undeflected was tested at sufficient canard incidence angles (fig. 6) so that trimmed drag polars and trim parameters could be determined (fig. 16). A maximum trimmed lift-drag ratio (fig. 16(c)) of about 8.8 was obtained at $M = 0.40$, remained nearly constant up to $M = 0.80$, and decreased to 7.7 at $M = 0.90$. At $M = 1.20$, the maximum trimmed lift-drag ratio was 4.7 or about one-half the low speed value. The canard incidence angle for maximum trimmed lift-drag ratio was in the range from 1° to 5° for all the Mach numbers investigated.

At $M = 0.40$ to 0.90, the model was trimmed up to a lift coefficient of 0.80 within the angle-of-attack range investigated. The variation with lift coefficient of canard incidence angle required for trim is shown in figure 16(a) for various Mach numbers. A cross plot of trim angle of attack with Mach number for constant values of lift coefficient (fig. 16(b)) indicated only small variations in trim angle of attack over the Mach number range.

Effect of Canard Flap Deflections

With the canard at incidence angles of 0° and 10° (fig. 7) deflection of the canard leading- and trailing-edge flaps produced nearly constant positive pitching-moment coefficient increments over the lift-coefficient range at all free-stream Mach numbers.

With the canard at 18° incidence angle, a 15° deflection of the canard leading- and trailing-edge flaps (figs. 6 and 11) increased the longitudinal stability of the model at low

Mach numbers. Comparison of the $C_{m_{C_L}}$ variation with Mach number for the model with the canard leading- and trailing-edge flaps undeflected (fig. 15(c)) and deflected 15^o (fig. 18(a)) indicates that deflecting the flaps doubled the low lift stability at $M = 0.40$ and had essentially no effect at $M = 0.90$.

Effect of Wing Trailing-Edge Flap Deflection

The effects of wing trailing-edge flap deflection on the basic longitudinal aerodynamic characteristics of the model with the canard on are presented in figures 9, 10, and 11. Summary data for figures 9 and 11 are presented in figures 17 ($\delta_c = 0^o$) and 18 ($\delta_c = 18^o$), respectively. Although the canard leading- and trailing-edge flaps were at 15^o for the data of figure 11 ($\delta_c = 18^o$) and at 0^o for the data of figure 9 ($\delta_c = 0^o$), the effects of wing trailing-edge flap deflection were quite similar. The data shown in figure 13 indicate that the difference in outboard wing leading-edge flap deflection of 5^o between the configurations of figures 9 and 11 has no effect on the model longitudinal aerodynamic characteristics for the free-stream Mach number and angle-of-attack range of this discussion.

The negative pitch increments due to wing trailing-edge flap deflection were constant over the lift range for both canard incidence angles (figs. 9 and 11). However, wing trailing-edge flap pitch effectiveness was greater with 0^o canard incidence than with 18^o incidence. (Compare figs. 17(c) and 18(c).) Wing trailing-edge flap pitch effectiveness increased with Mach number for 0^o canard incidence but remained essentially constant with Mach number for 18^o canard incidence.

The effects of wing trailing-edge flap deflection on the basic longitudinal aerodynamic characteristics of the model with the canard off are presented in figure 8 and in summary form in figure 17. Because of the aft wing location, the model longitudinal stability $C_{m_{C_L}}$ (fig. 17(a)) was greater (about -0.22) without the canard. Lift and pitch effectiveness parameters at $\alpha = 0^o$ for the wing trailing-edge flap (fig. 17(c)) were essentially the same with or without the canard over the free-stream Mach number range.

Trim Angle-of-Attack Range at Constant Lift Coefficient

With the canard at an incidence angle of 18^o and the canard leading- and trailing-edge flaps deflected 15^o, the model was tested with wing trailing-edge flaps at $0^o/0^o$, $5^o/5^o$, and $10^o/10^o$ (fig. 11). Trim points were obtained for the two higher wing trailing-edge flap settings at moderate to high lift coefficients at $M = 0.40$ to 0.90 (fig. 19). The model trimmed at lift-drag ratios between 3.2 and 4.3 for lift coefficients between 0.88 and 0.50. A cross plot of trim angle of attack with Mach number for lift coefficients of 0.60 and 0.80 (fig. 19(b)) shows only a small variation in trim angle of attack over the Mach number range. Comparison of the trim angle of attack cross plots (figs. 16(b)

and 19(b)) indicates the trim angle-of-attack range the model can be pitched through at a given lift coefficient and Mach number by different combinations of control settings. That is, model trim angle of attack can be varied over an incremental range (nose-pointing capability) between 3.0° and 3.8°, depending on Mach number, at a lift coefficient of 0.60. It can also be varied over an incremental range of 2.6° at a lift coefficient of 0.80.

Trimmed Lift-Drag Ratios at Constant Lift Coefficients

Examination of the drag polars and pitching-moment curves of figures 6, 7, and 11 indicates that to trim with the canard for the least drag at a given high lift, it is best to use the full deflection capability of the canard trailing-edge flaps before increasing canard incidence. This is illustrated in figure 20 where the variation of drag coefficient with pitching-moment coefficient for all the control variables (canard on) is presented for constant values of lift coefficient at $M = 0.40$. Figure 20 is constructed from cross plots of the basic data; the symbols there indicate discrete geometric control settings and not actual data points. For the free-stream Mach number illustrated by figure 20, trimming the model by increasing canard incidence from 0° to approximately 5° (at $C_L = 0.80$) results in a lift-drag ratio of 3.9, while trimming by deflecting the canard leading- and trailing-edge flaps to 5° and 15° ($\delta_c = 0^{\circ}$), respectively, results in a lift-drag ratio of 4.3. This is about a 15-percent increase in lift-drag ratio. At lift coefficients of 0.60 and 0.40 there were comparable increases in trimmed lift-drag ratio although the percent increases were smaller because of the larger lift-drag ratios. At a lift coefficient of 0.20, trimmed lift-drag ratio showed no improvement when using canard flap deflection instead of canard incidence.

The trends exhibited in figure 20 for deflection of the wing leading-edge flaps at high lift coefficients (to improve wing leading-edge suction) indicate that additional improvement in trimmed lift-drag ratio should be attainable when the wing leading-edge flaps are deflected in conjunction with the canard leading- and trailing-edge flaps.

SUMMARY OF RESULTS

An investigation of the longitudinal aerodynamic characteristics of a fighter model with a close-coupled canard mounted above the wing chord plane has been conducted. Canard incidence was varied from -5° to 18°, and selected canard and wing flap deflections were investigated. The results of the investigation which was conducted over a free-stream Mach number range from 0.40 to 1.20 and at angles of attack from -4° to 15° are summarized as follows:

1. The model could be trimmed by changing canard incidence (canard and wing flaps at 0^{o}) for lift coefficients up to 0.80 at subsonic free-stream Mach numbers.

2. Maximum trimmed lift-drag ratios of about 8.8, 7.7, and 4.7 were obtained at free-stream Mach numbers of 0.40, 0.90, and 1.20, respectively, by using the canard incidence for trim (with canard and wing flaps at 0^{o}).

3. With the canard at 18^{o} incidence and the canard leading- and trailing-edge flaps deflected 15^{o}, the model trimmed at lift coefficients between 0.50 and 0.88 using wing trailing-edge flaps (0^{o} to 10^{o} deflection) as the trimming surfaces at subsonic free-stream Mach numbers.

4. At a lift coefficient of 0.60, model trim angle of attack could be varied over an incremental range (nose-pointing capability) between 3.0^{o} and 3.8^{o}, depending on Mach number, by different combinations of control settings.

5. At high lift coefficients, larger trimmed lift-drag ratios were obtained by using the full deflection capability of the canard leading- and trailing-edge flaps before increasing canard incidence angle. At a lift coefficient of 0.80, trimming with canard incidence (canard flaps undeflected) resulted in a lift-drag ratio of 3.9, while holding the canard at 0^{o} incidence and trimming by deflecting the canard leading- and trailing-edge flaps 5^{o} and 15^{o}, respectively, resulted in a lift-drag ratio of 4.3.

Langley Research Center
National Aeronautics and Space Administration
Hampton, VA 23665
May 23, 1978

REFERENCES

1. Gloss, Blair B.; and McKinney, Linwood W.: Canard-Wing Lift Interference Related to Maneuvering Aircraft at Subsonic Speeds. NASA TM X-2897, 1973.

2. Dollyhigh, Samuel M.: Static Longitudinal Aerodynamic Characteristics of Close-Coupled Wing-Canard Configurations at Mach Numbers From 1.60 to 2.86. NASA TN D-6597, 1971.

3. Gloss, Blair B.: Effect of Canard Location and Size on Canard-Wing Interference and Aerodynamic-Center Shift Related to Maneuvering Aircraft at Transonic Speeds. NASA TN D-7505, 1974.

4. Gloss, Blair B.: The Effect of Canard Leading-Edge Sweep and Dihedral Angle on the Longitudinal and Lateral Aerodynamic Characteristics of a Close-Coupled Canard-Wing Configuration. NASA TN D-7814, 1974.

5. Henderson, William P.: The Effect of Canard and Vertical Tails on the Aerodynamic Characteristics of a Model With a 59° Sweptback Wing at a Mach Number of 0.30. NASA TM X-3088, 1974.

6. Gloss, Blair B.: Effect of Wing Planform and Canard Location and Geometry on the Longitudinal Aerodynamic Characteristics of a Close-Coupled Canard Wing Model at Subsonic Speeds. NASA TN D-7910, 1975.

7. McKinney, Linwood W.; and Dollyhigh, Samuel M.: Some Trim Drag Considerations for Maneuvering Aircraft. J. Aircraft, vol. 8, no. 8, Aug. 1971, pp. 623-629.

8. Fink, Donald E.: Improved Fighter Capabilities Sought. Aviat. Week & Space Technol., vol. 107, no. 1, July 4, 1977, pp. 56-60.

9. Wetmore, Warren C.: Advanced Fighter Program Stress Shifts. Aviat. Week & Space Technol., vol. 104, no. 18, May 3, 1976, pp. 89-100.

10. Yaffee, Michael L.: New Controls To Shape Future Aircraft. Aviat. Week & Space Technol., vol. 97, no. 16, Oct. 16, 1972, pp. 46-50.

11. Lockenour, J. L.; and Williams, W. G.: Stability and Control Potential for Future Fighters. The Effects of Buffeting and Other Transonic Phenomena on Maneuvering Combat Aircraft, AGARD-AR-82, July 1975, pp. 54-62, 201-207.

12. Re, Richard J.; and Capone, Francis J.: An Investigation of a Close-Coupled Canard as a Direct Side-Force Generator on a Fighter Model at Mach Numbers From 0.40 to 0.90. NASA TN D-8510, 1977.

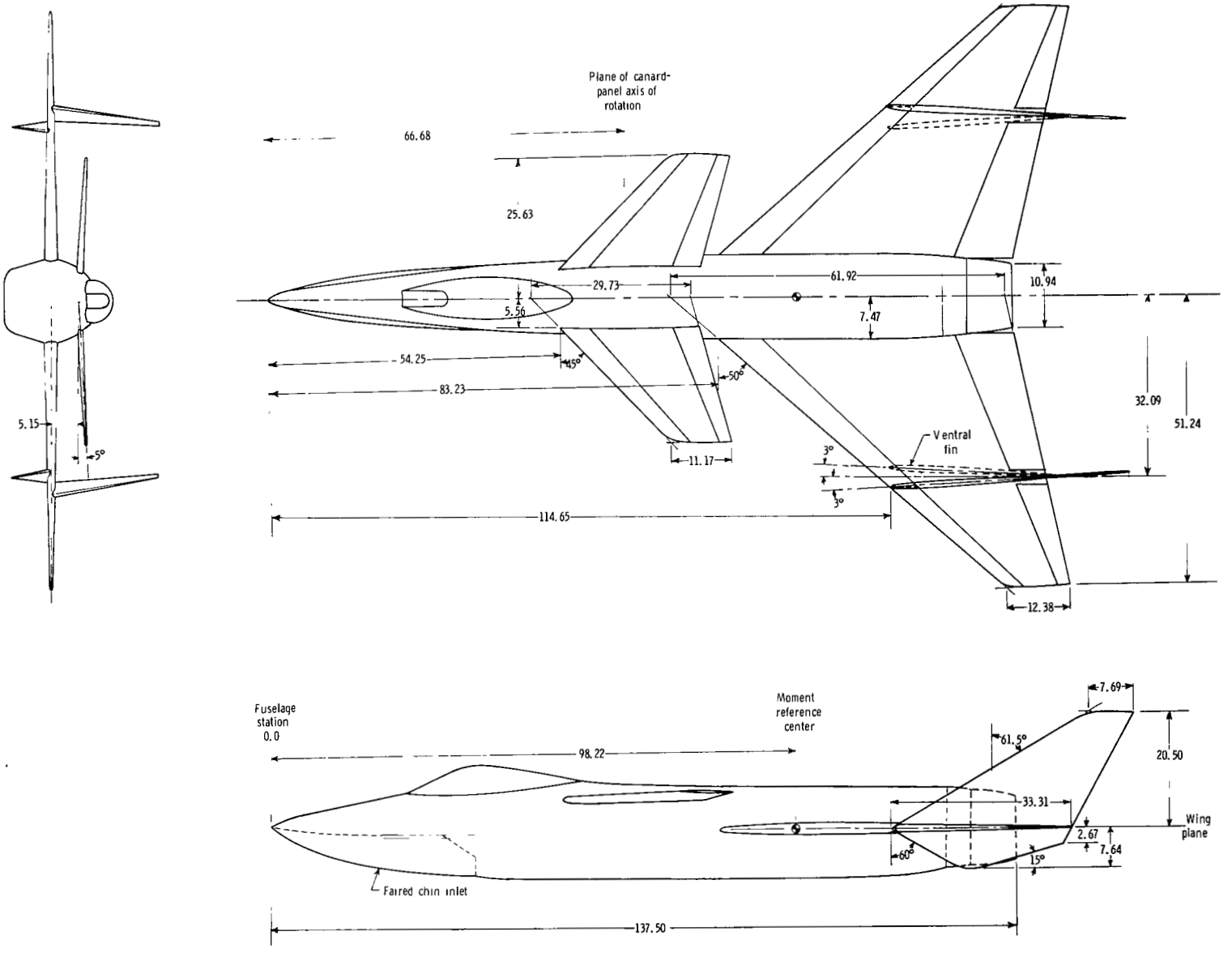

(a) General arrangement of model.

Figure 1.- Model geometry. (All dimensions are in cm unless otherwise indicated.)

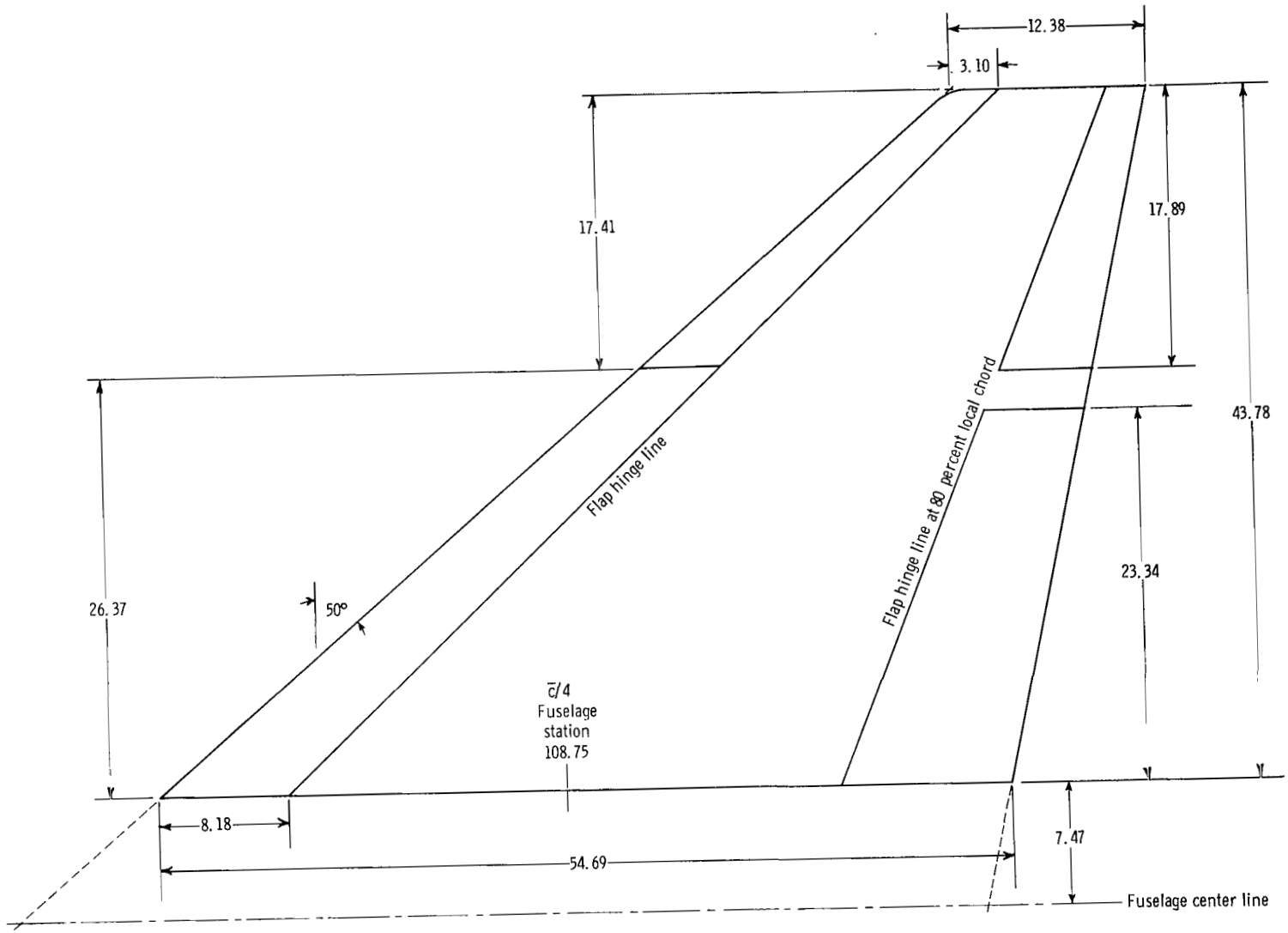

(b) Wing geometry.

Figure 1.- Continued.

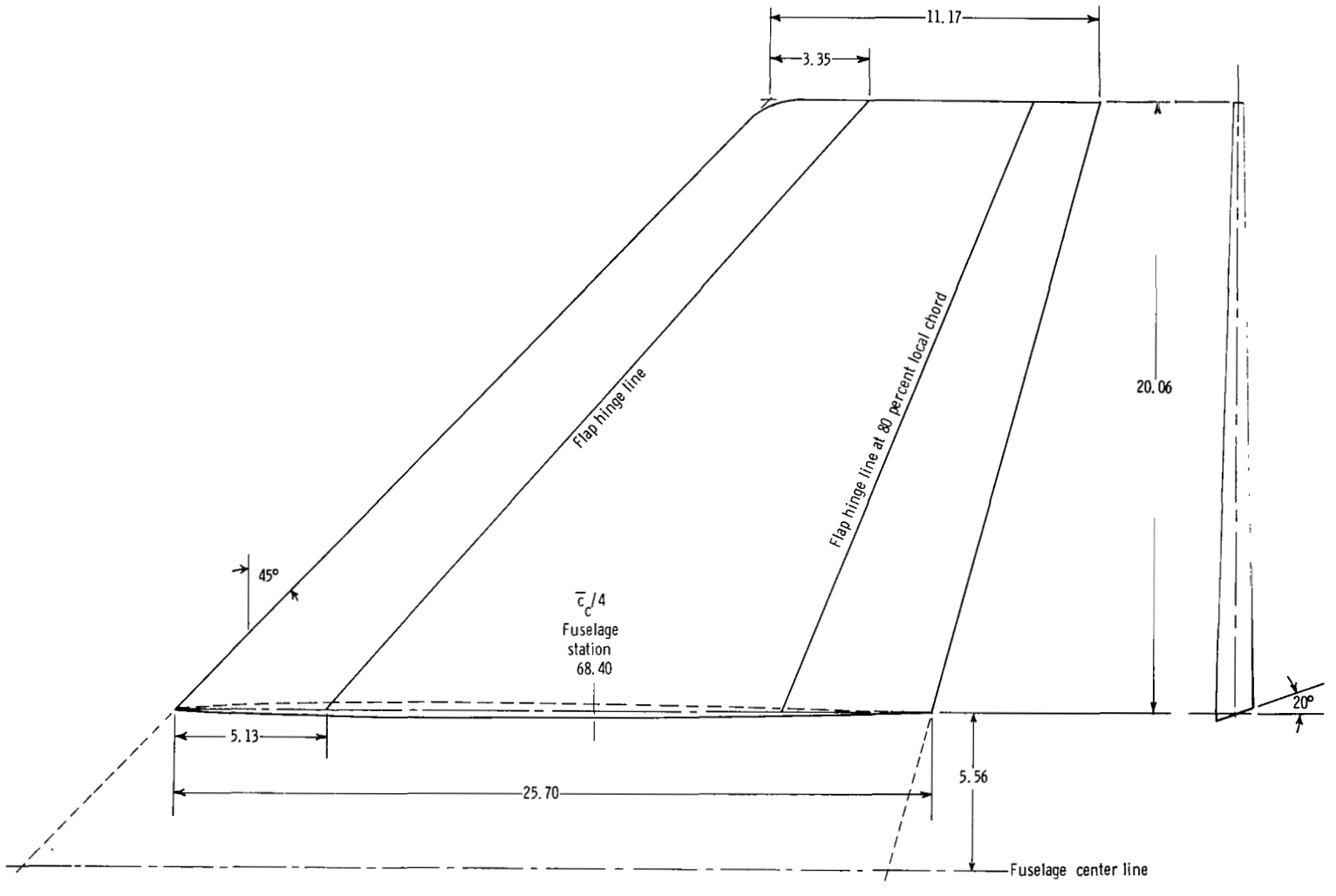

(c) Canard panel geometry (true view).

Figure 1.- Concluded.

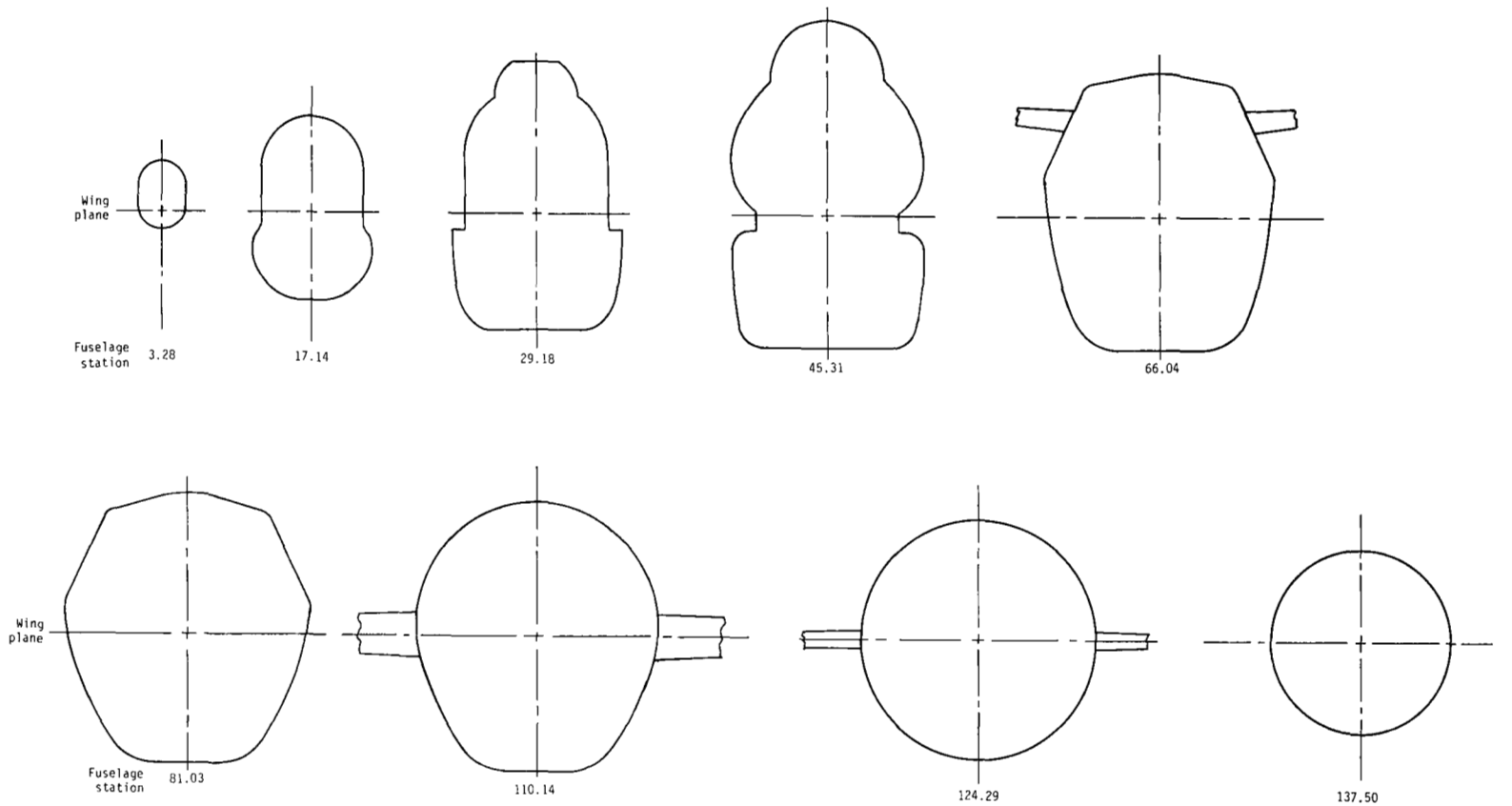

Figure 2.- Fuselage external contours. (All stations are in cm.)

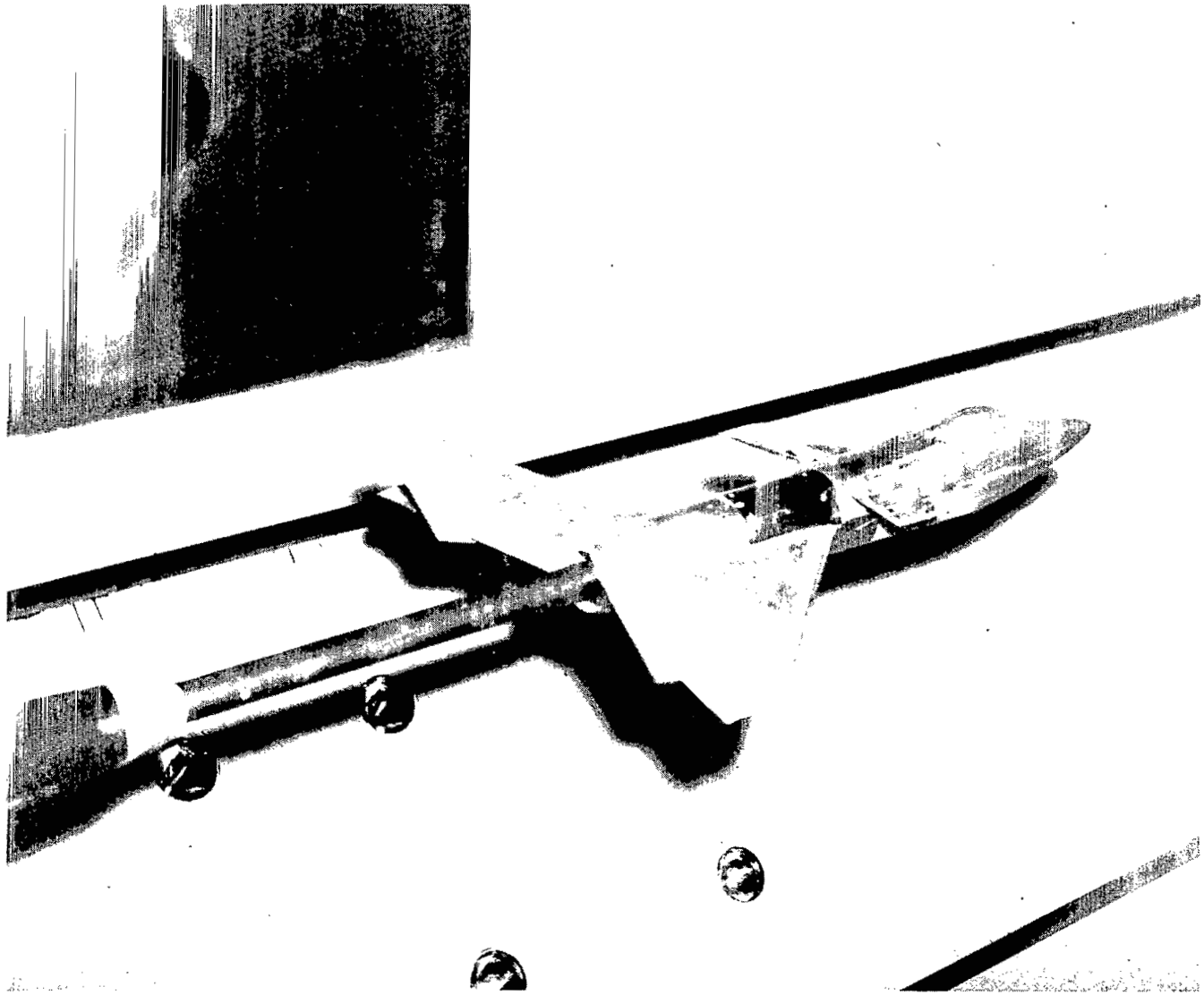

L-75-7712

Figure 3.- Model sting-mounted in wind-tunnel test section.

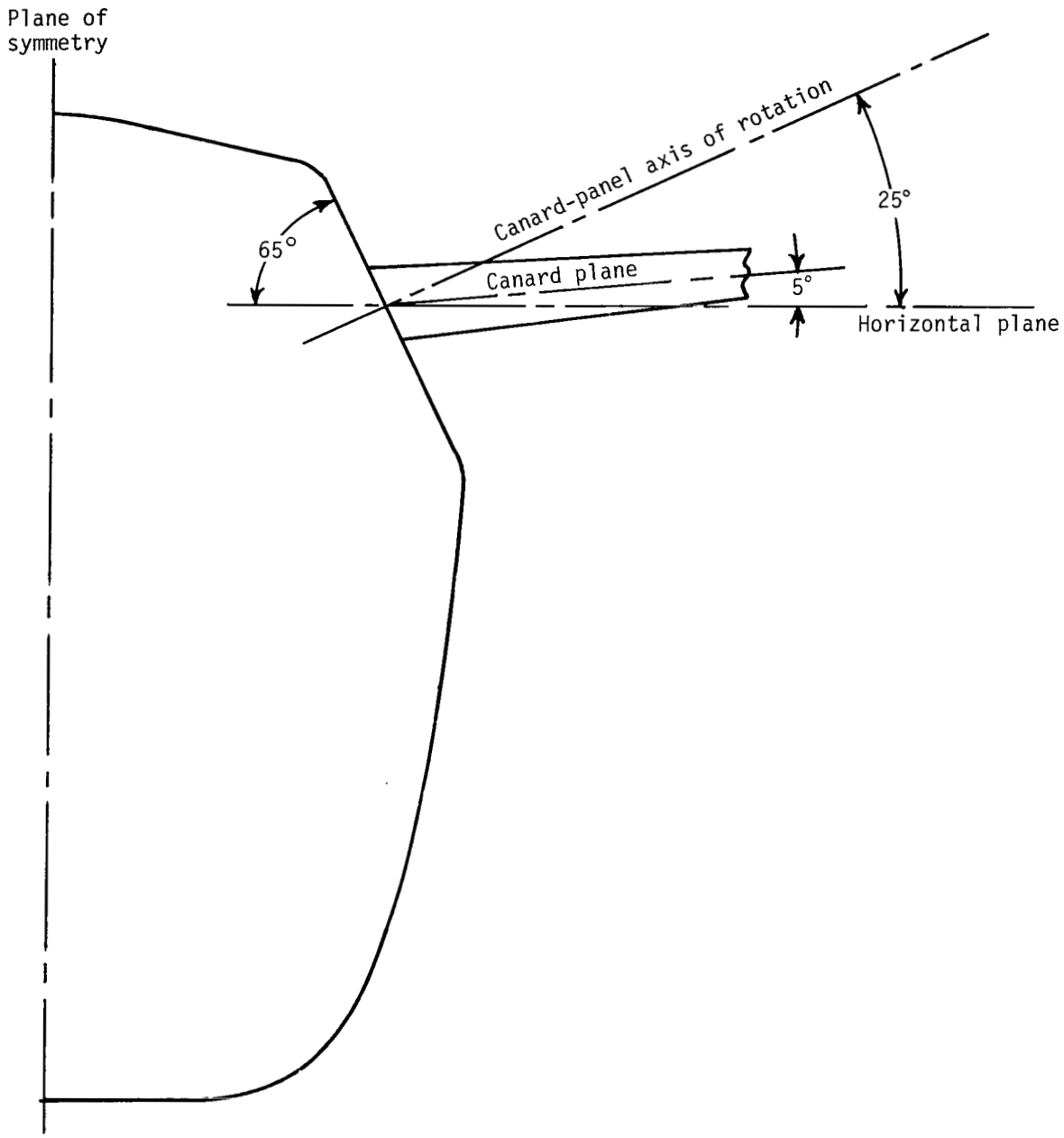

Figure 4.- Relative orientation of canard-panel axis of rotation to canard plane.

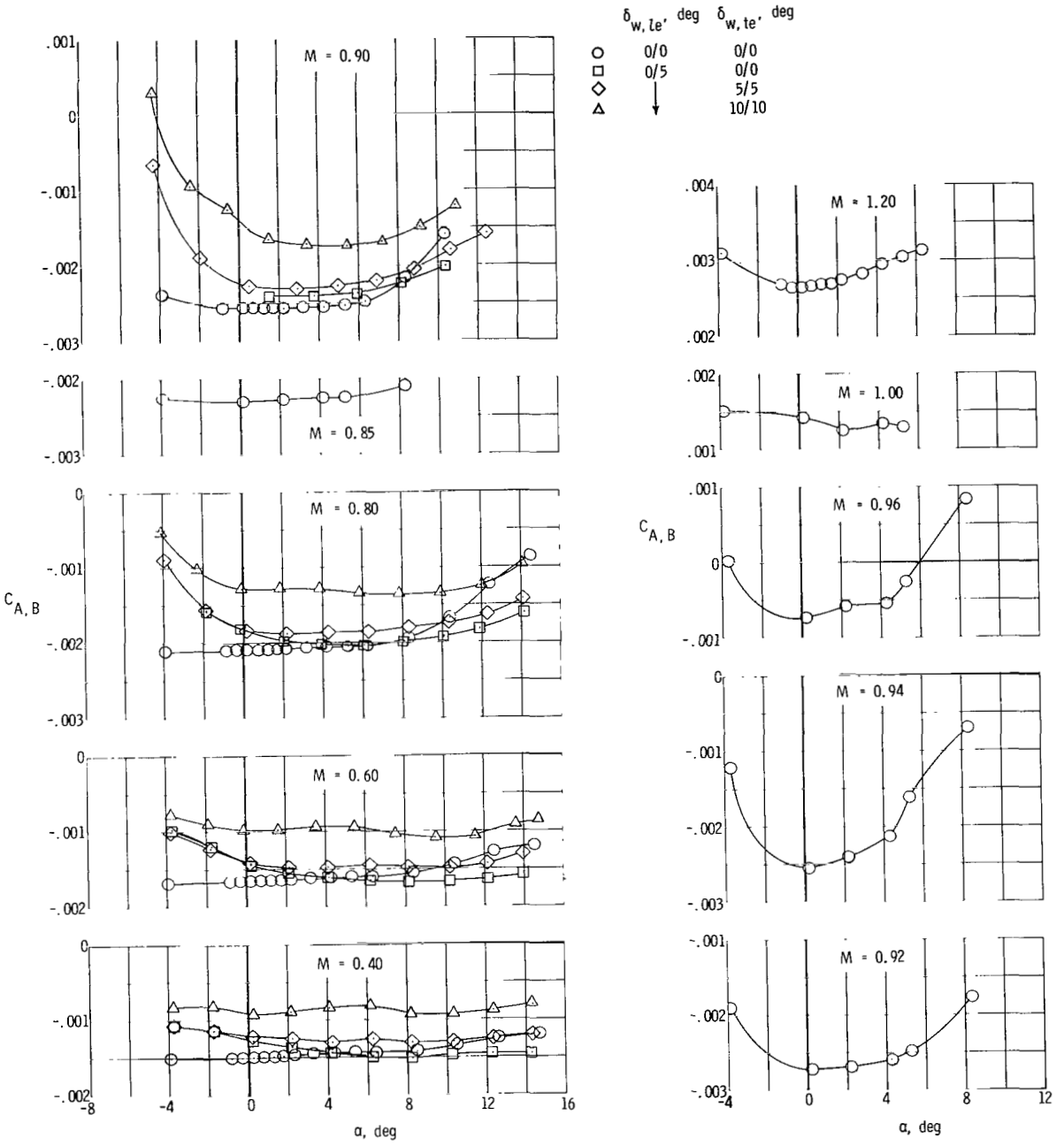

(a) Canard on; $\delta_c = 0^o$; $\delta_{c,le} = \delta_{c,te} = 0^o$.

Figure 5.- Variation of fuselage base axial-force coefficient with angle of attack for typical model configurations.

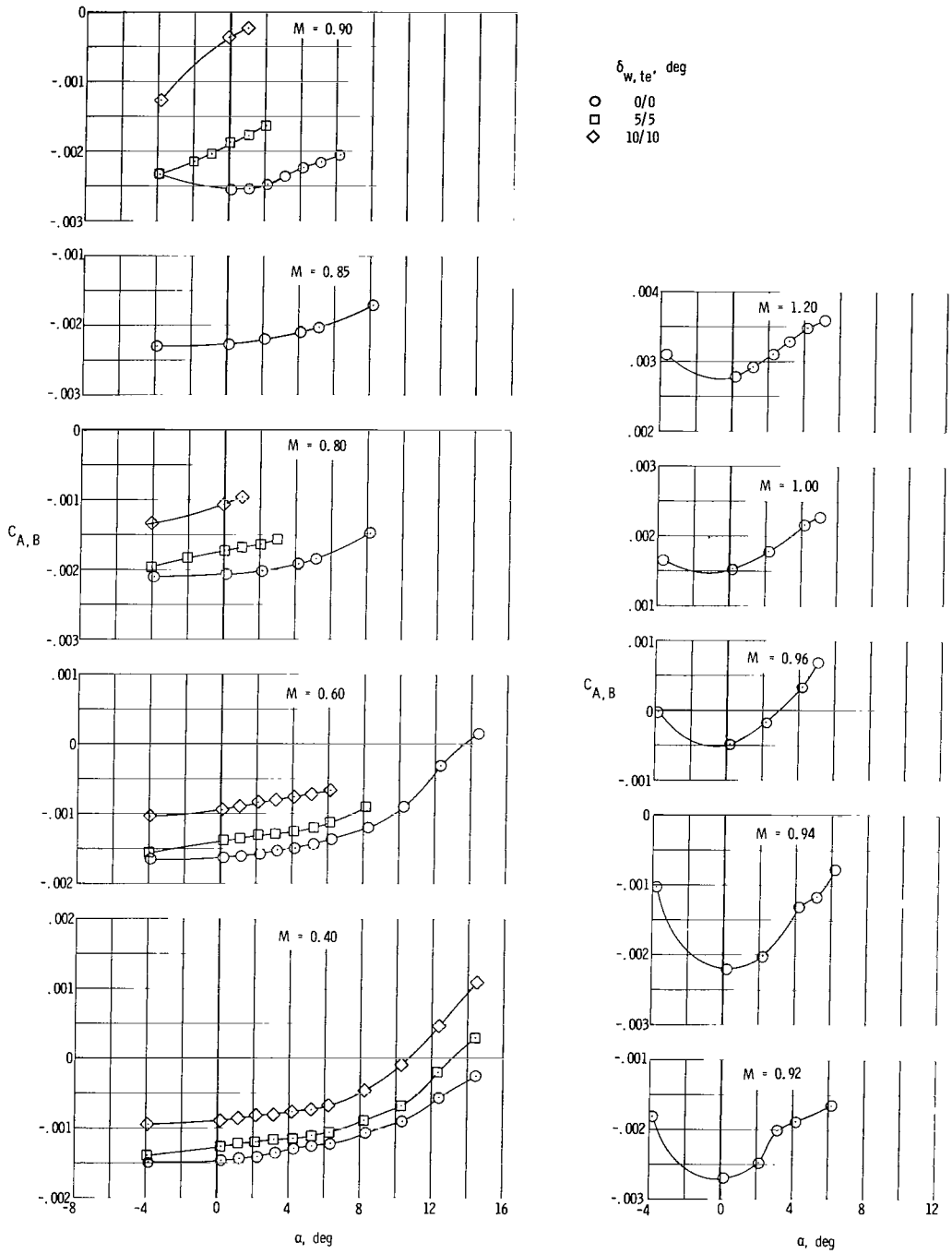

(b) Canard off; $\delta_{w,le} = 0^{o}/0^{o}$.

Figure 5.- Concluded.

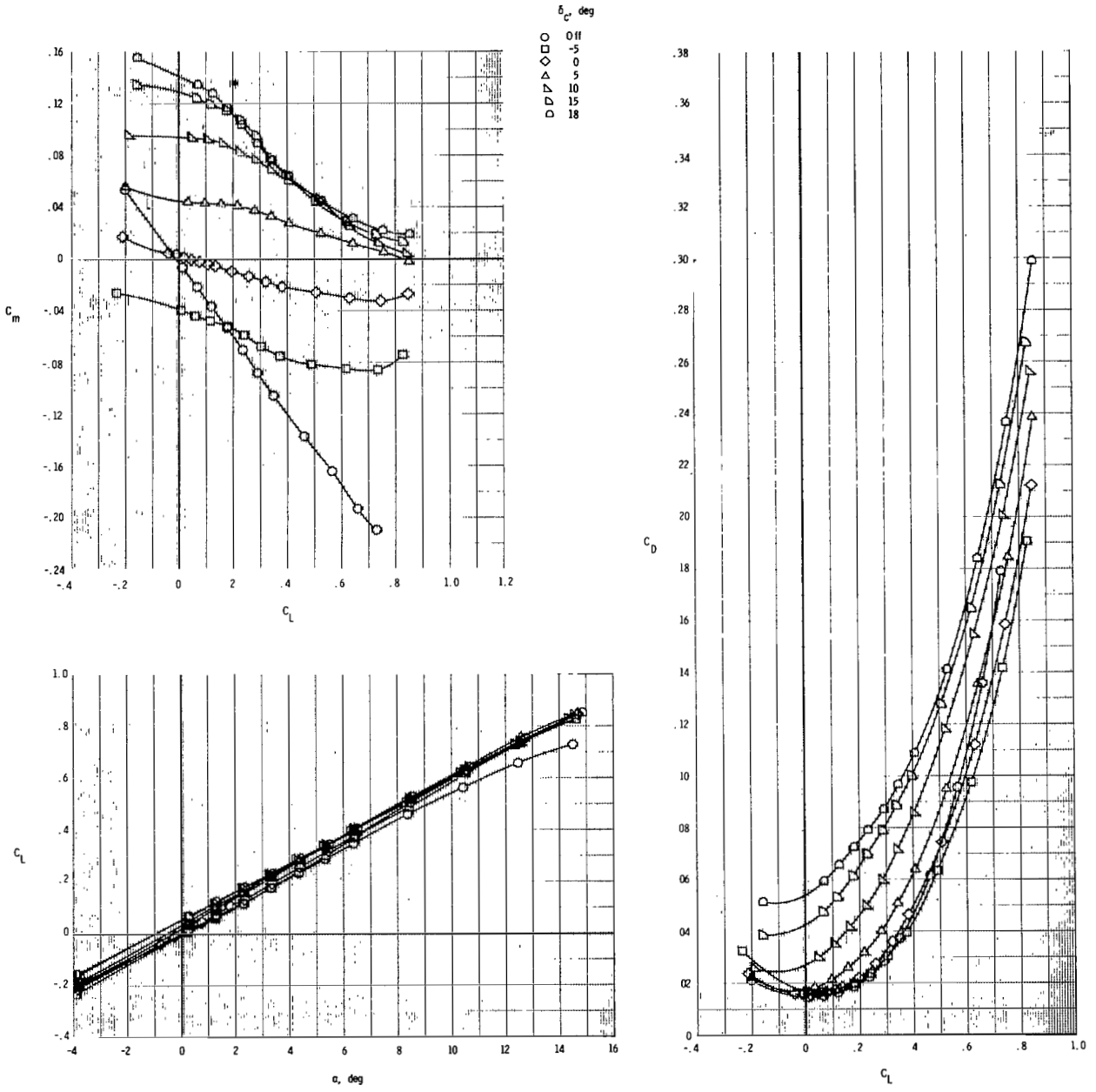

(a) M = 0.40.

Figure 6.- Effect of canard incidence on model longitudinal aerodynamic characteristics. All wing and canard flaps at 0^o deflection; vertical tails and ventrals on.

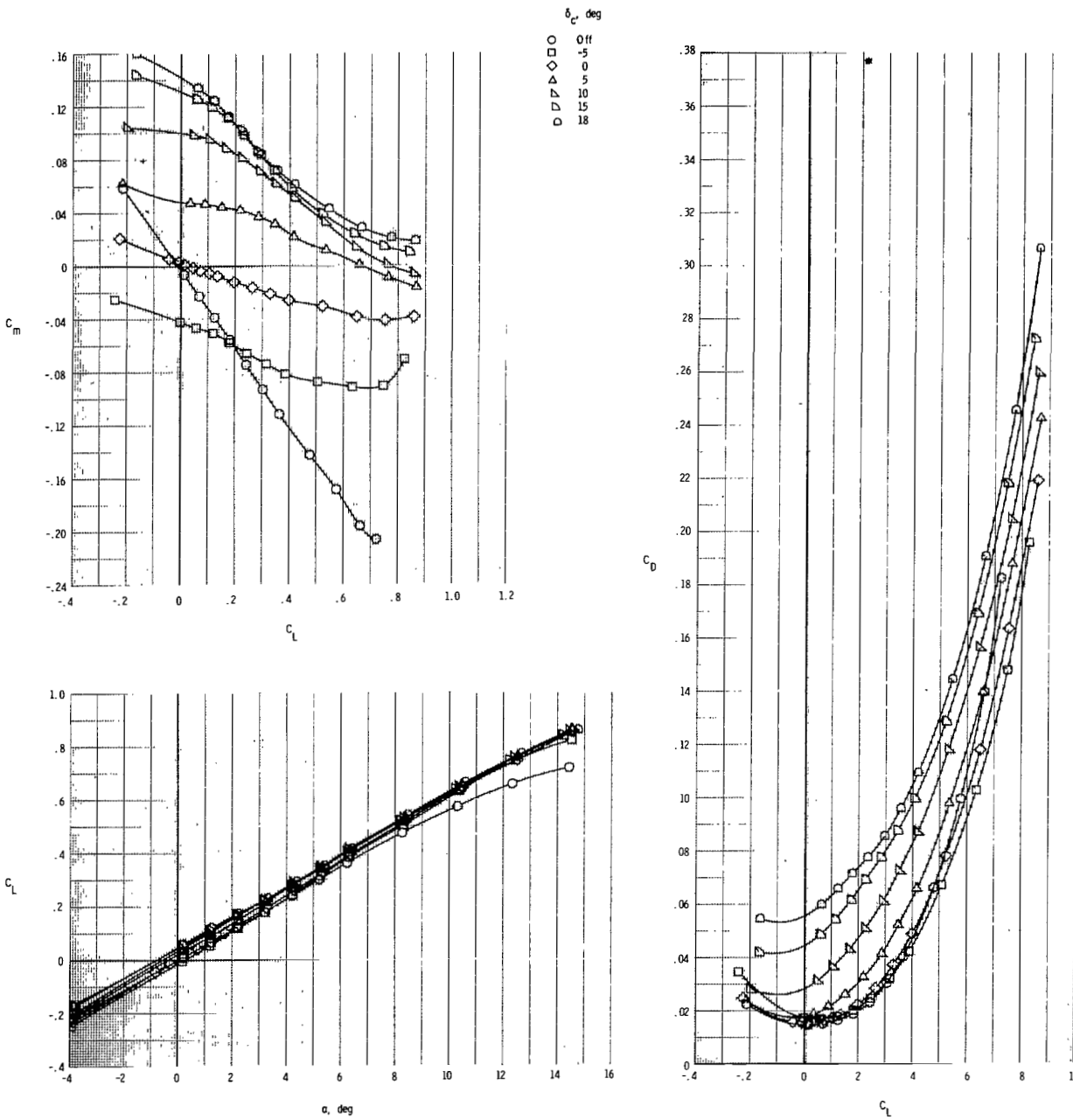

(b) M = 0.60.

Figure 6.- Continued.

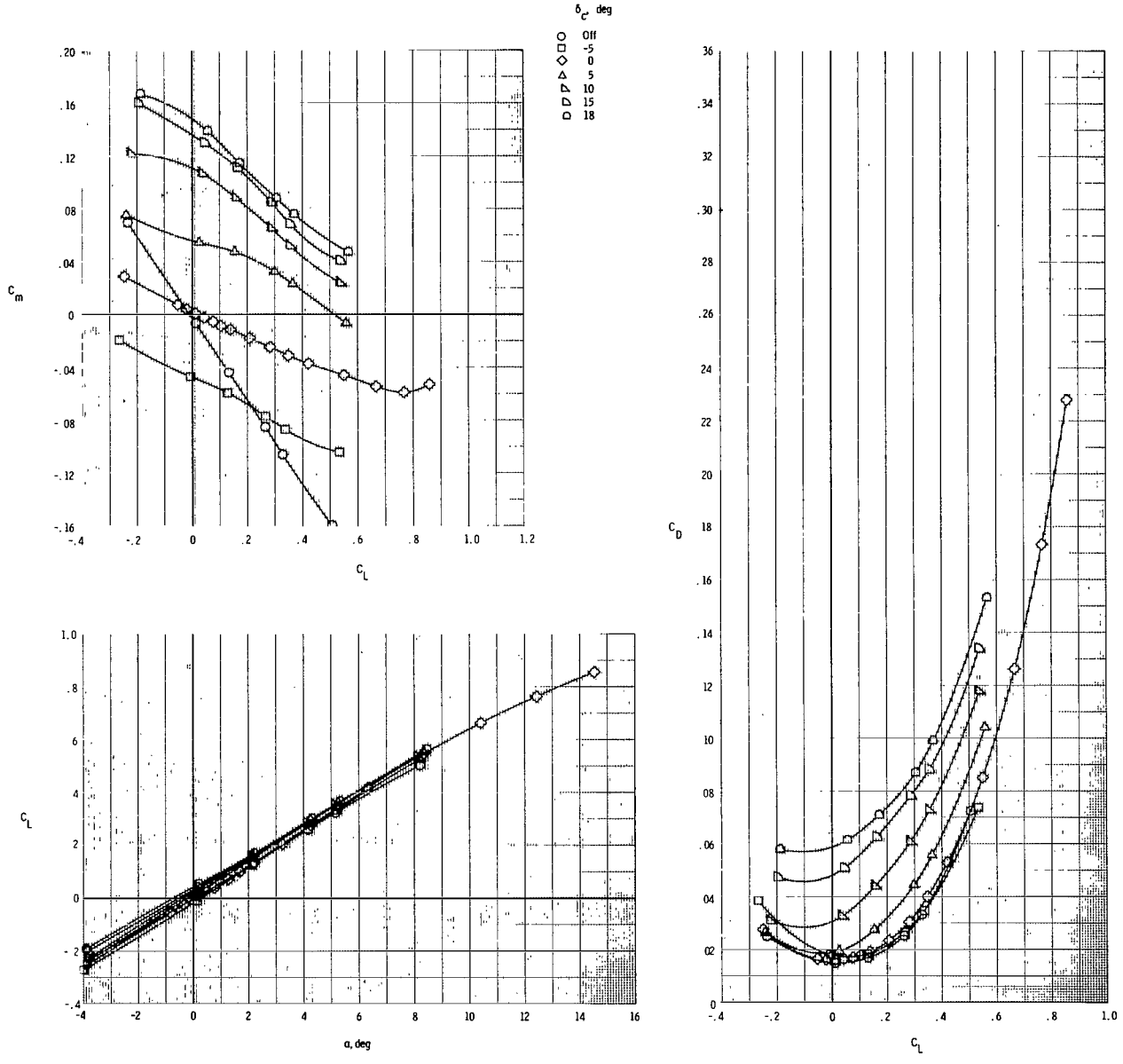

(c) M = 0.80.

Figure 6.- Continued.

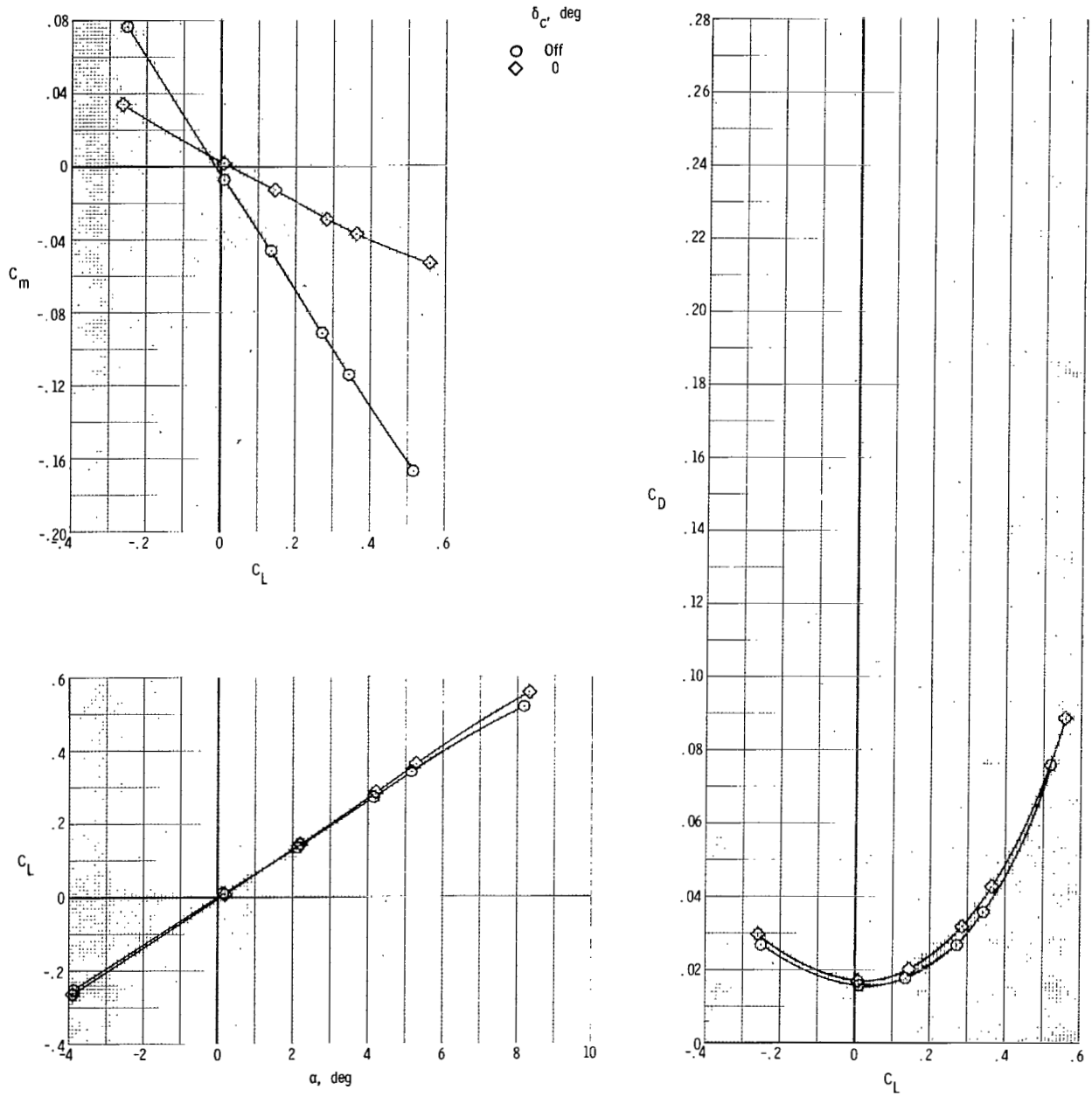

(d) M = 0.85.

Figure 6.- Continued.

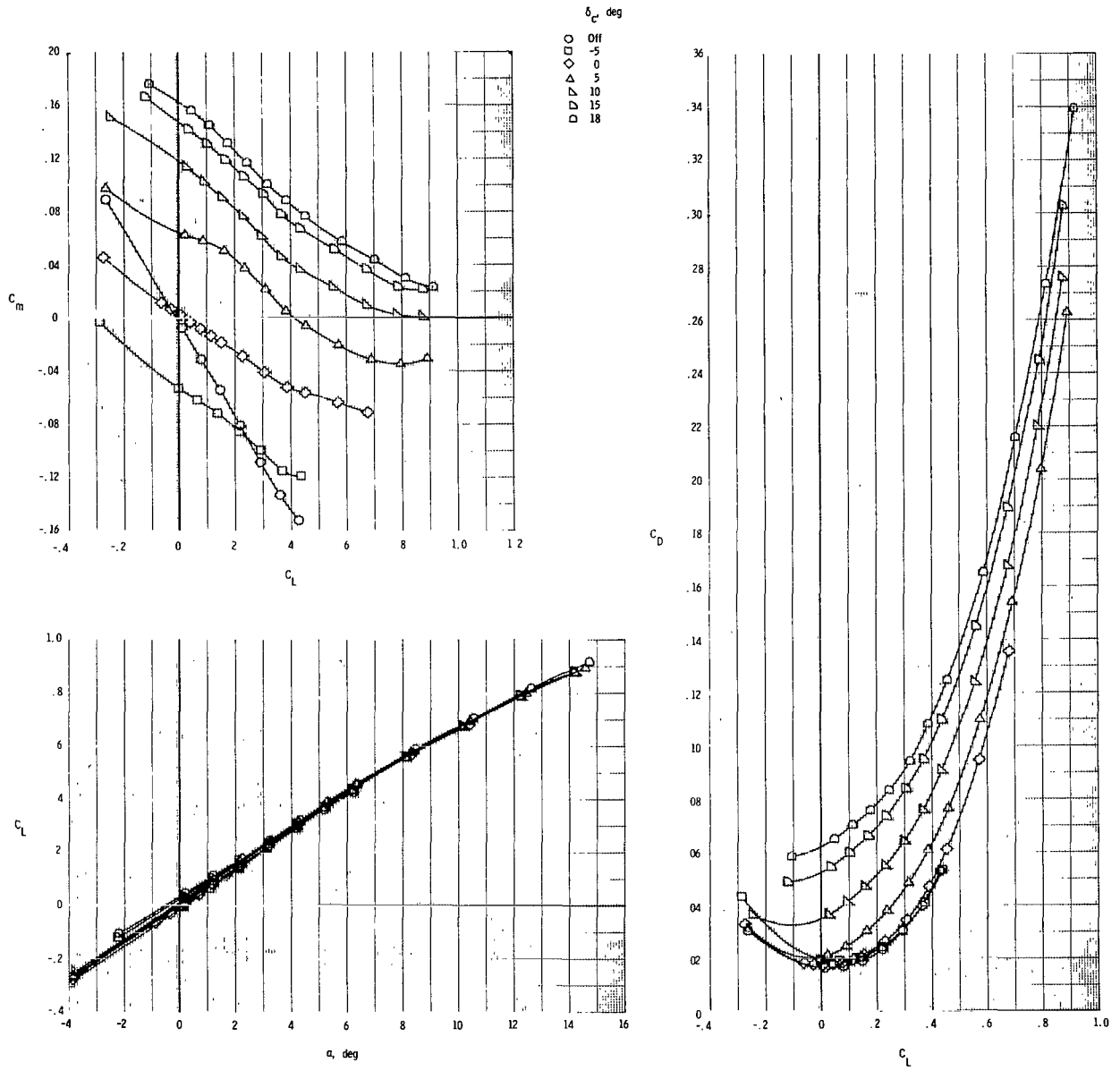

(e) M = 0.90.

Figure 6.- Continued.

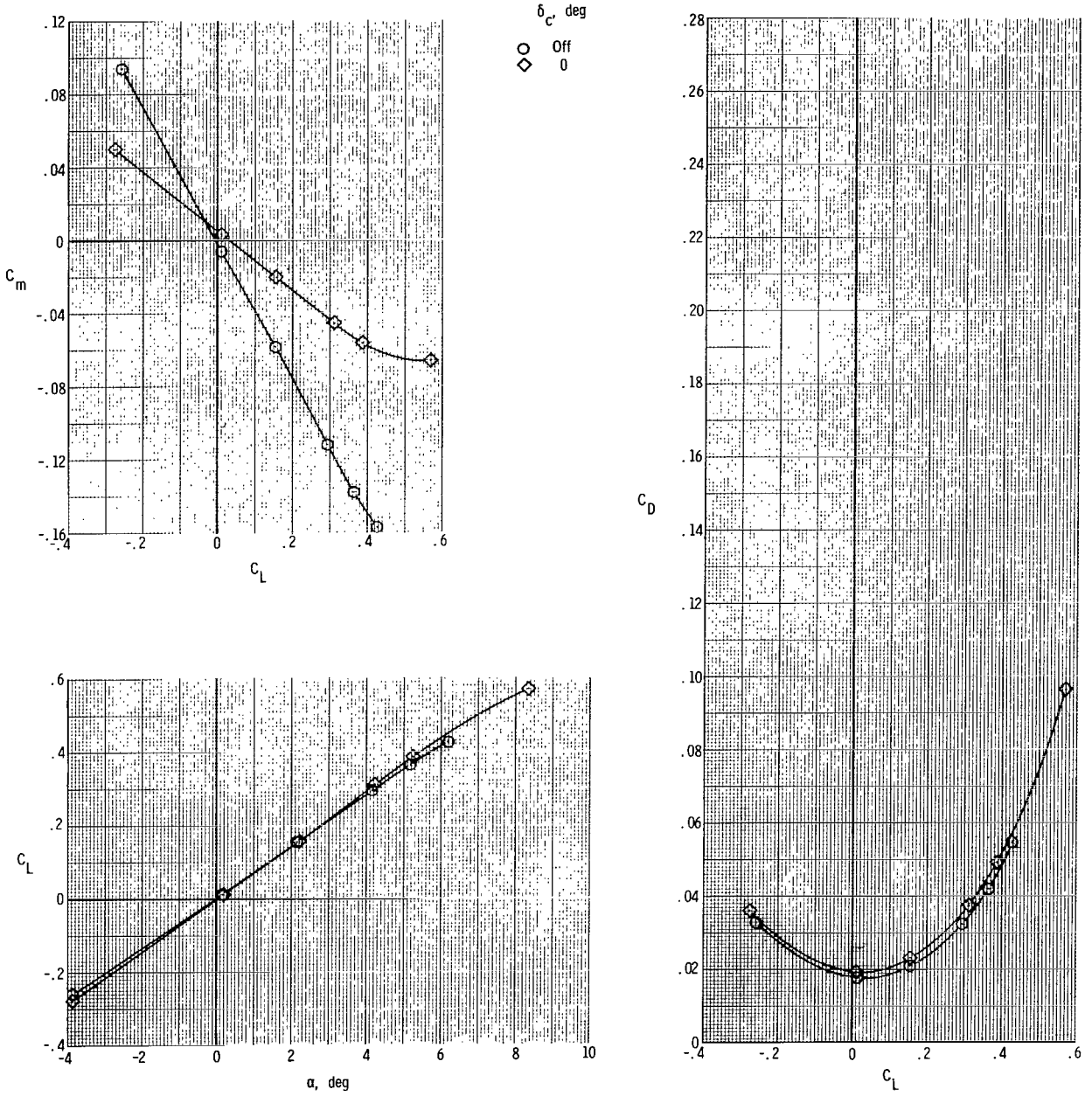

(f) M = 0.92.

Figure 6.- Continued.

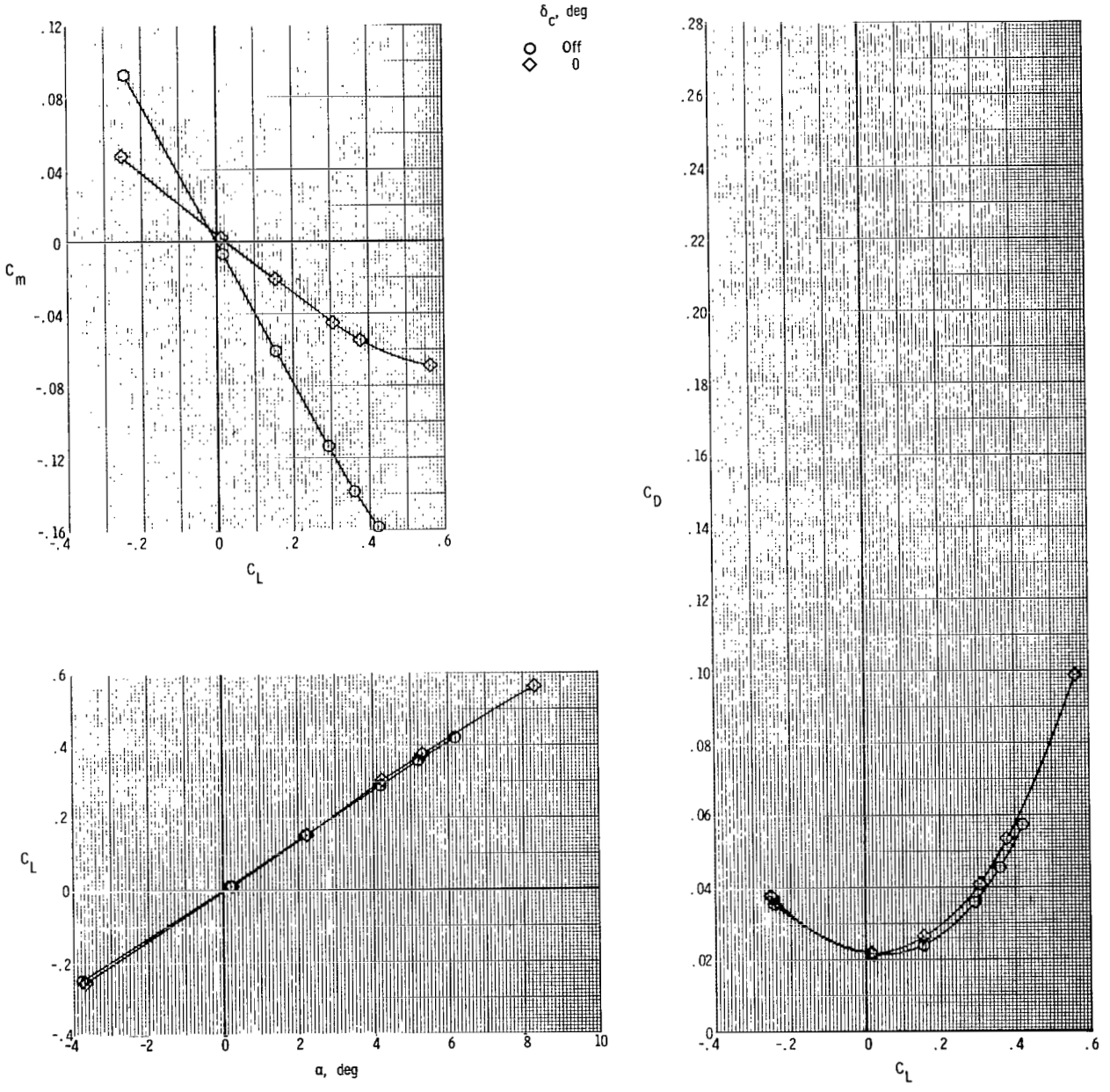

(g) M = 0.94.

Figure 6.- Continued.

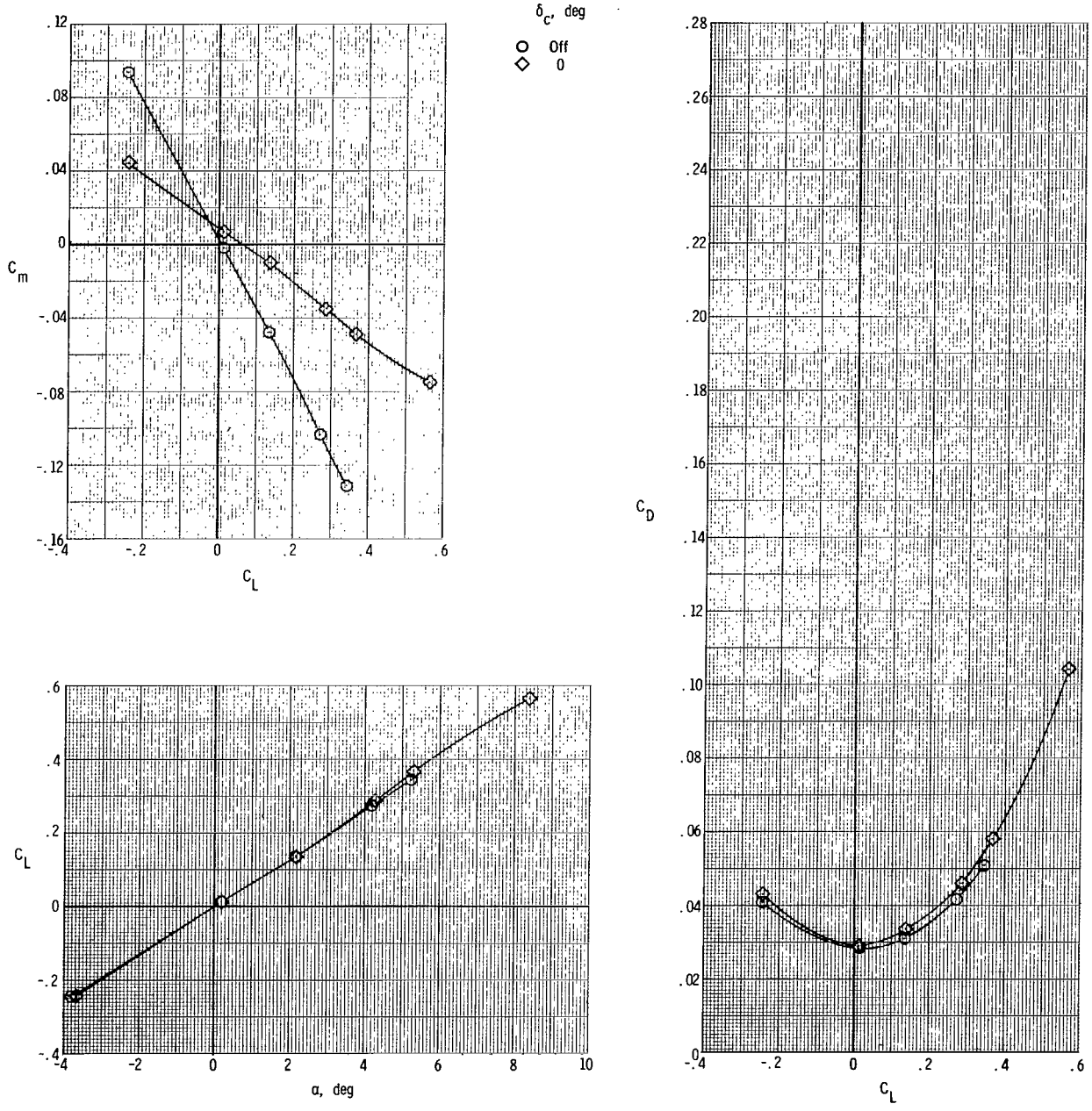

(h) M = 0.96.

Figure 6.- Continued.

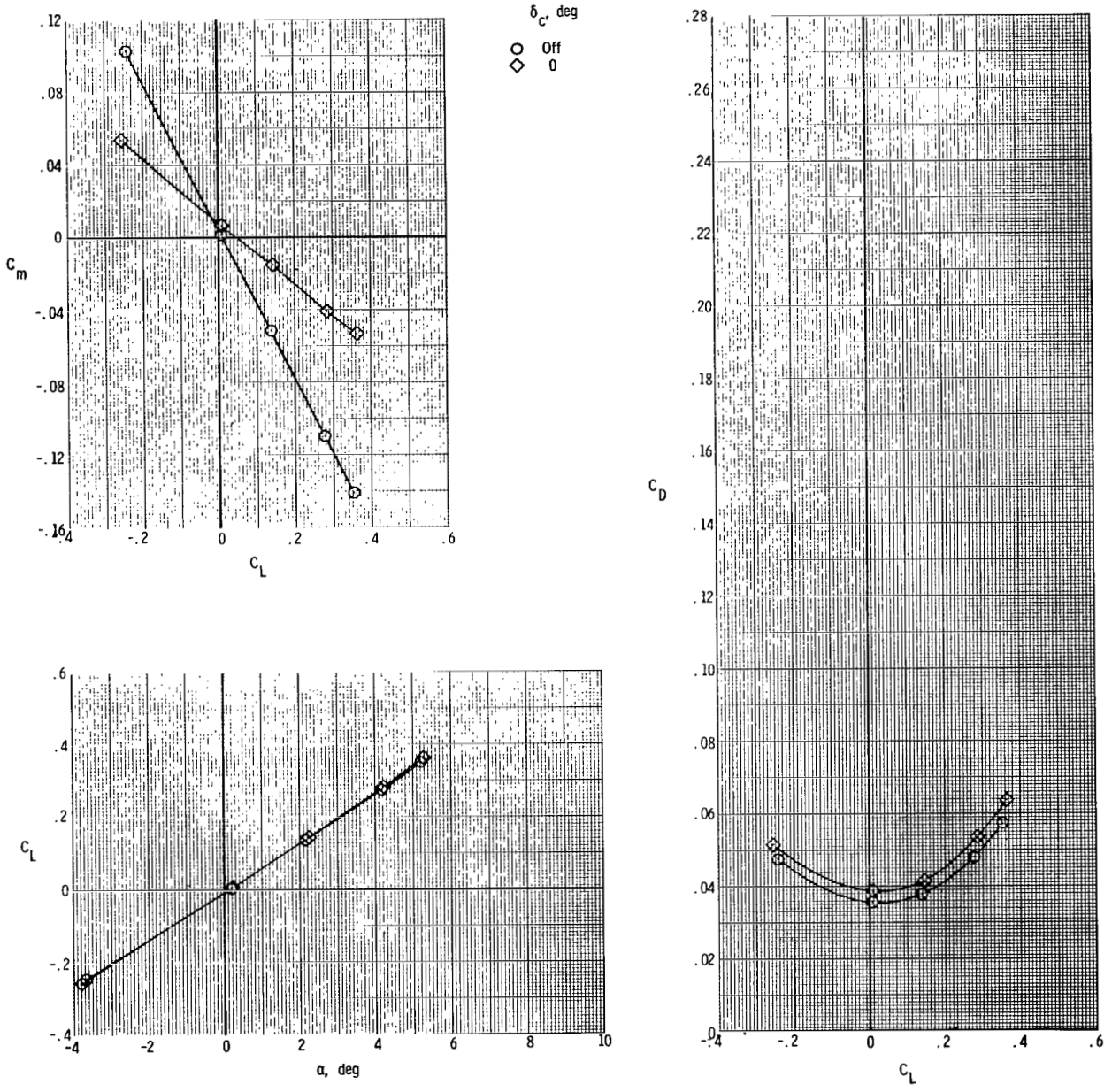

(i) M = 1.00.

Figure 6.- Continued.

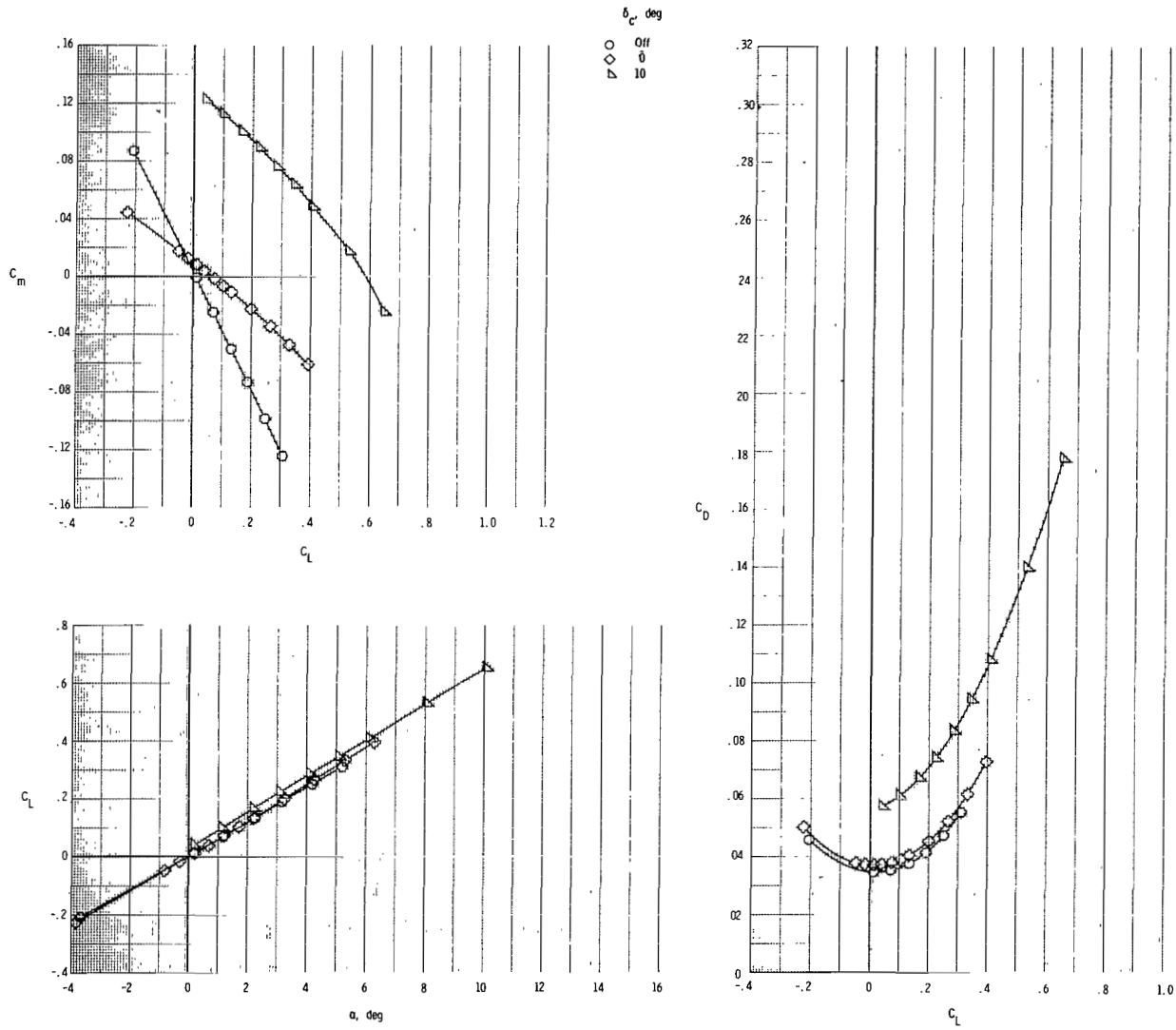

(j) M = 1.20.

Figure 6.- Concluded.

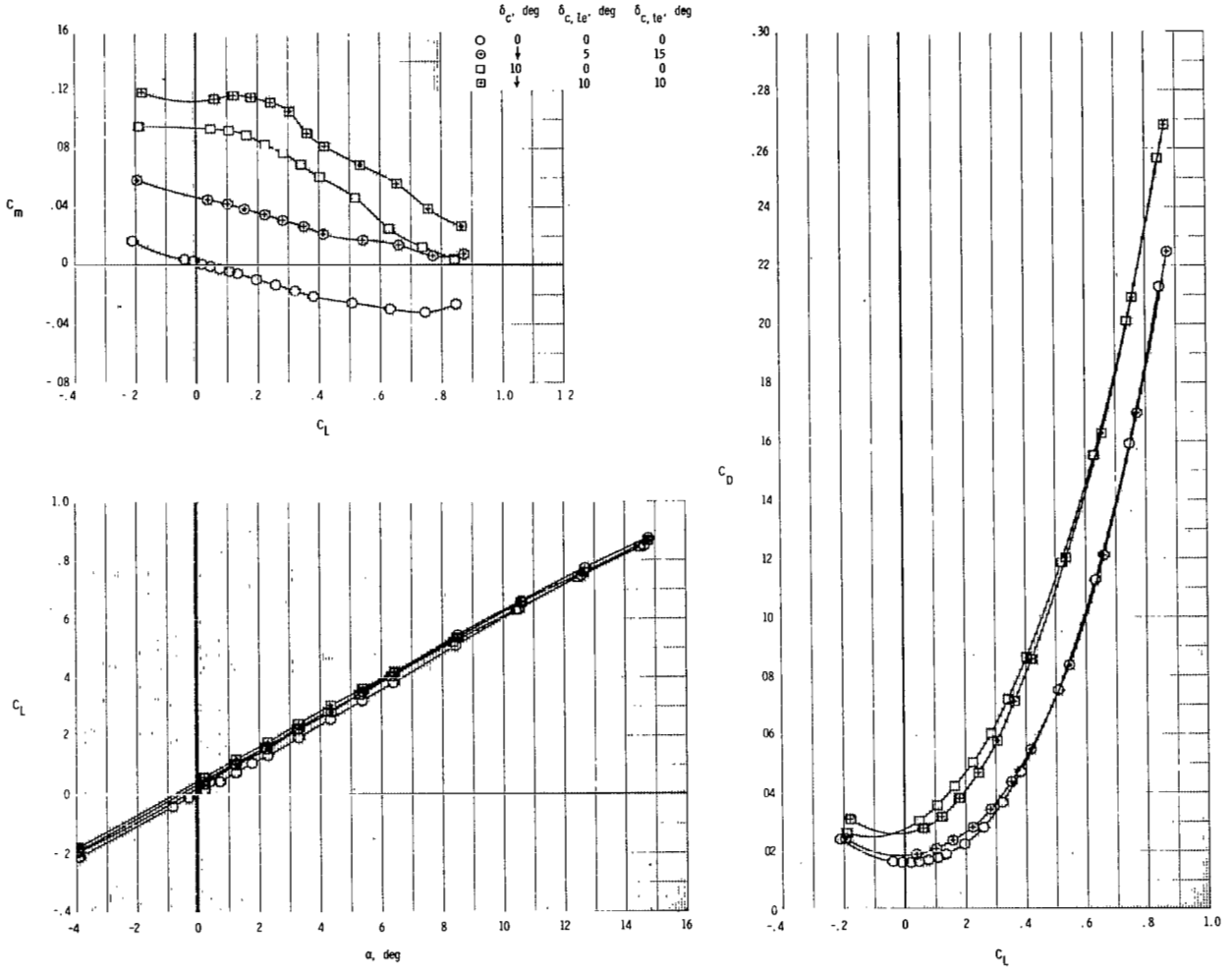

(a) M = 0.40.

Figure 7.- Effect of canard incidence and leading- and trailing-edge flap deflection on model longitudinal aerodynamic characteristics. $\delta_{w,le} = \delta_{w,te} = 0^{o}/0^{o}$; vertical tails and ventrals on.

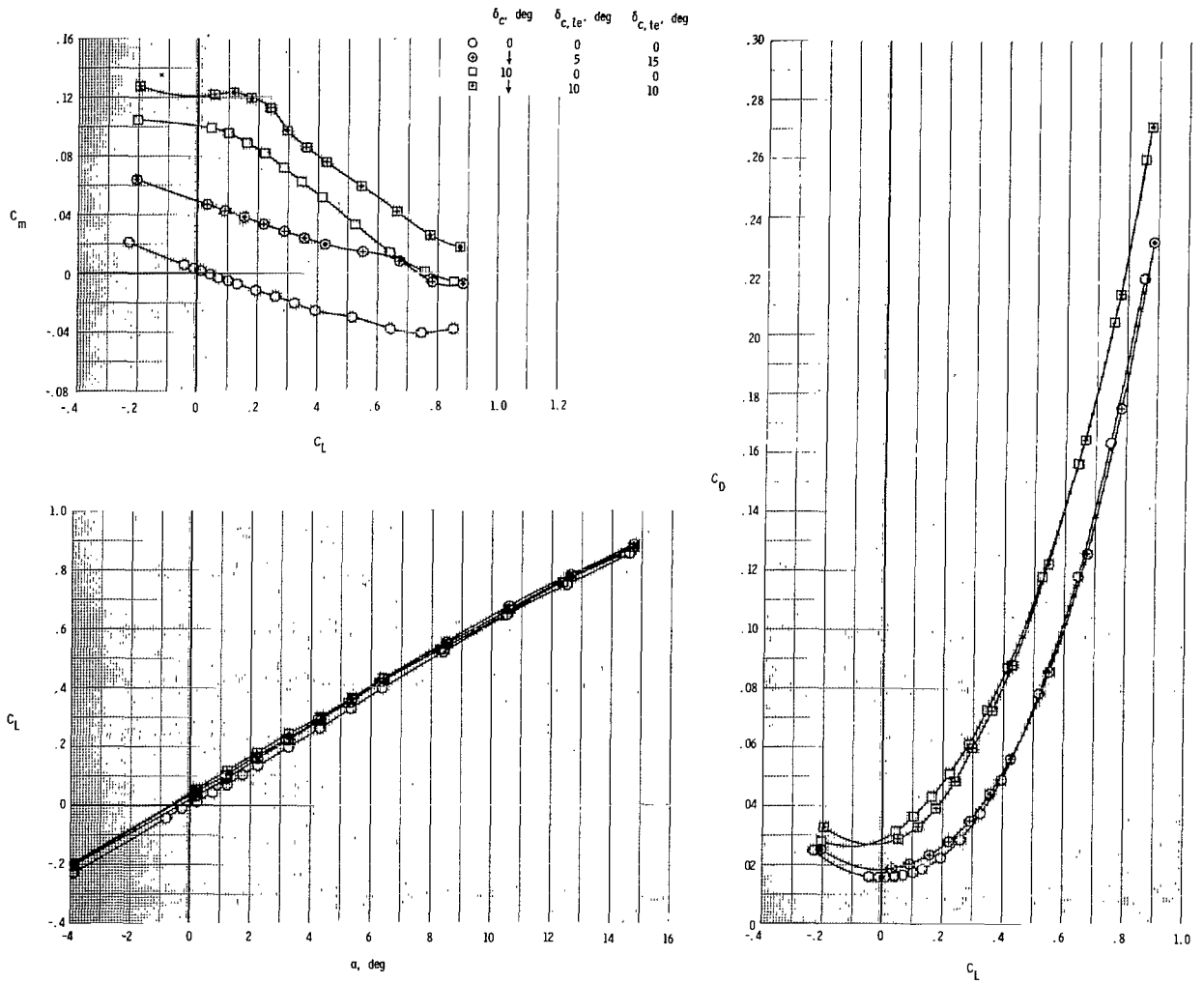

(b) M = 0.60.

Figure 7.- Continued.

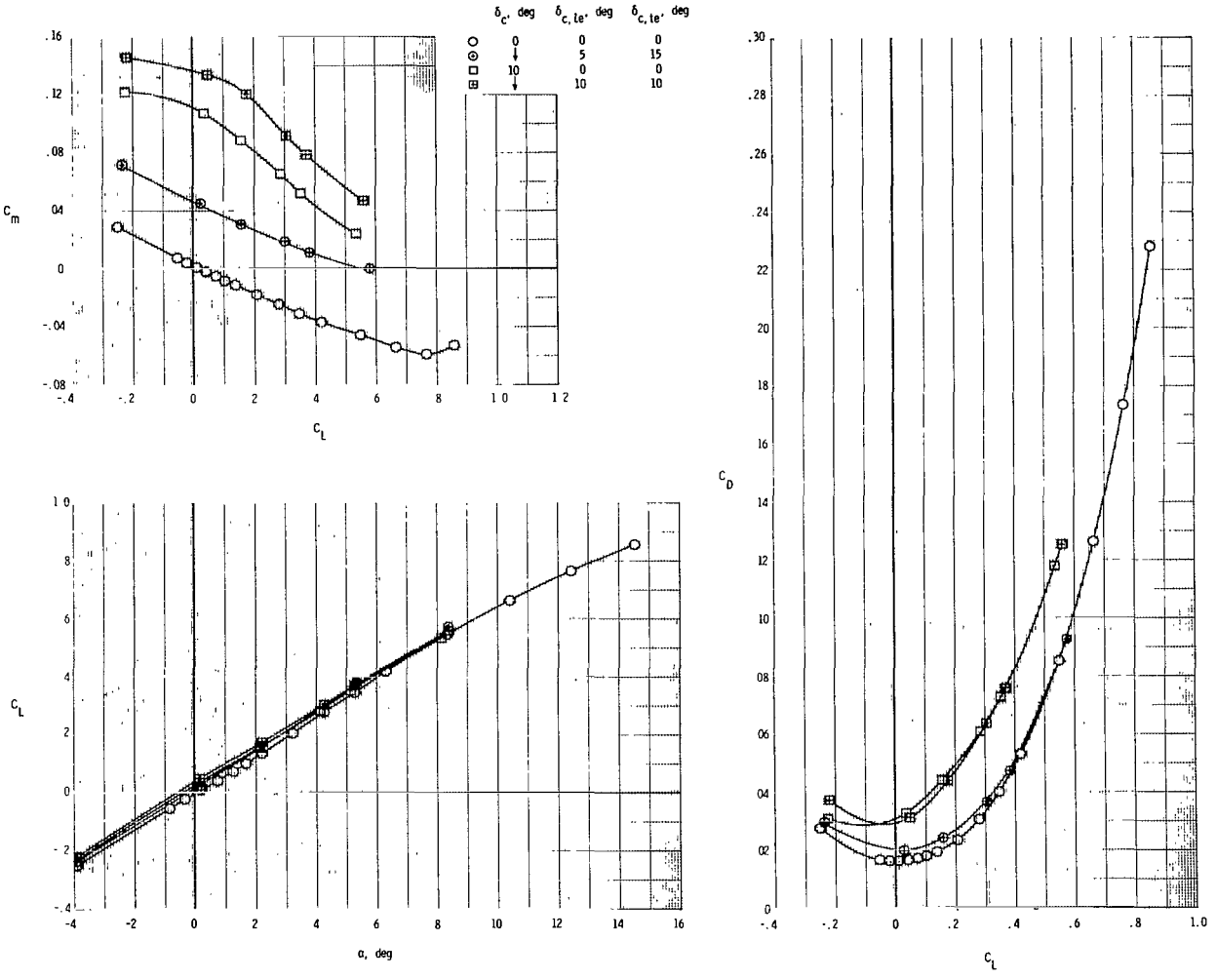

(c) M = 0.80.

Figure 7.- Continued.

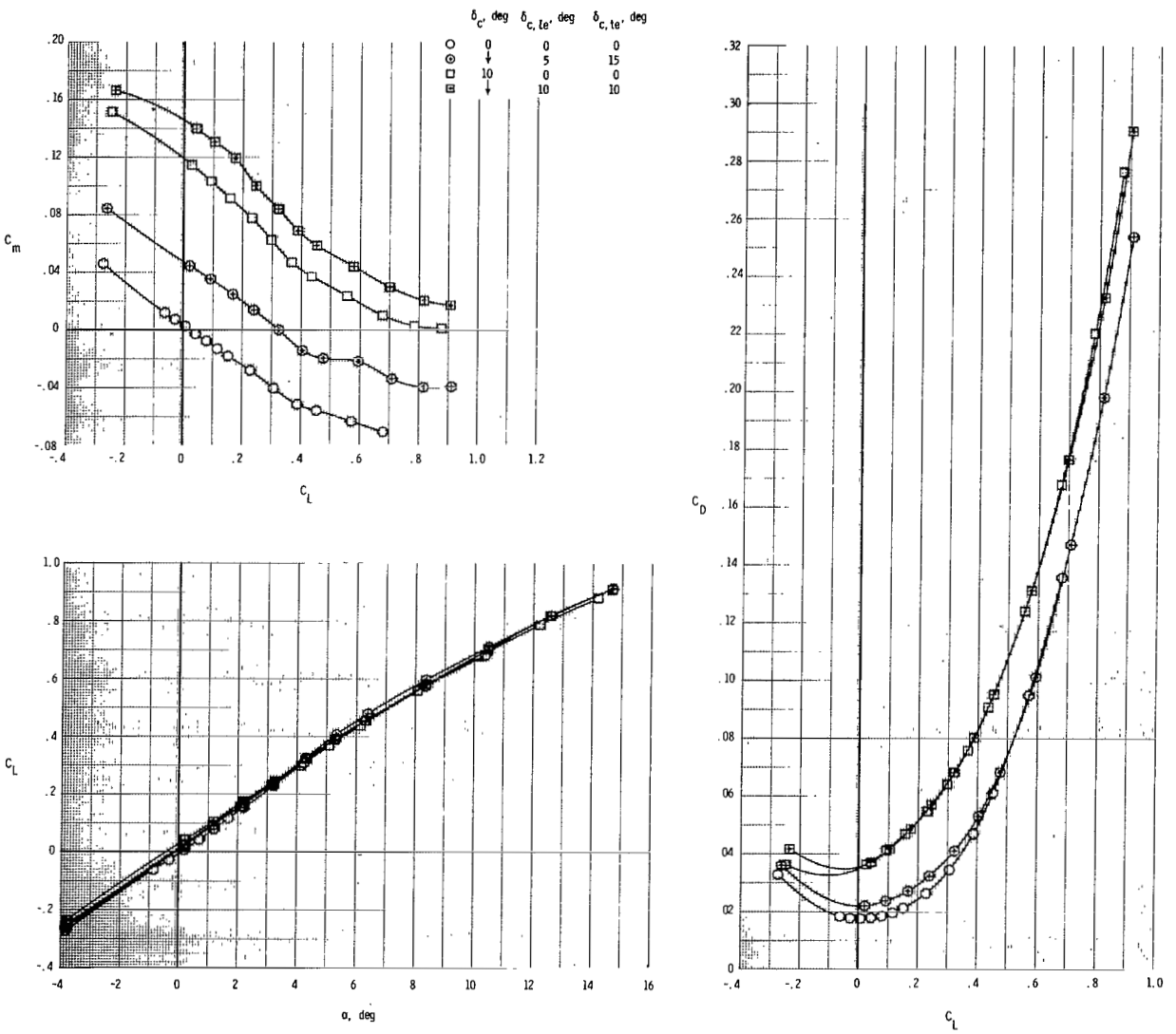

(d) M = 0.90.

Figure 7.- Concluded.

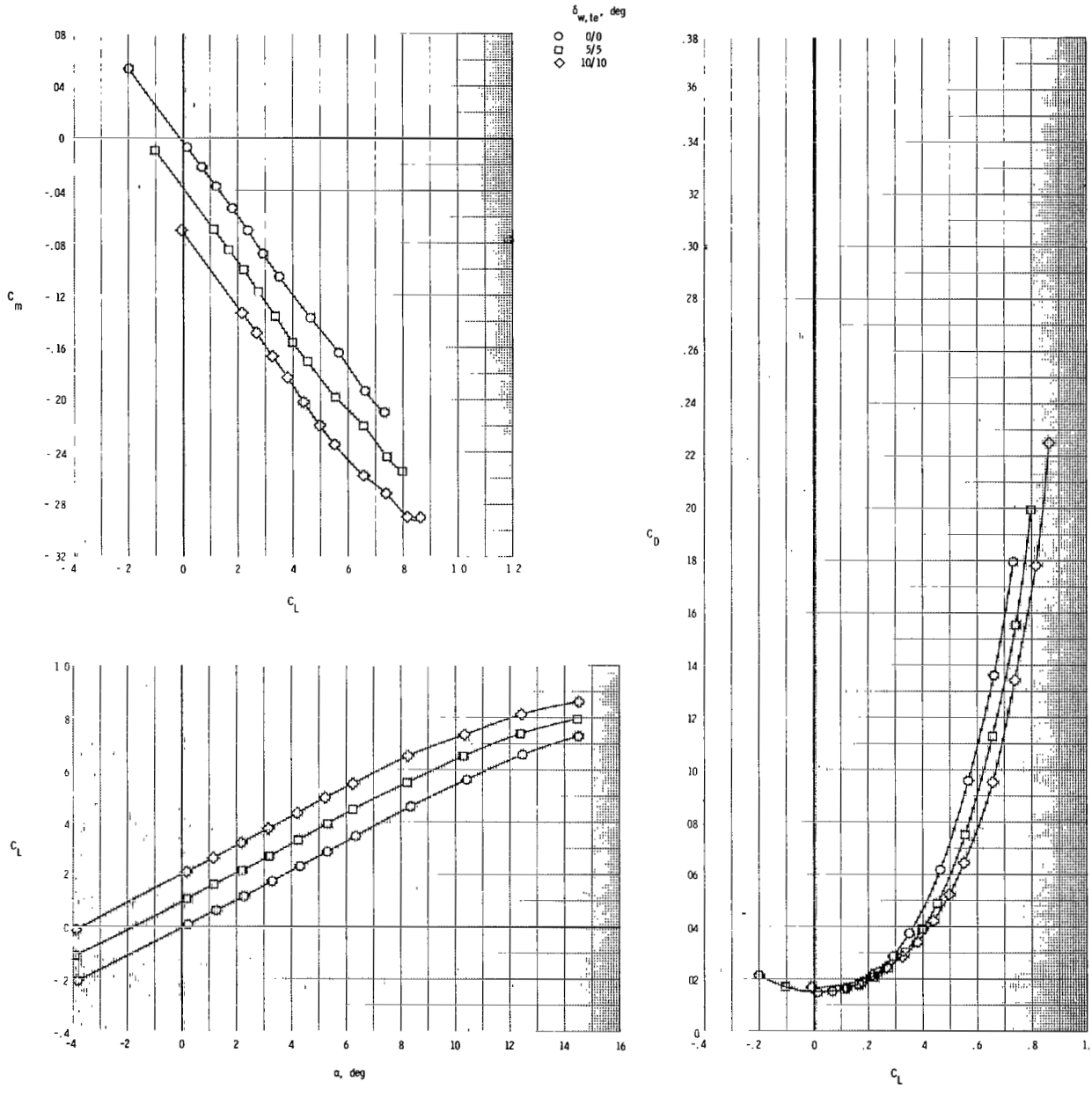

(a) M = 0.40.

Figure 8.- Effect of wing trailing-edge flap deflection on model longitudinal aerodynamic characteristics with canard off. $\delta_{w,le} = 0^o/0^o$; vertical tails and ventrals on.

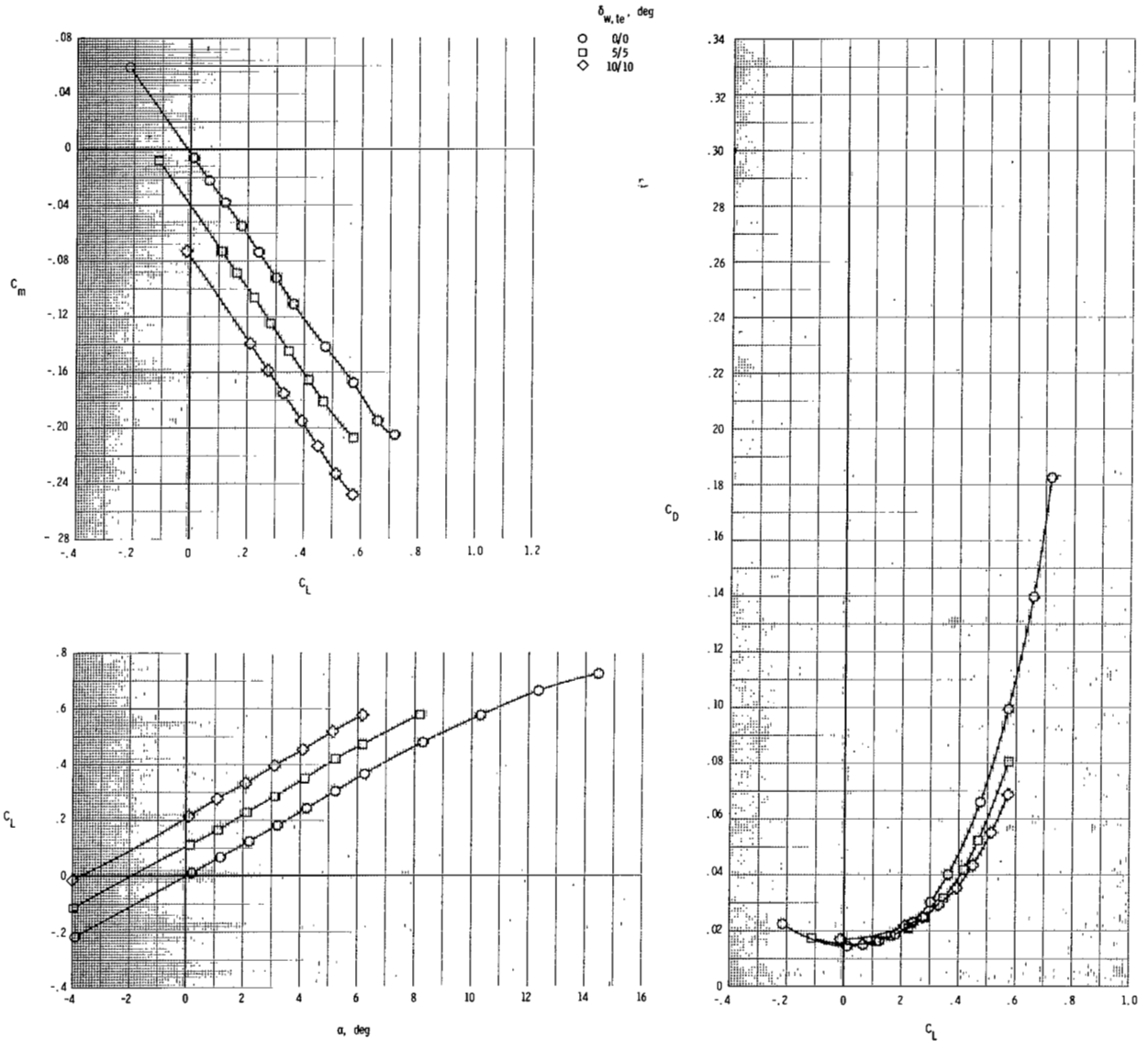

(b) M = 0.60.

Figure 8.- Continued.

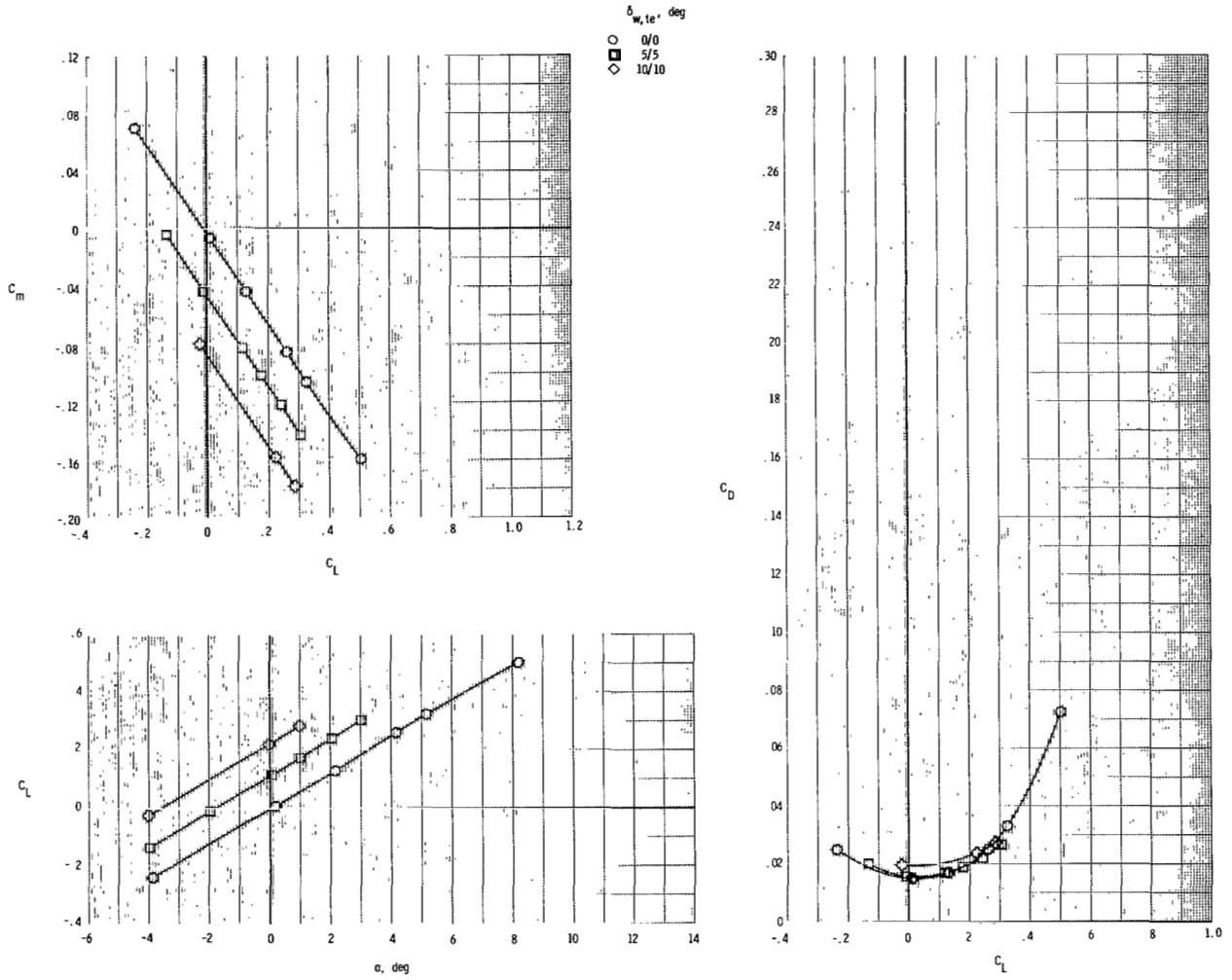

(c) M = 0.80.

Figure 8.- Continued.

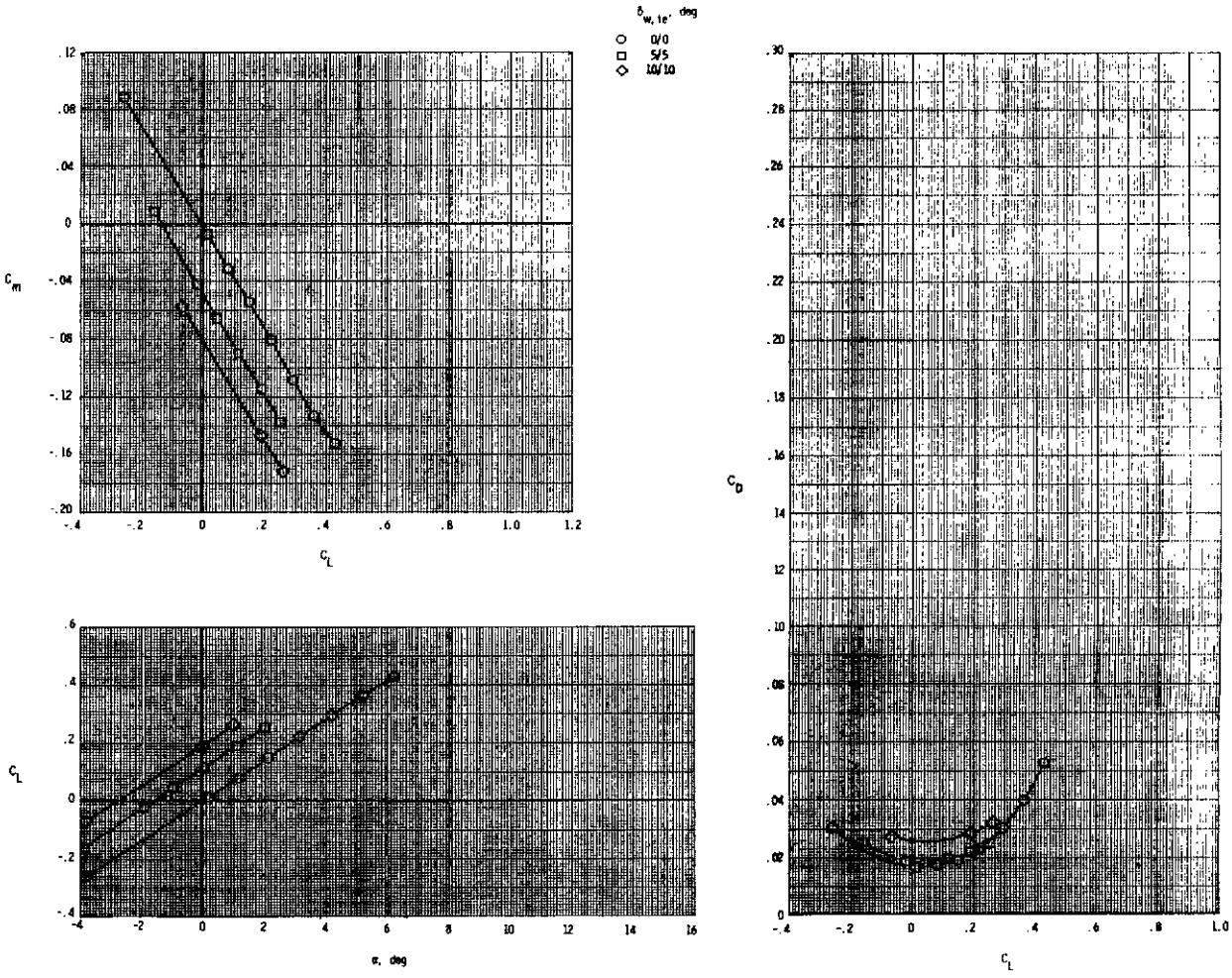

(d) M = 0.90.

Figure 8.- Concluded.

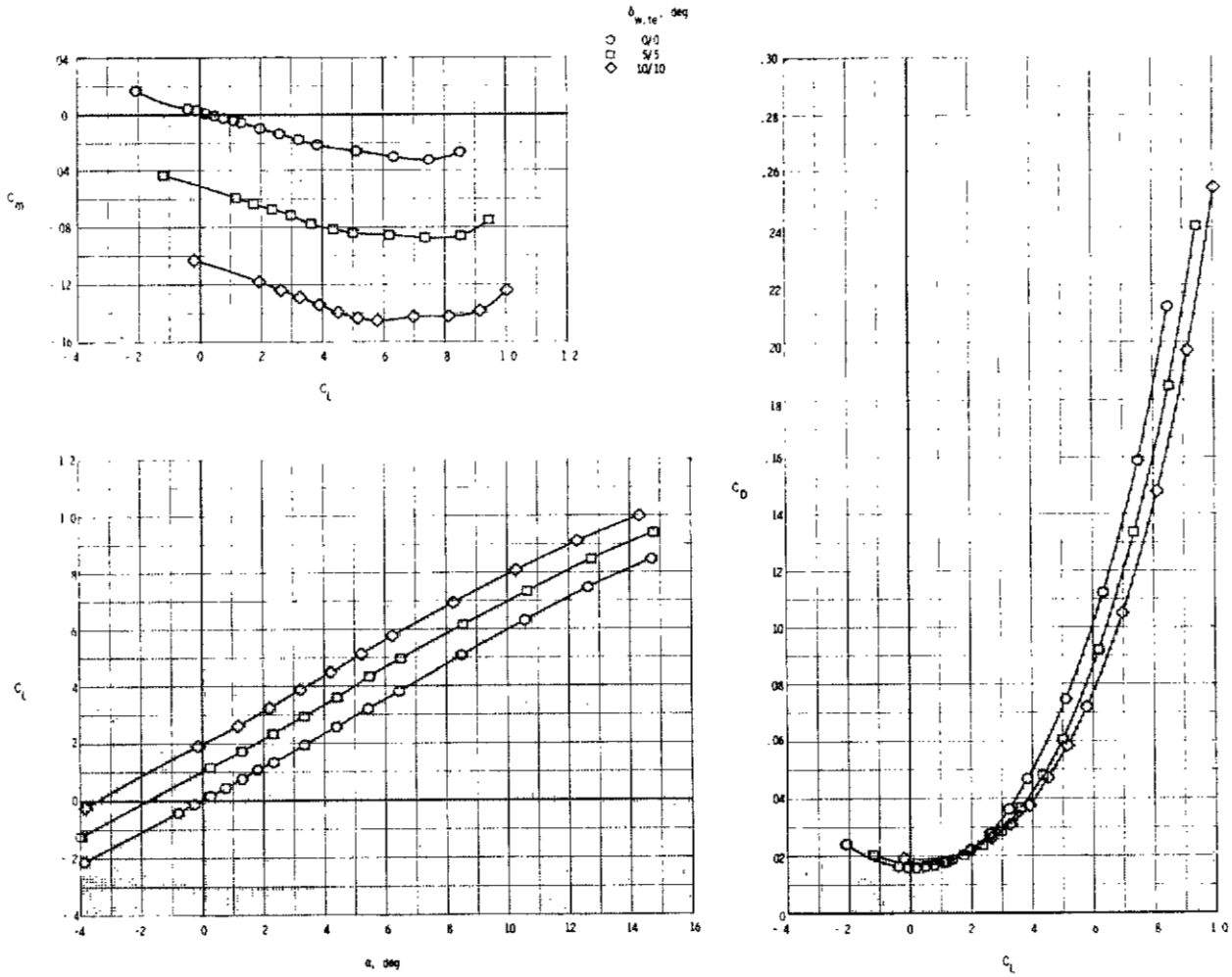

(a) M = 0.40.

Figure 9.- Effect of wing trailing-edge flap deflection on model longitudinal aerodynamic characteristics with canard on. $\delta_{w,le} = 0^o/0^o$; $\delta_c = 0^o$; $\delta_{c,le} = \delta_{c,te} = 0^o$; vertical tails and ventrals on.

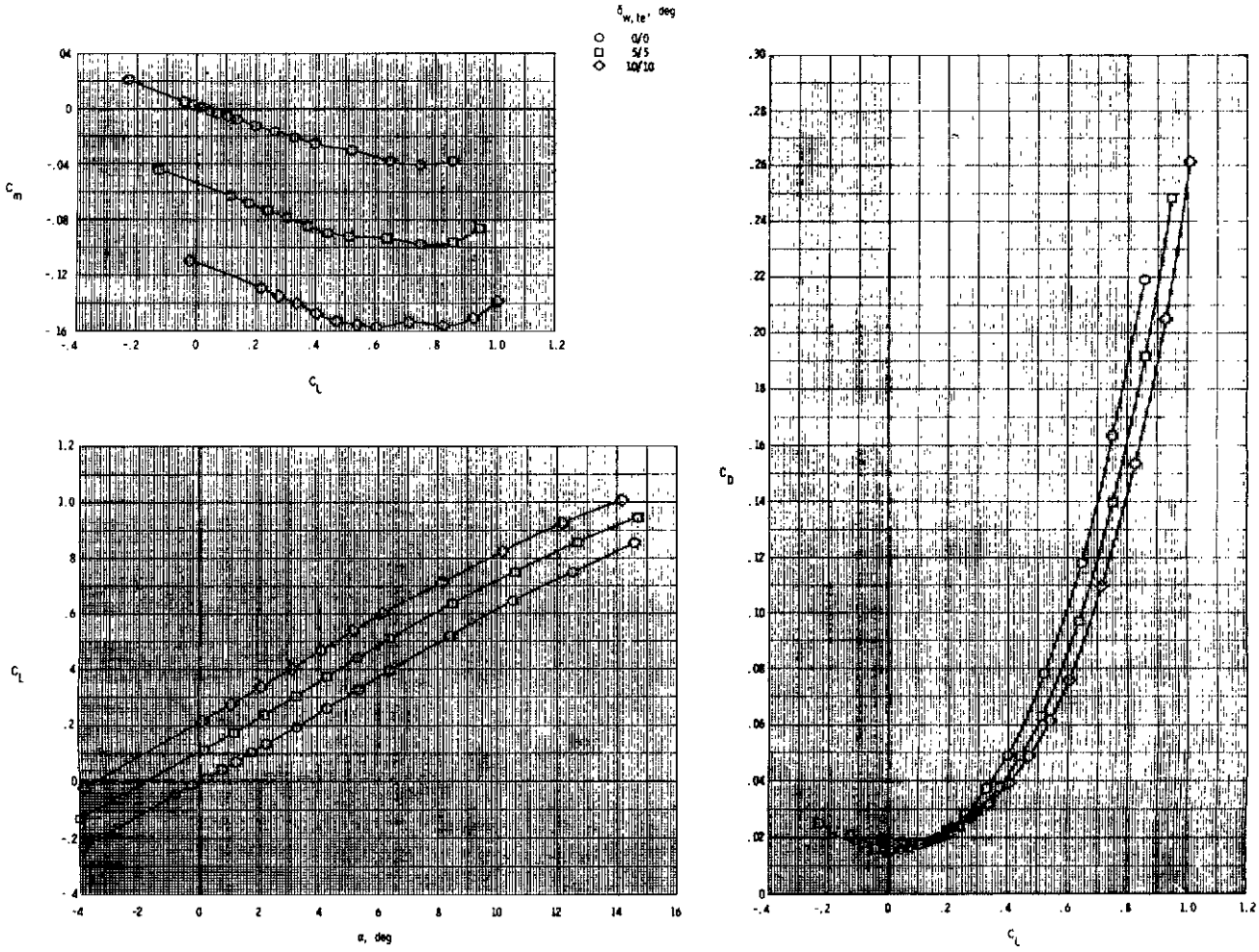

(b) M = 0.60.

Figure 9.- Continued.

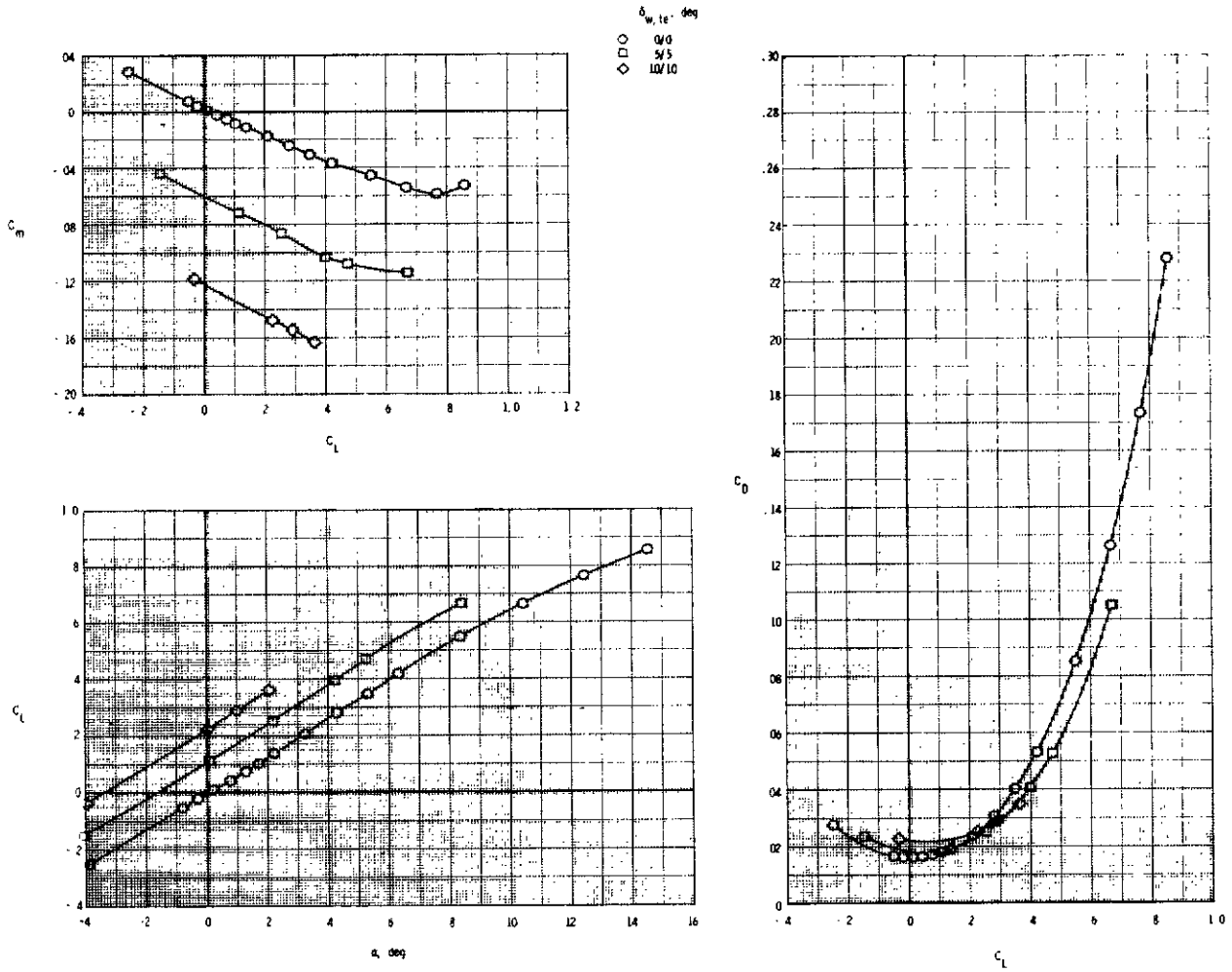

(c) M = 0.80.

Figure 9.- Continued.

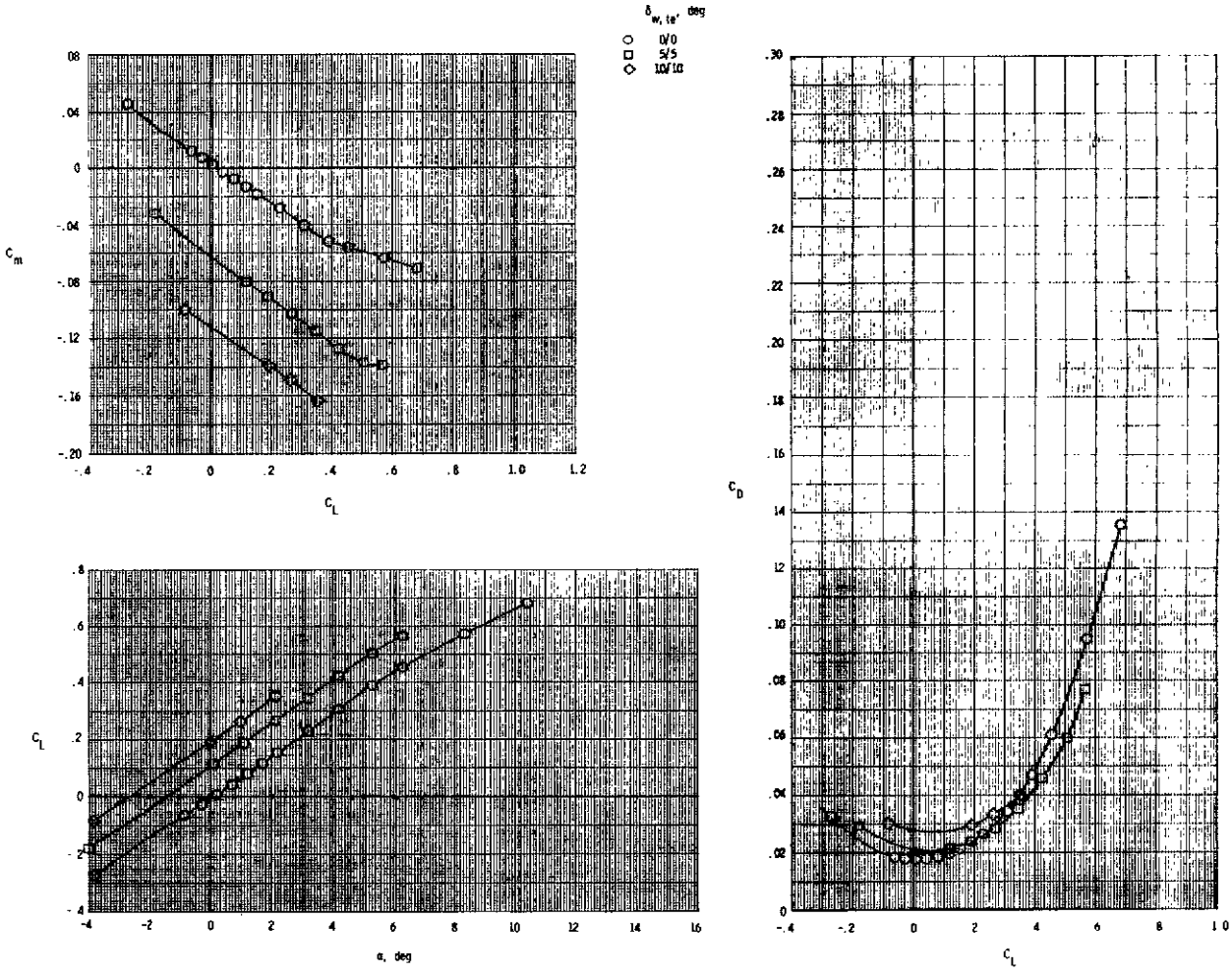

(d) M = 0.90.

Figure 9.- Concluded.

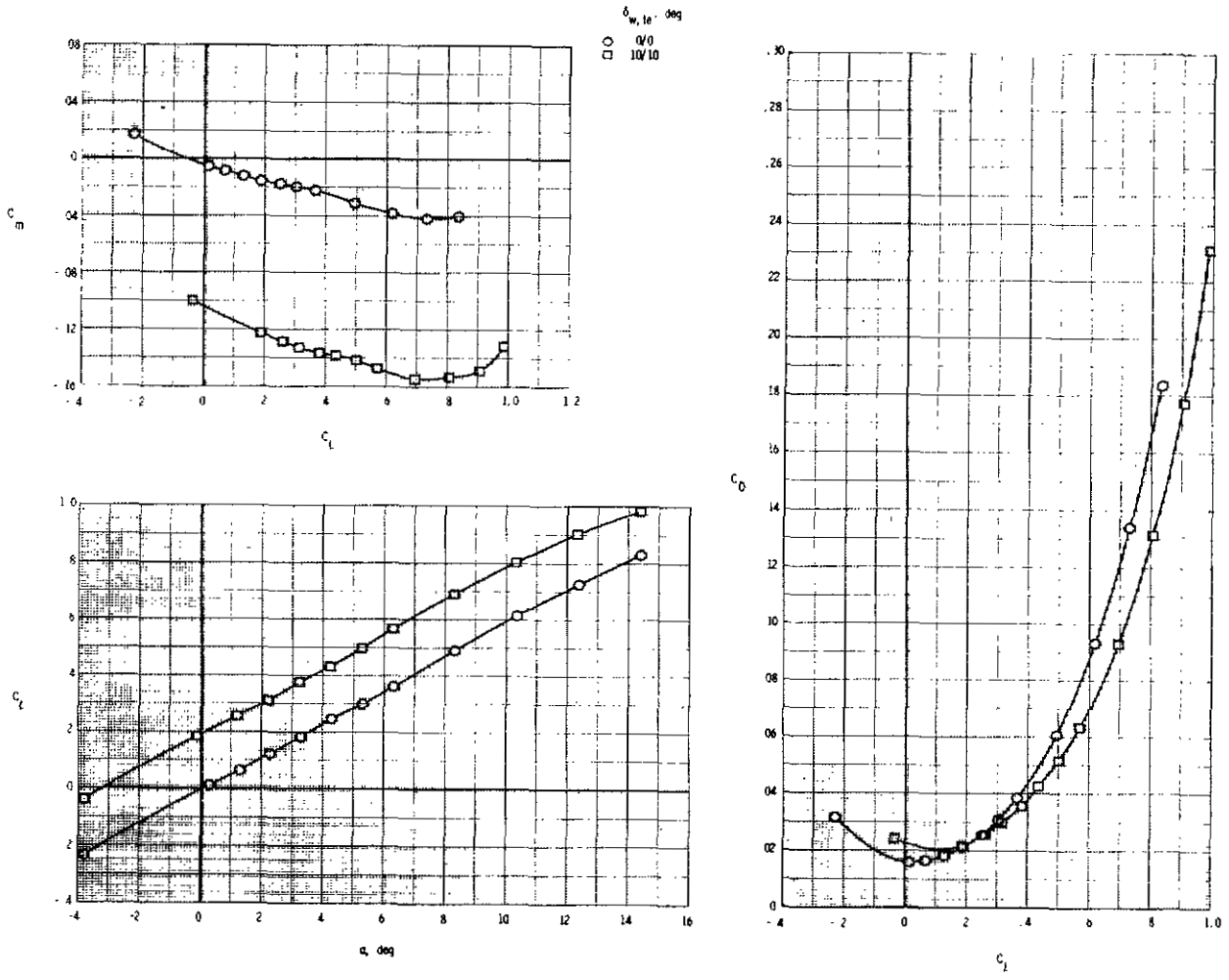

(a) M = 0.40.

Figure 10.- Effect of wing trailing-edge flap deflection on model longitudinal aerodynamic characteristics with canard on. $\delta_{w,le} = 10^o/10^o$; $\delta_c = 0^o$; $\delta_{c,le} = \delta_{c,te} = 0^o$; vertical tails and ventrals on.

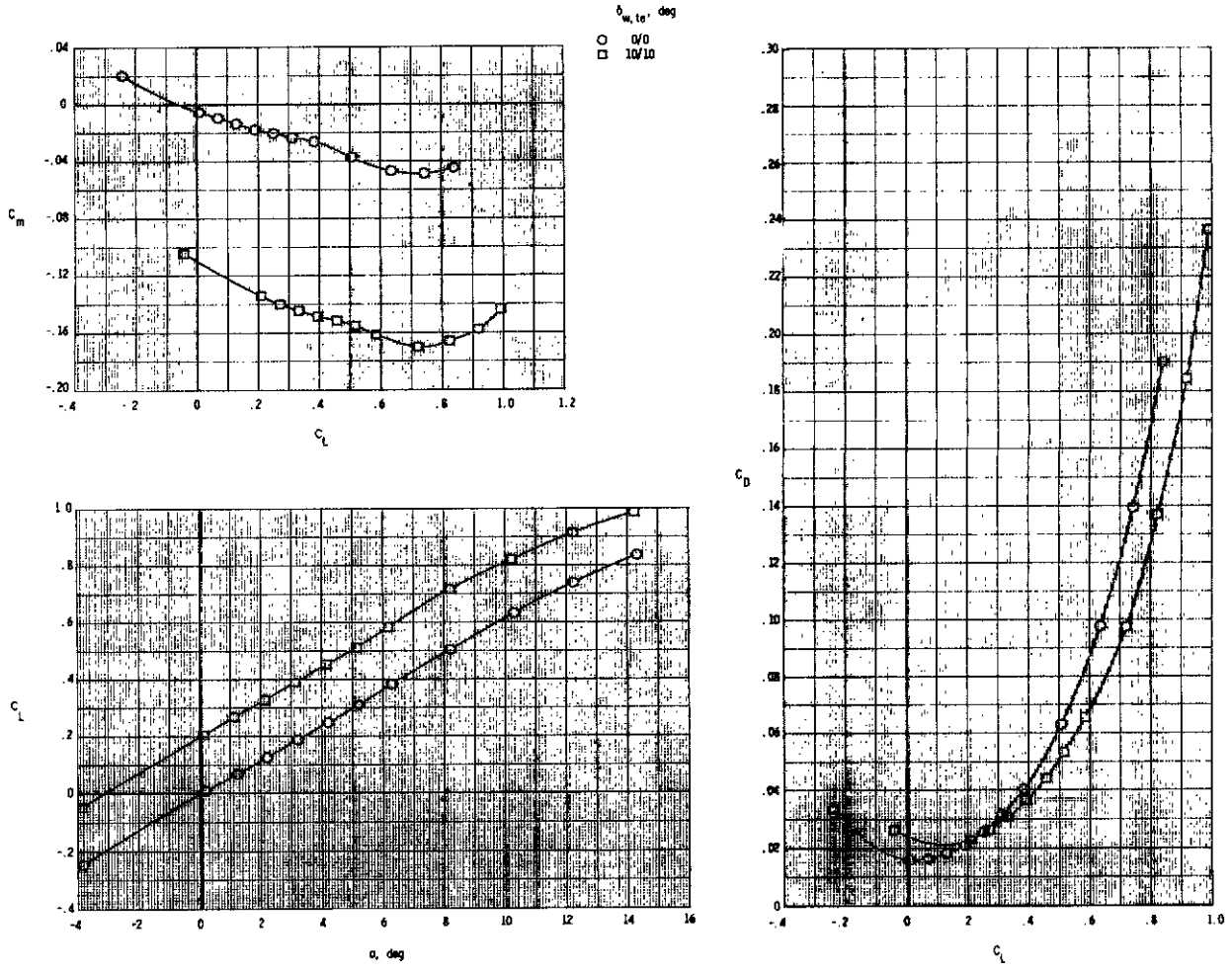

(b) M = 0.60.

Figure 10.- Continued.

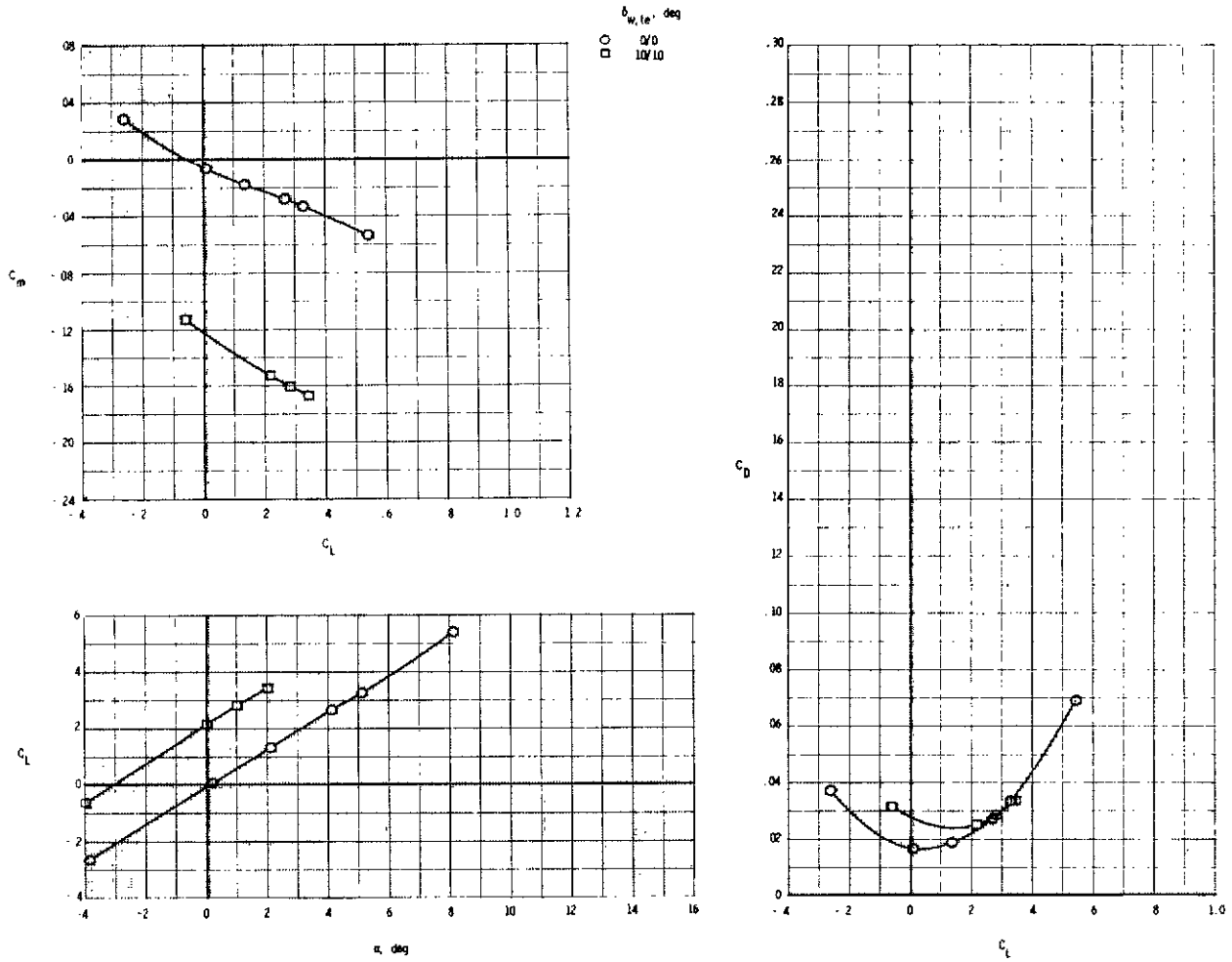

(c) M = 0.80.

Figure 10.- Continued.

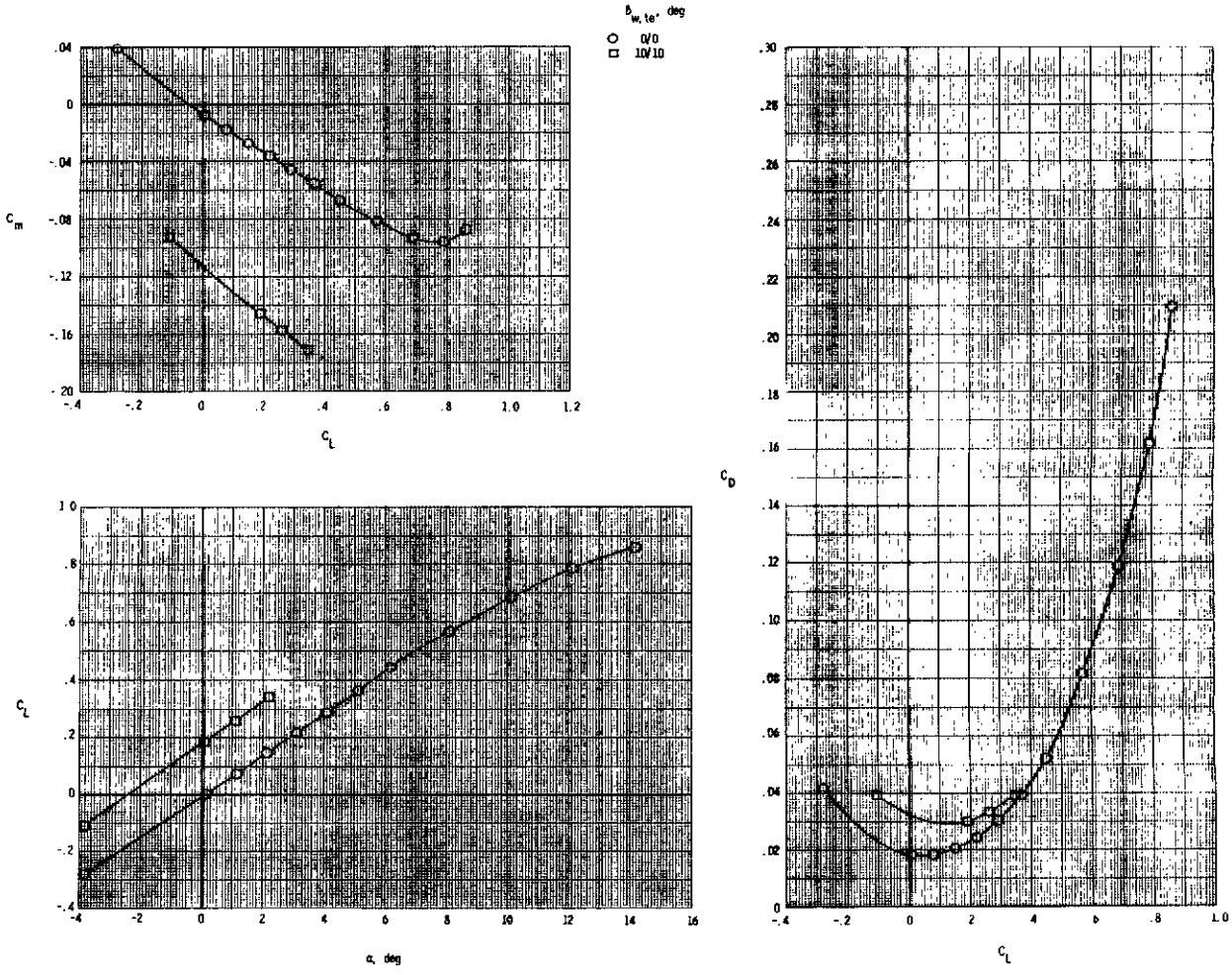

(d) M = 0.90.

Figure 10.- Concluded.

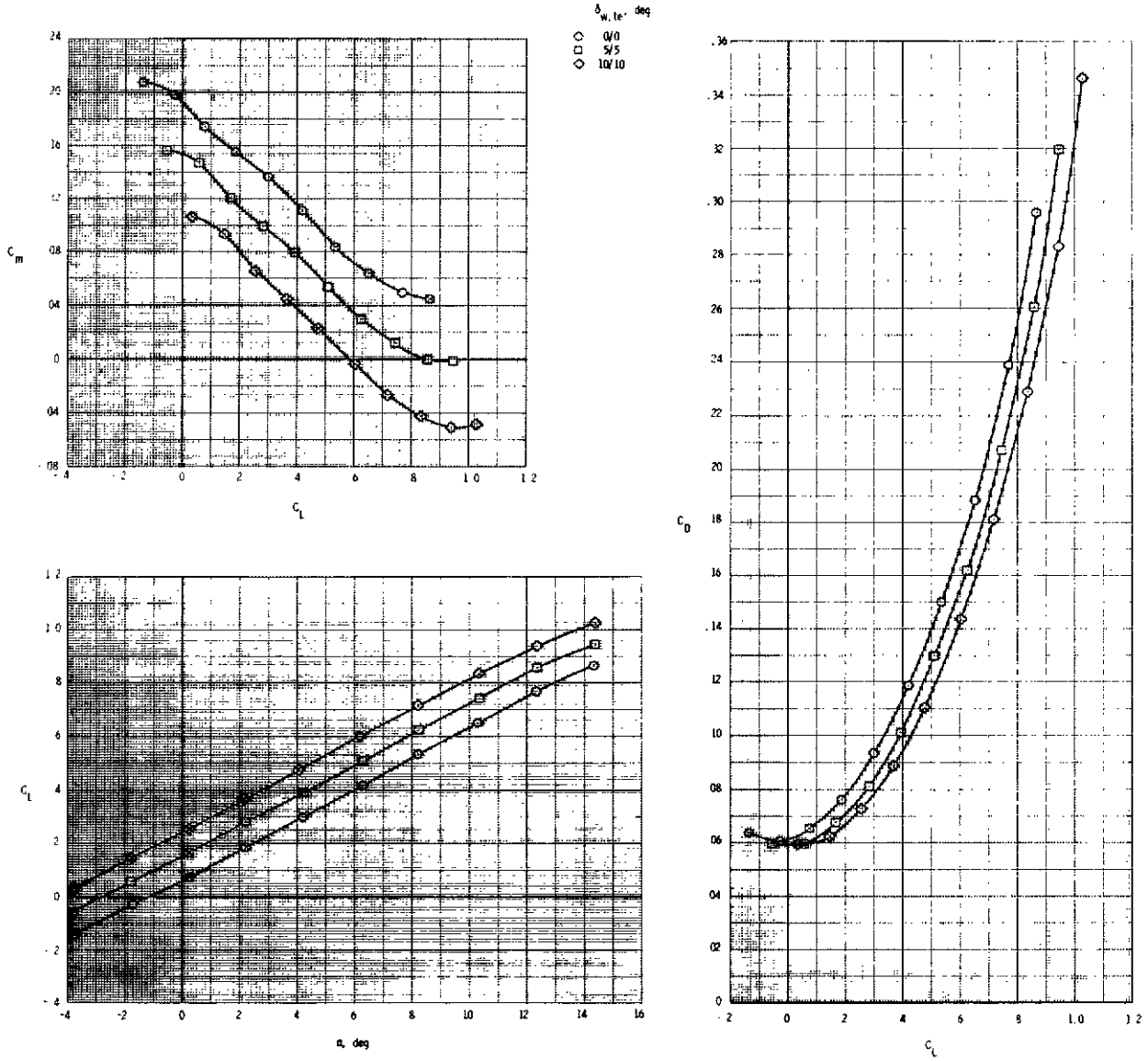

(a) M = 0.40.

Figure 11.- Effect of wing trailing-edge flap deflection on model longitudinal aerodynamic characteristics with canard on. $\delta_{w,le} = 0^o/5^o$; $\delta_c = 18^o$; $\delta_{c,le} = \delta_{c,te} = 15^o$; vertical tails and ventrals on.

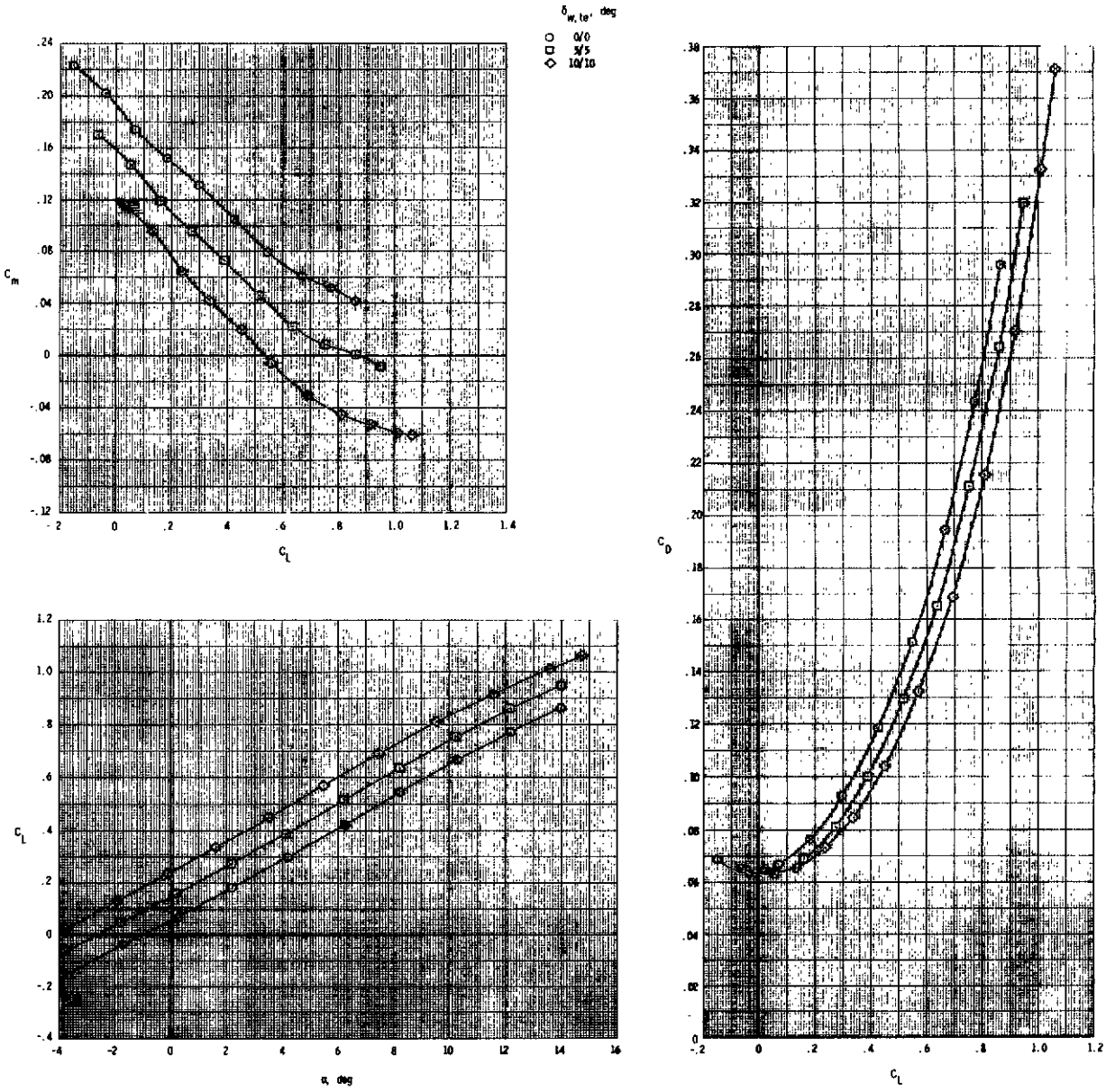

(b) M = 0.60.

Figure 11.- Continued.

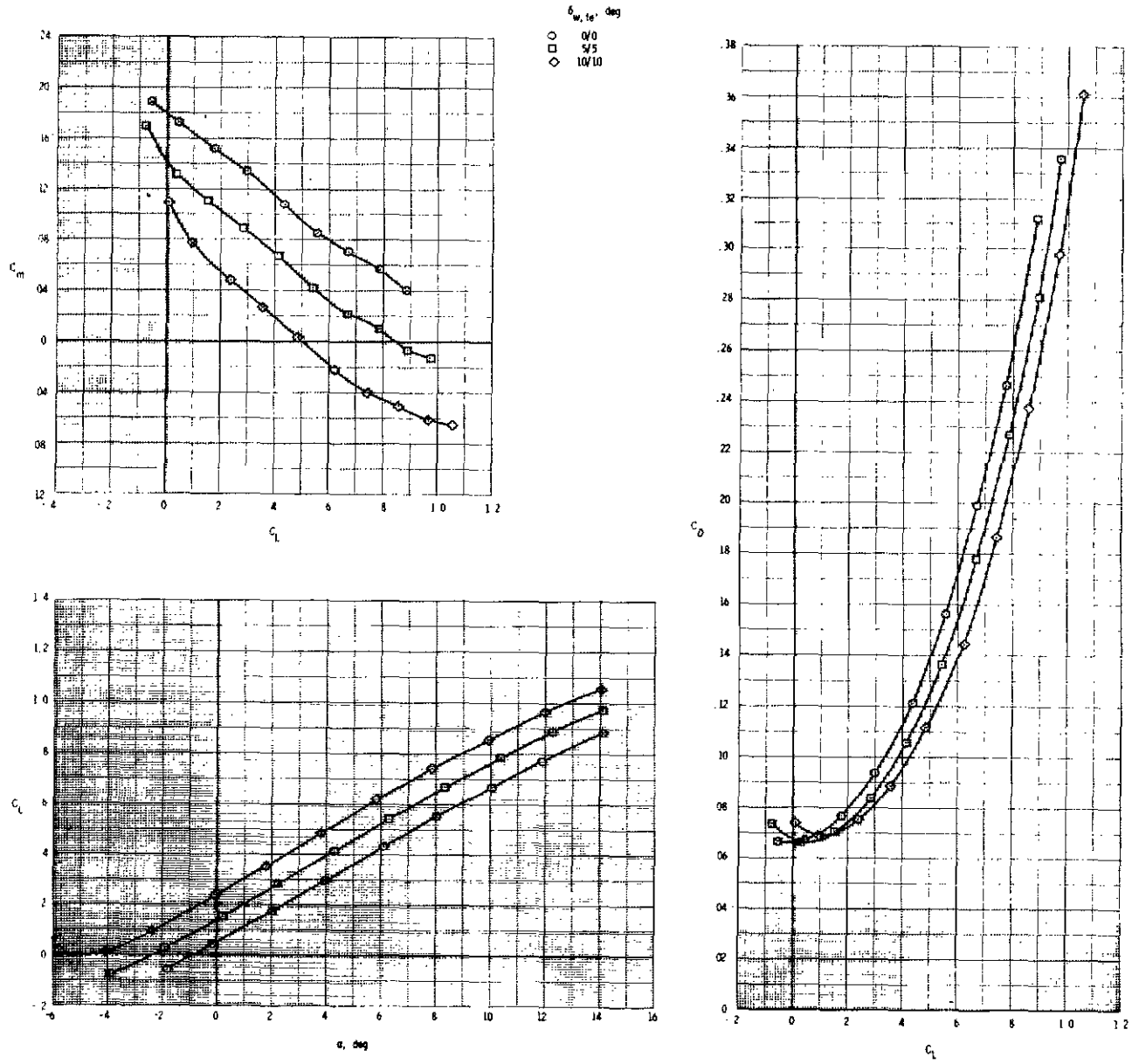

(c) M = 0.80.

Figure 11.- Continued.

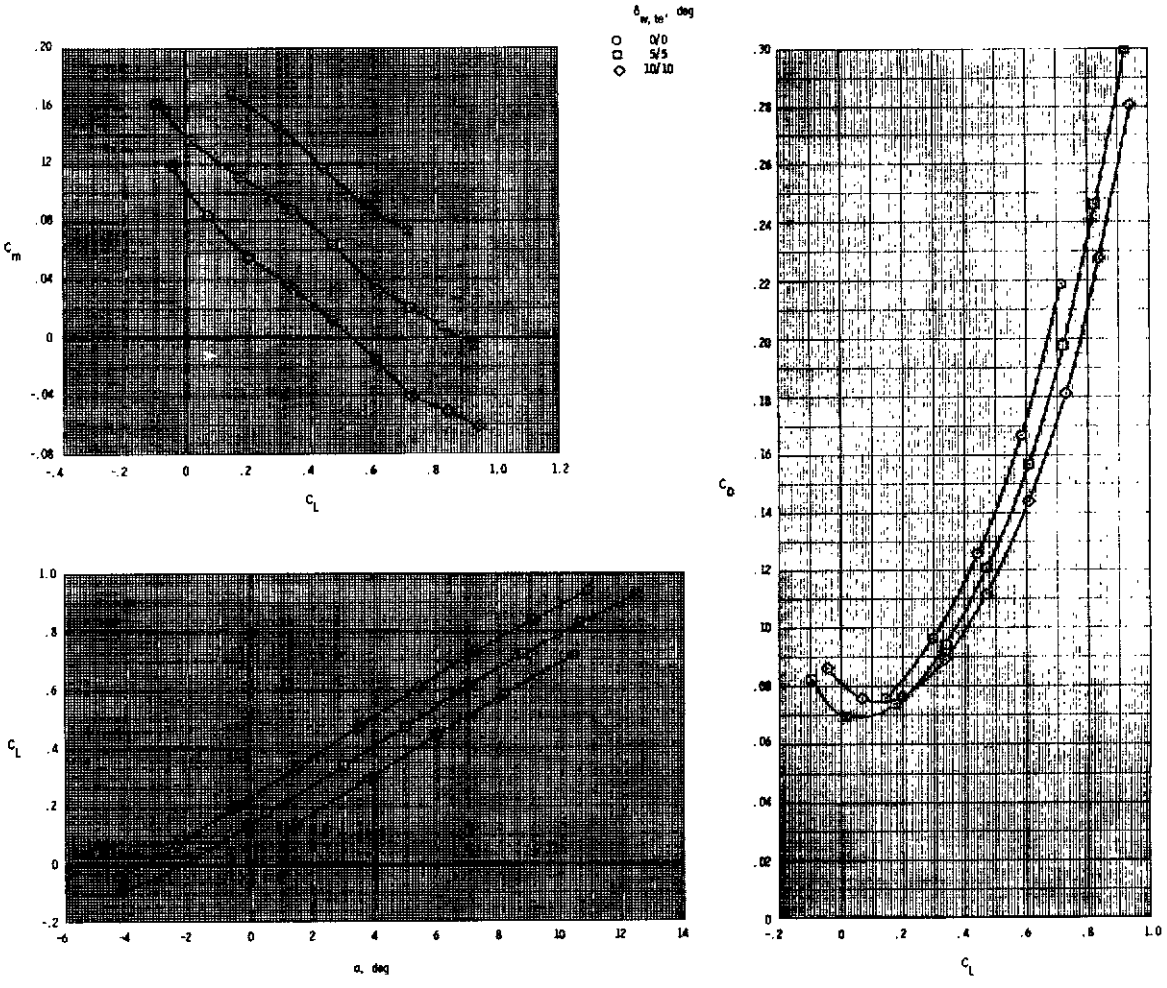

(d) M = 0.90.

Figure 11.- Concluded.

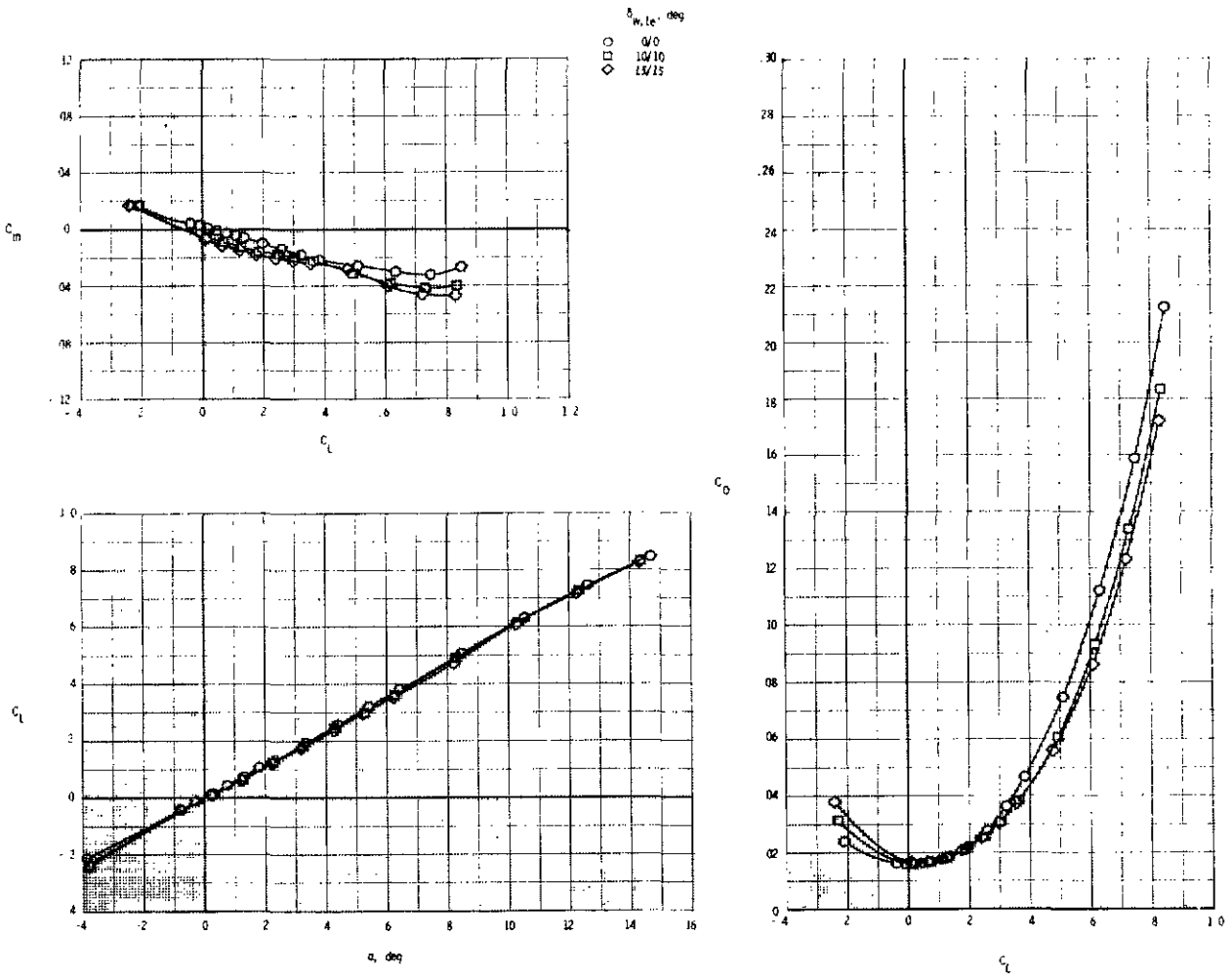

(a) M = 0.40.

Figure 12.- Effect of wing leading-edge flap deflection on model longitudinal aerodynamic characteristics with canard on. $\delta_{w,te} = 0^o/0^o$; $\delta_c = 0^o$; $\delta_{c,le} = \delta_{c,te} = 0^o$; vertical tails and ventrals on.

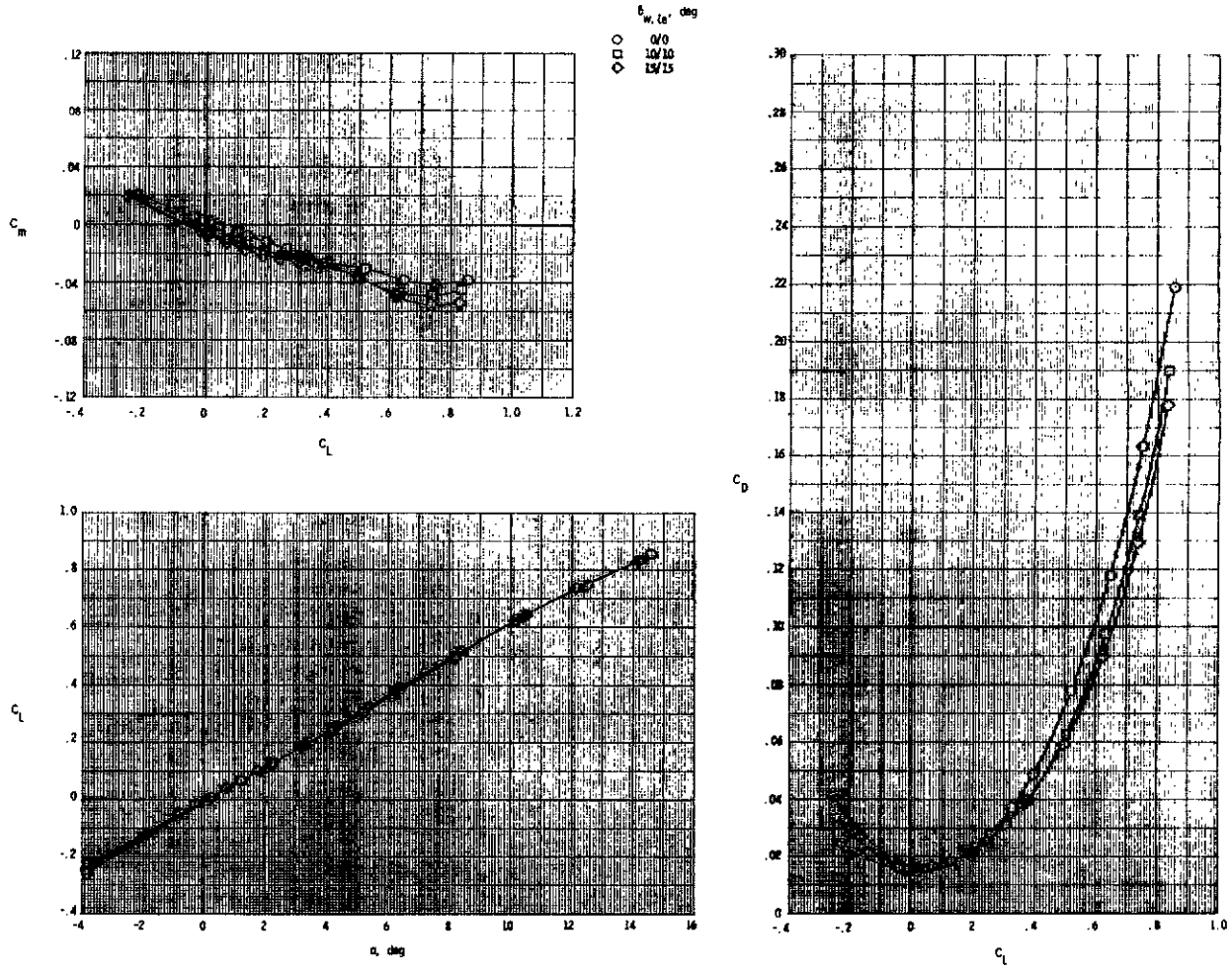

(b) M = 0.60.

Figure 12.- Continued.

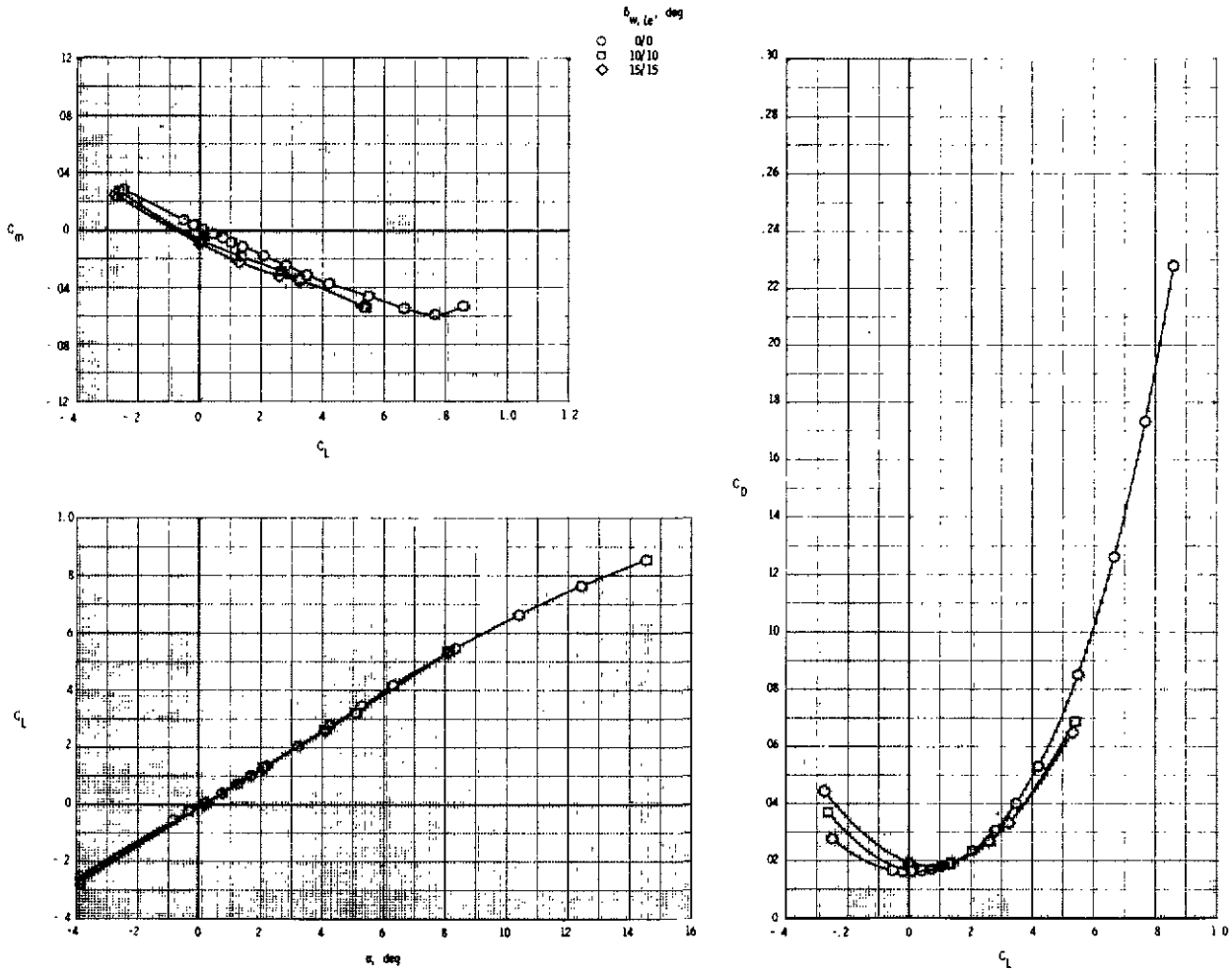

(c) M = 0.80.

Figure 12.- Continued.

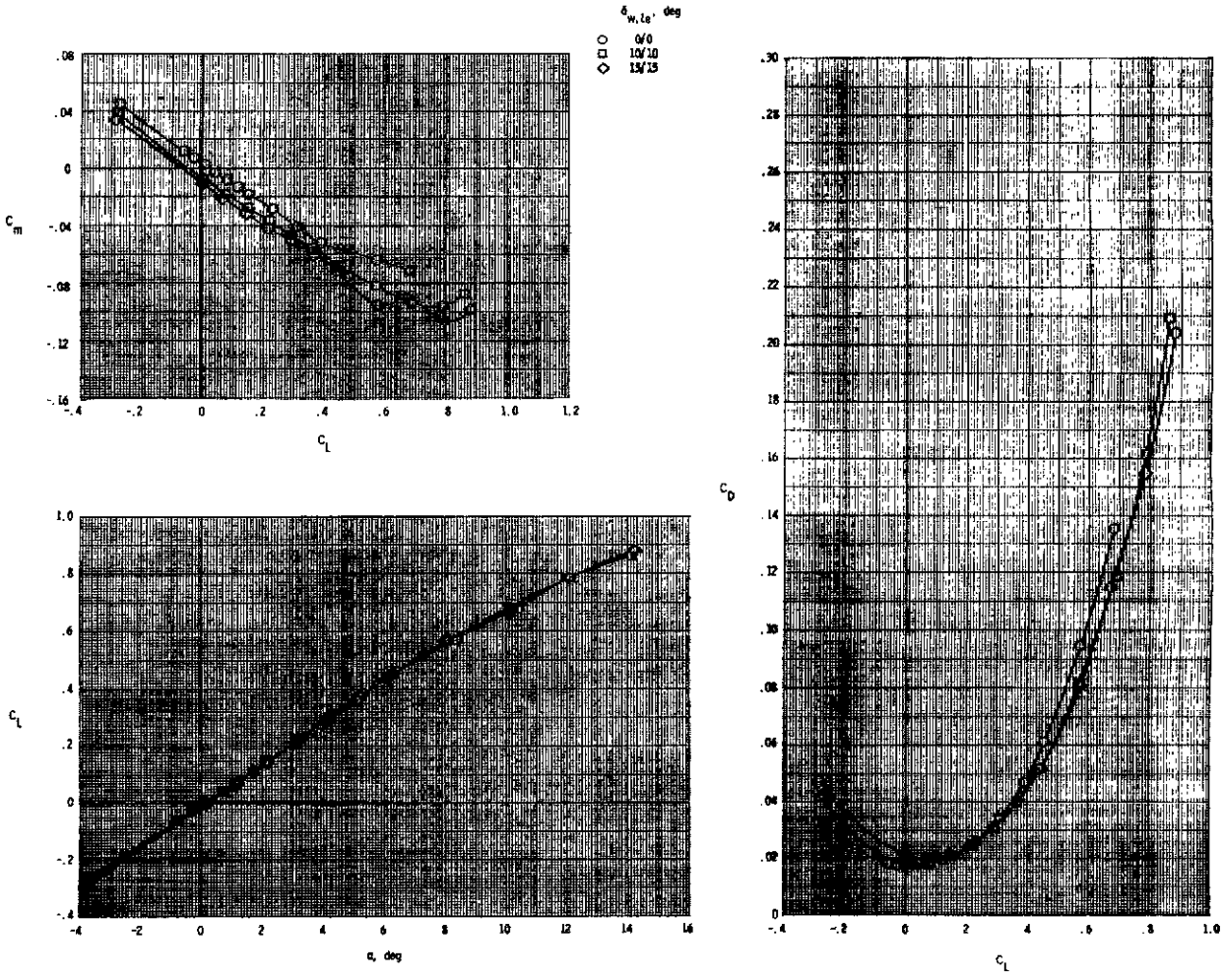

(d) M = 0.90.

Figure 12.- Concluded.

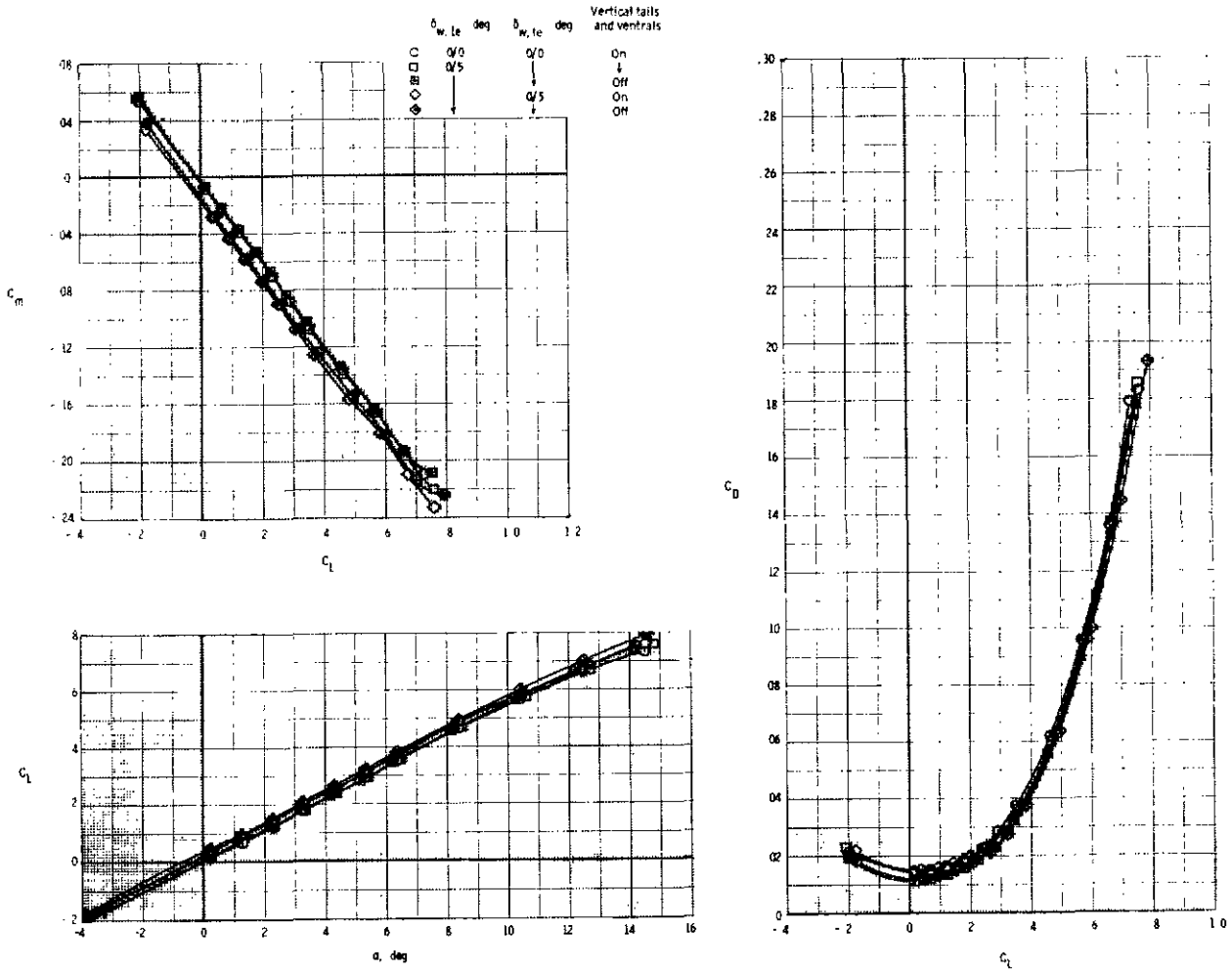

(a) M = 0.40.

Figure 13.- Effect of wing outboard leading- and trailing-edge flap deflections and vertical surfaces on model longitudinal aerodynamic characteristics with canard off.

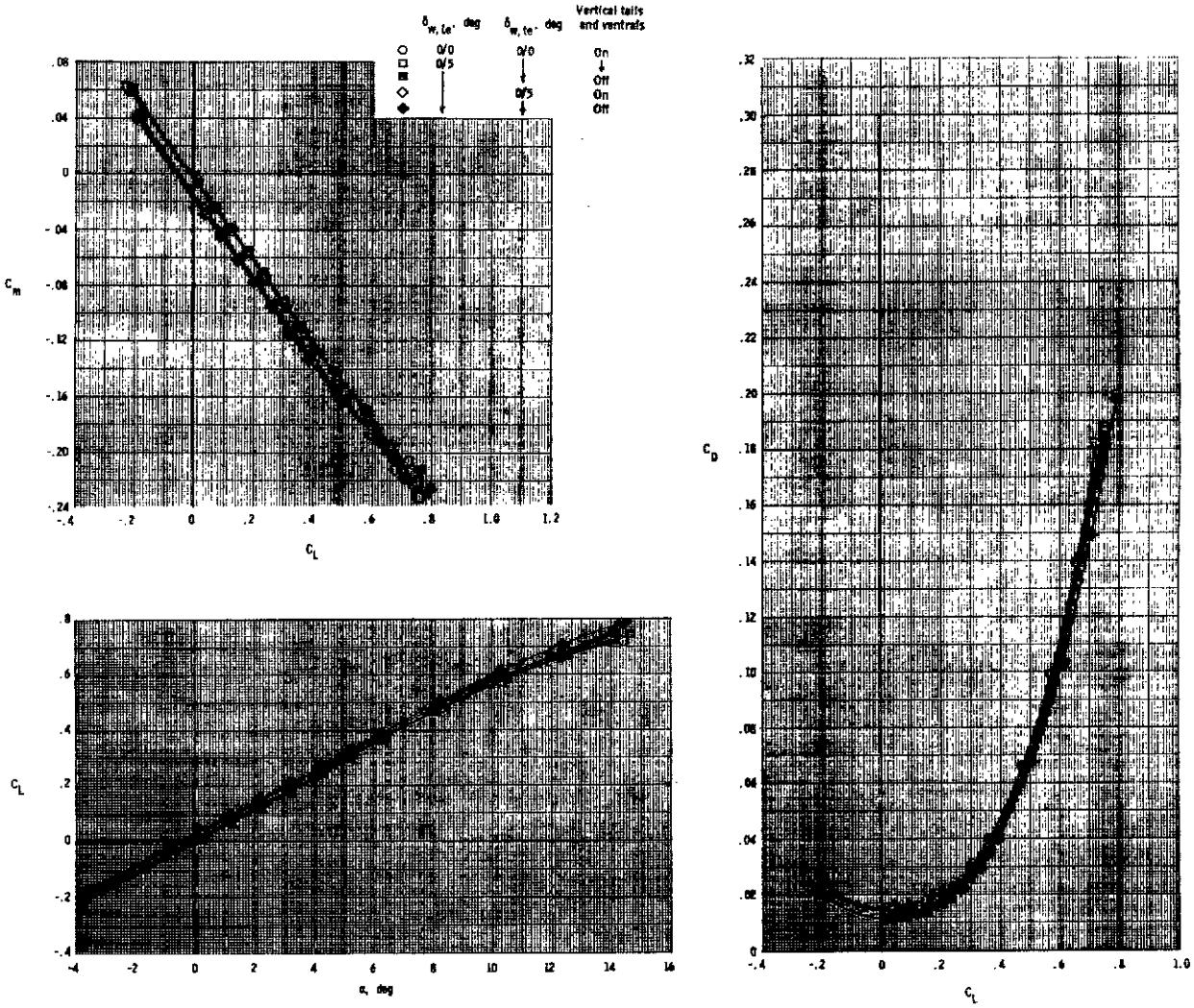

(b) M = 0.60.

Figure 13.- Continued.

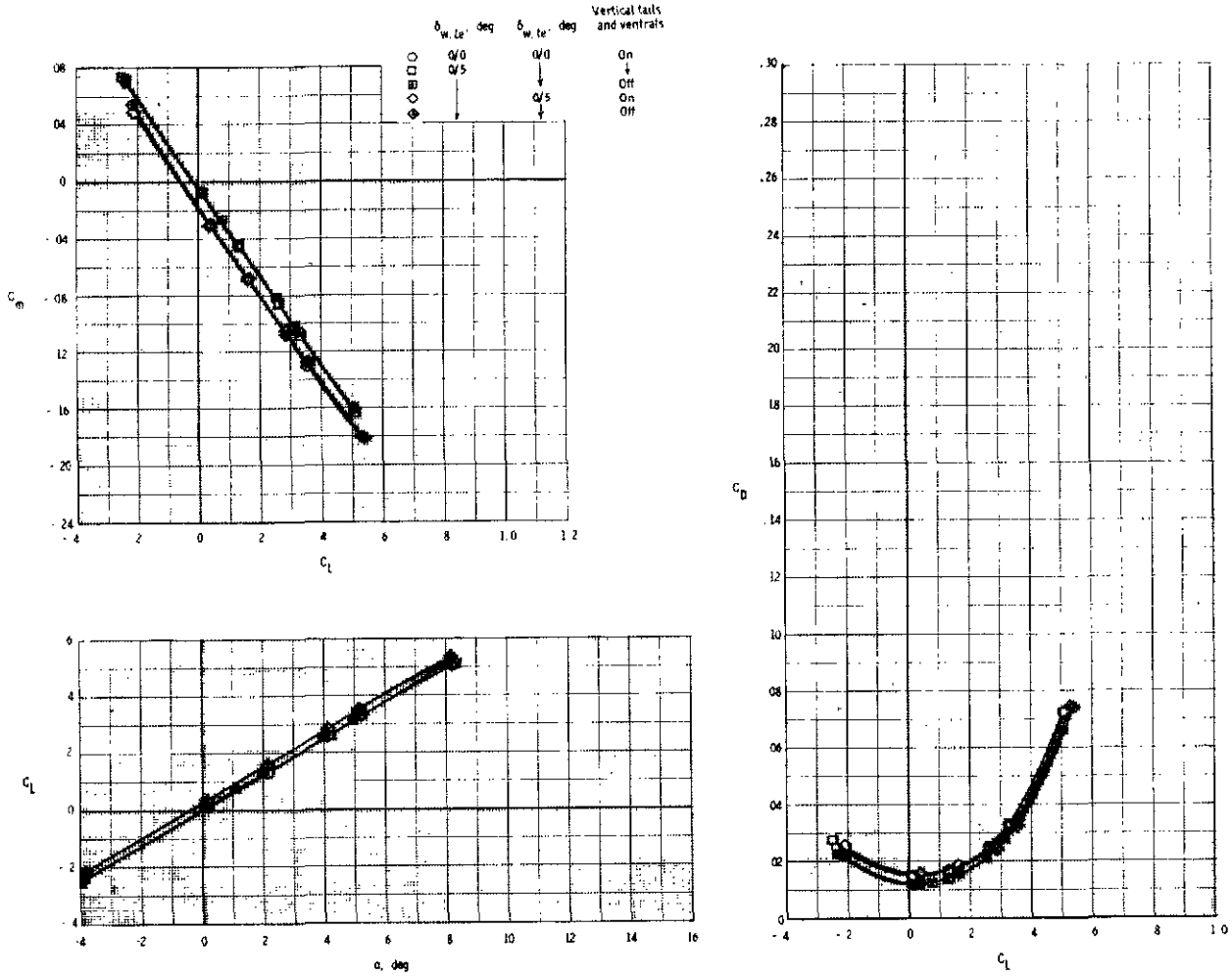

(c) M = 0.80.

Figure 13.- Continued.

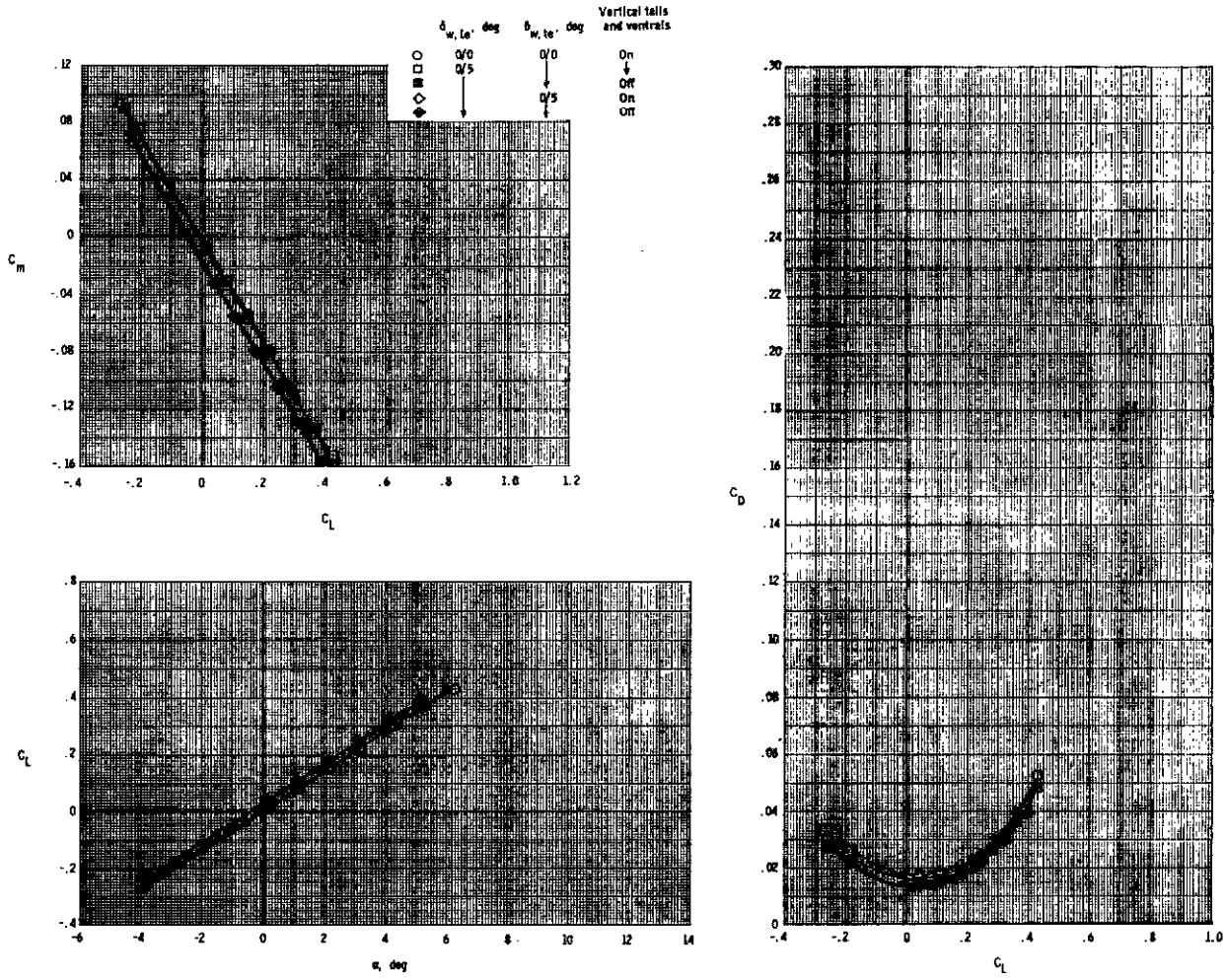

(d) M = 0.90.

Figure 13.- Concluded.

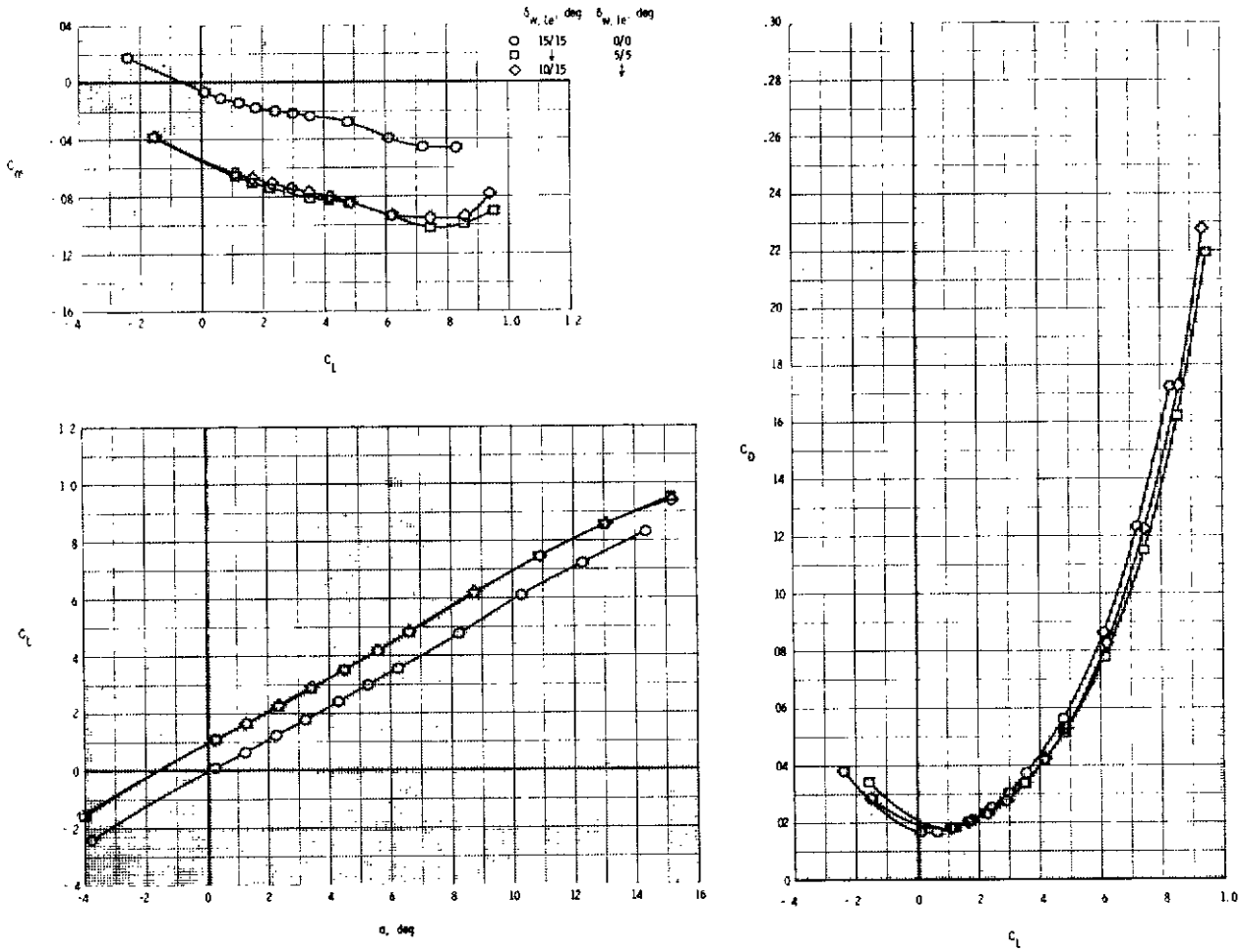

(a) M = 0.40.

Figure 14.- Effect of wing trailing-edge flap deflection and wing inboard leading-edge flap deflection on model longitudinal aerodynamic characteristics with canard on. $\delta_C = 0^O$; $\delta_{C,le} = \delta_{C,te} = 0^O$; vertical tails and ventrals on.

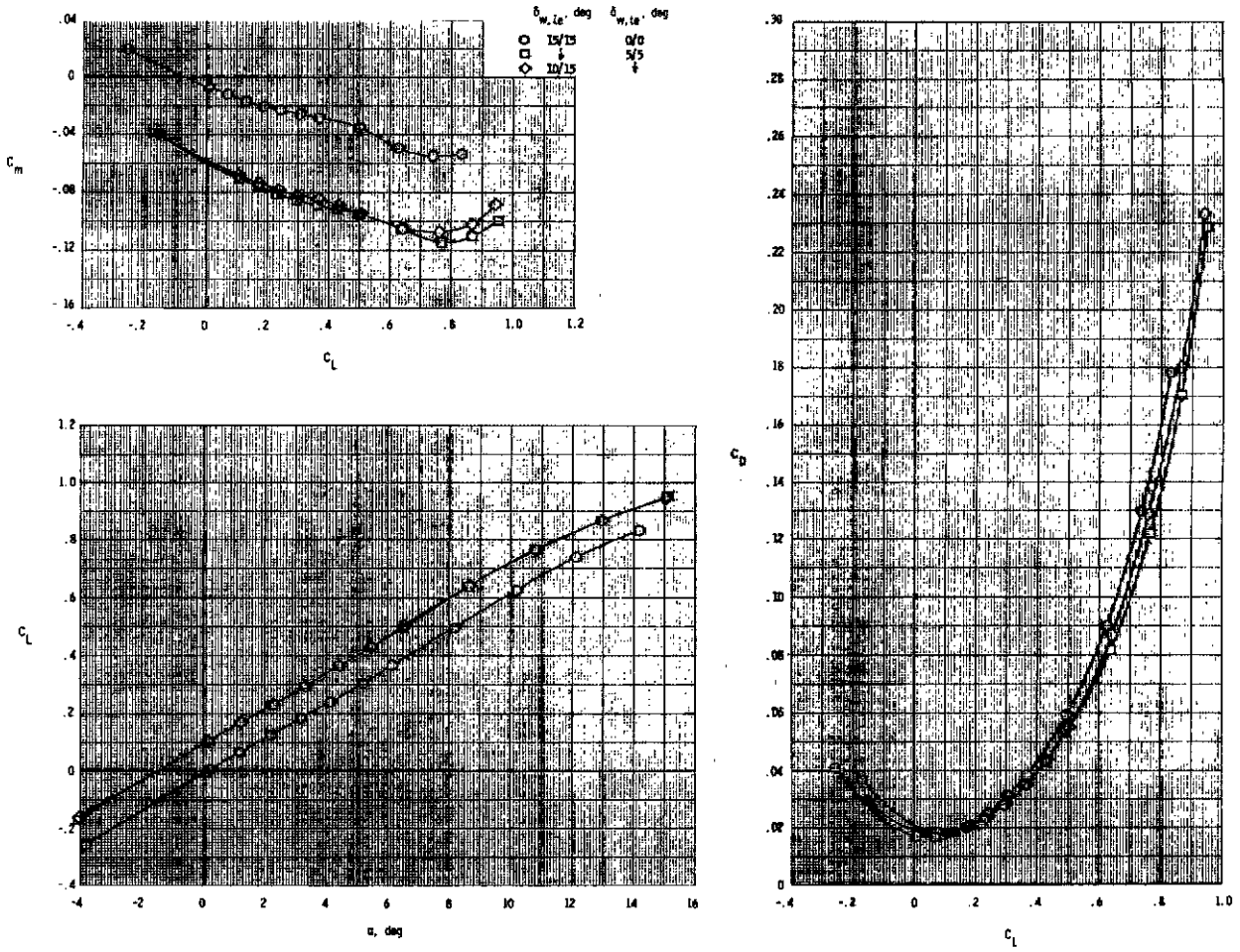

(b) M = 0.60.

Figure 14.- Continued.

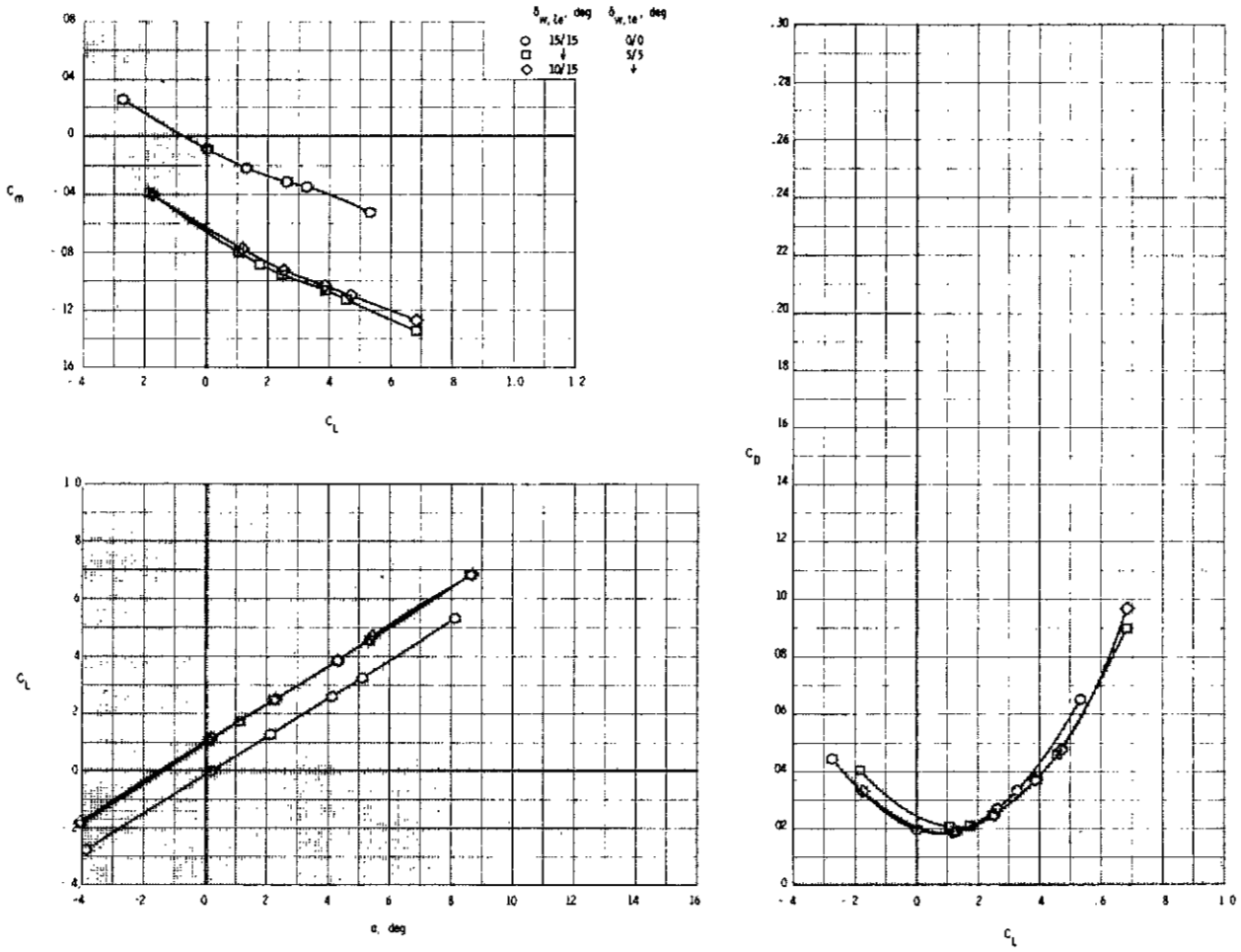

(c) M = 0.80.

Figure 14.- Continued.

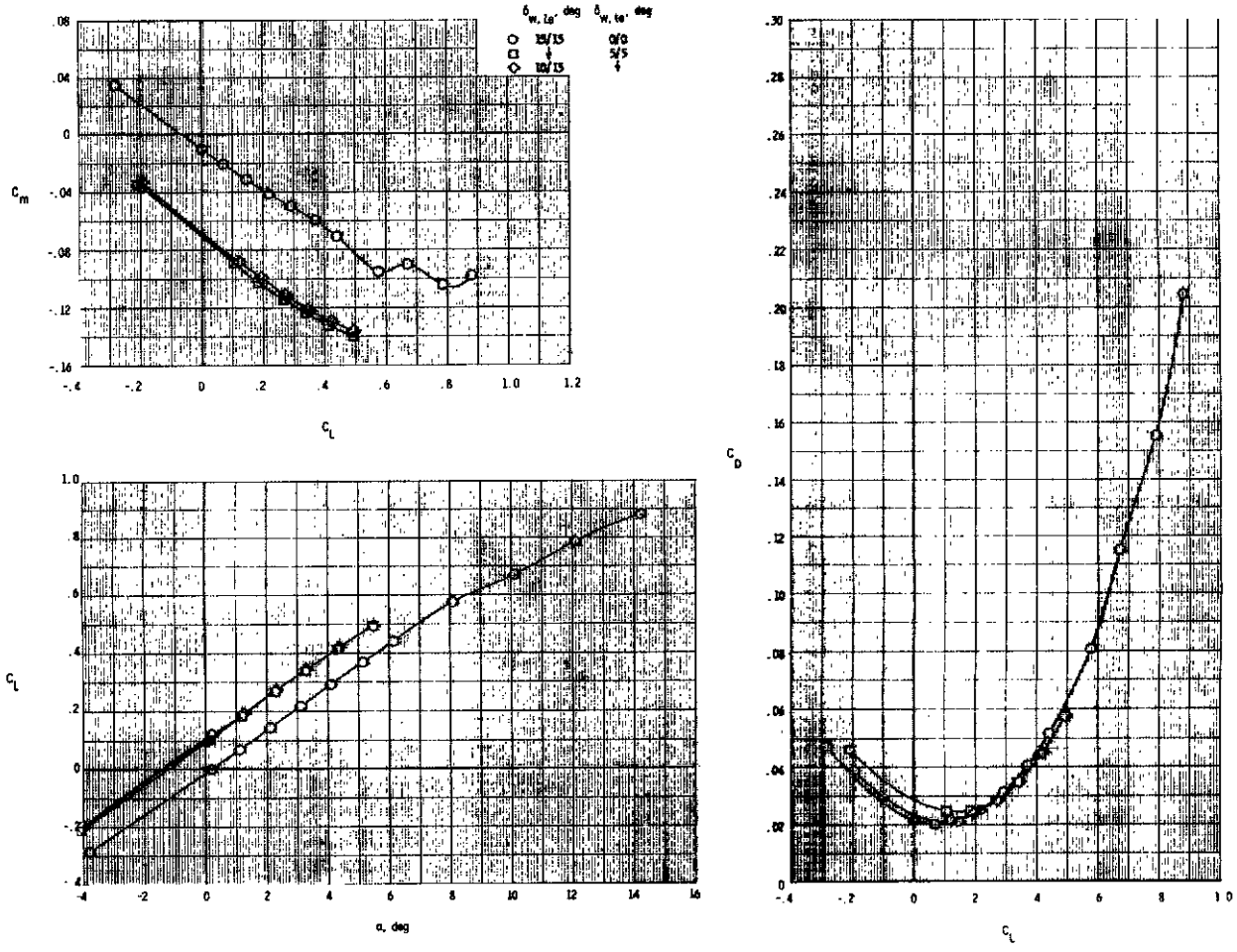

(d) M = 0.90.

Figure 14.- Concluded.

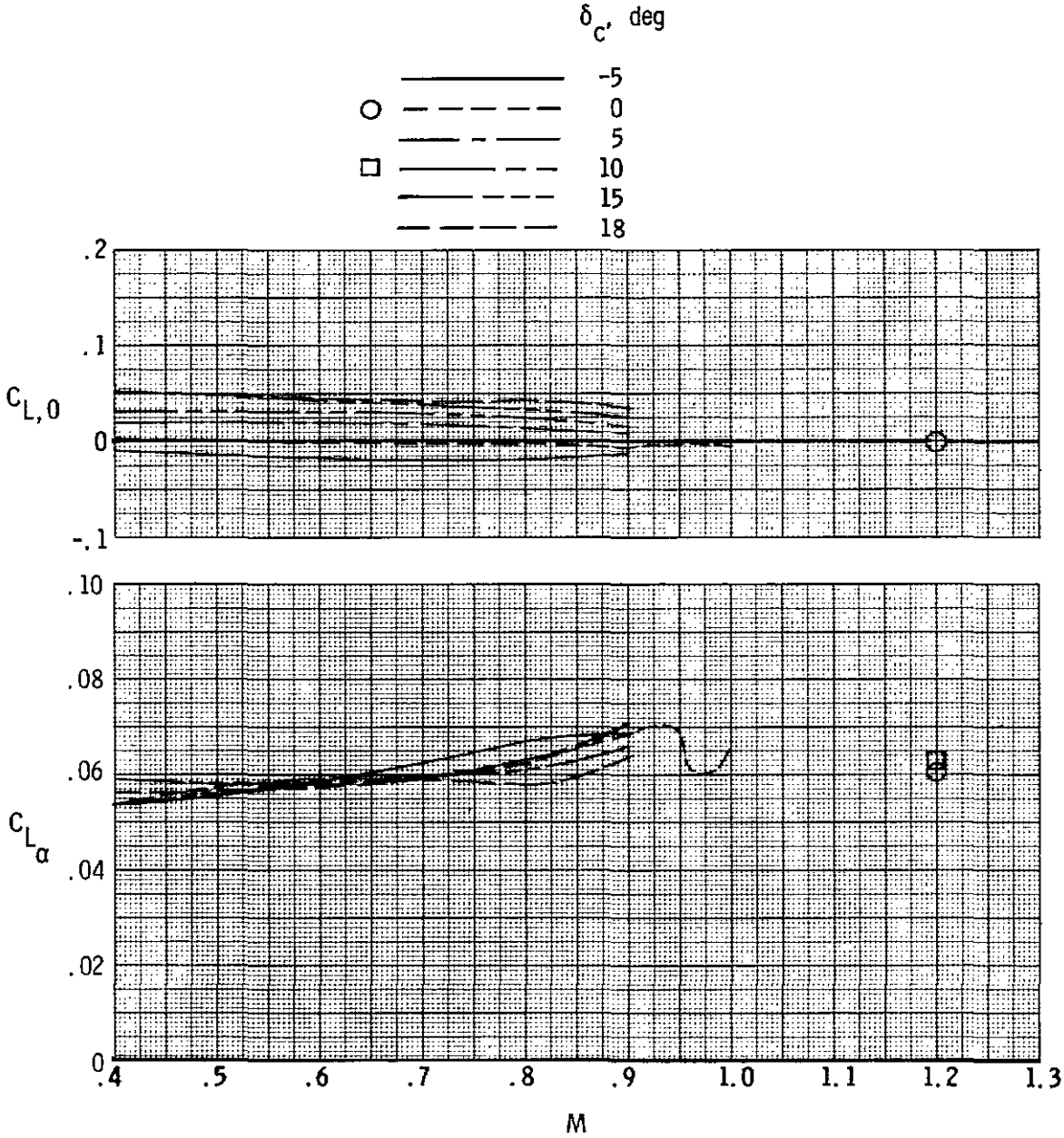

(a) $C_{L,0}$ and C_{L_α}.

Figure 15.- Effect of canard incidence on model longitudinal aerodynamic parameters. $\delta_{w,le} = \delta_{w,te} = 0^o/0^o$; $\delta_{c,le} = \delta_{c,te} = 0^o$; vertical tails and ventrals on.

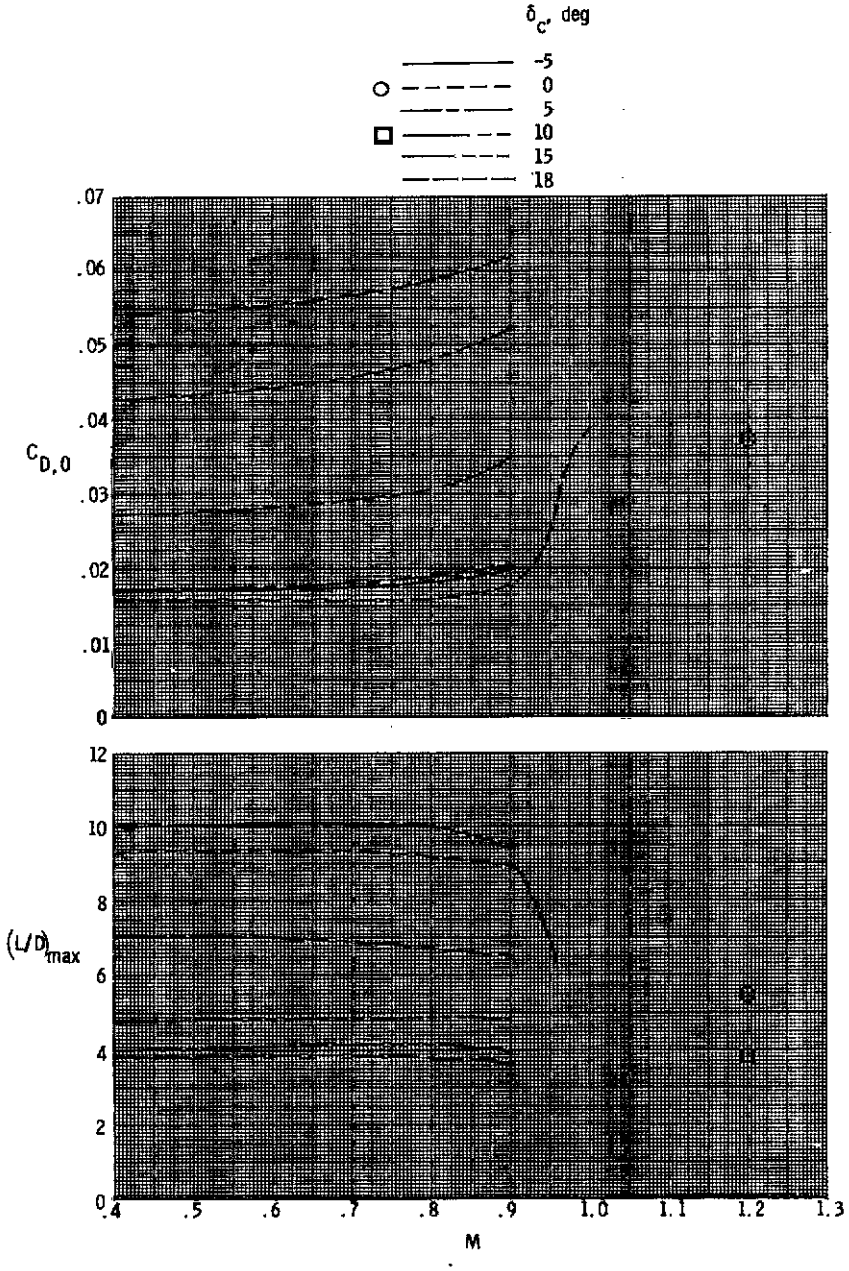

(b) $C_{D,0}$ and $(L/D)_{max}$.

Figure 15.- Continued.

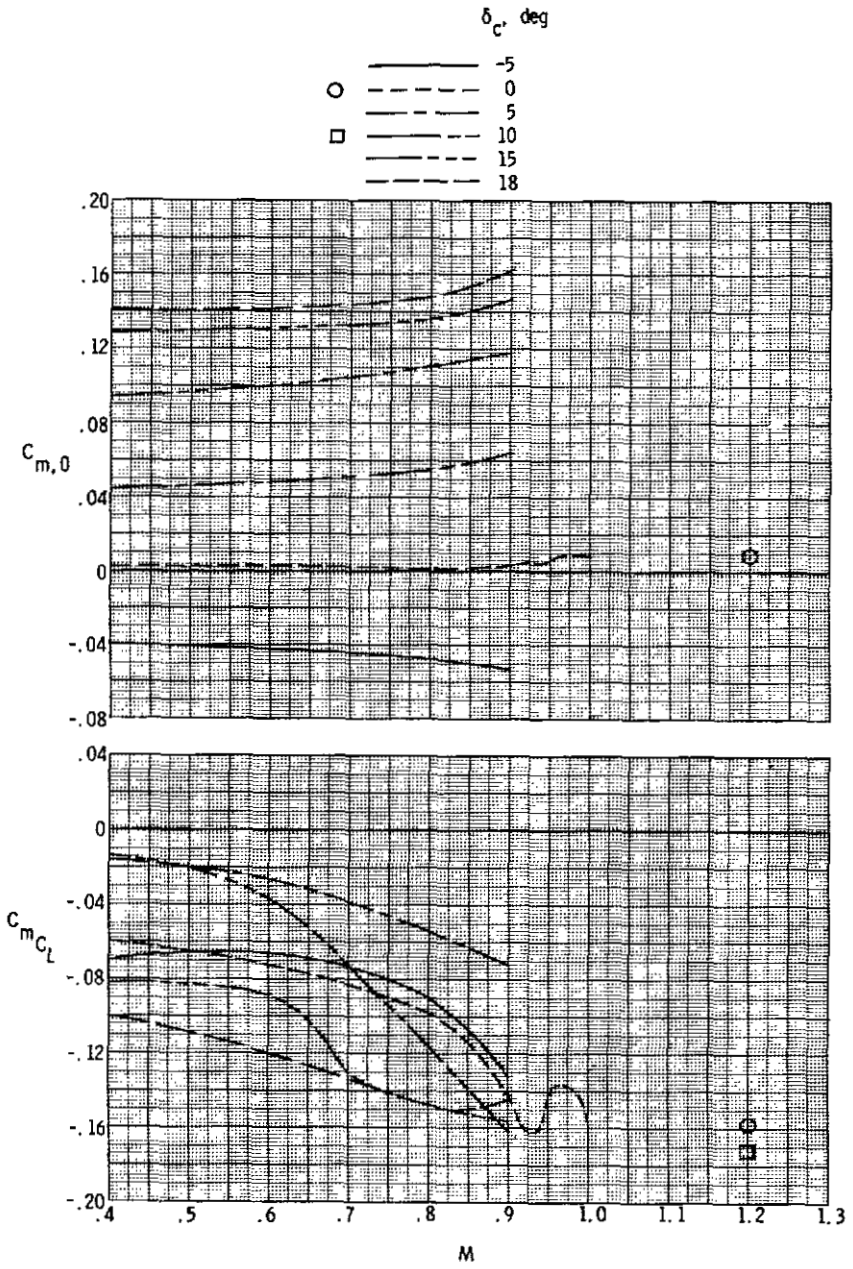

(c) $C_{m,0}$ and $C_{m_{C_L}}$.

Figure 15.- Continued.

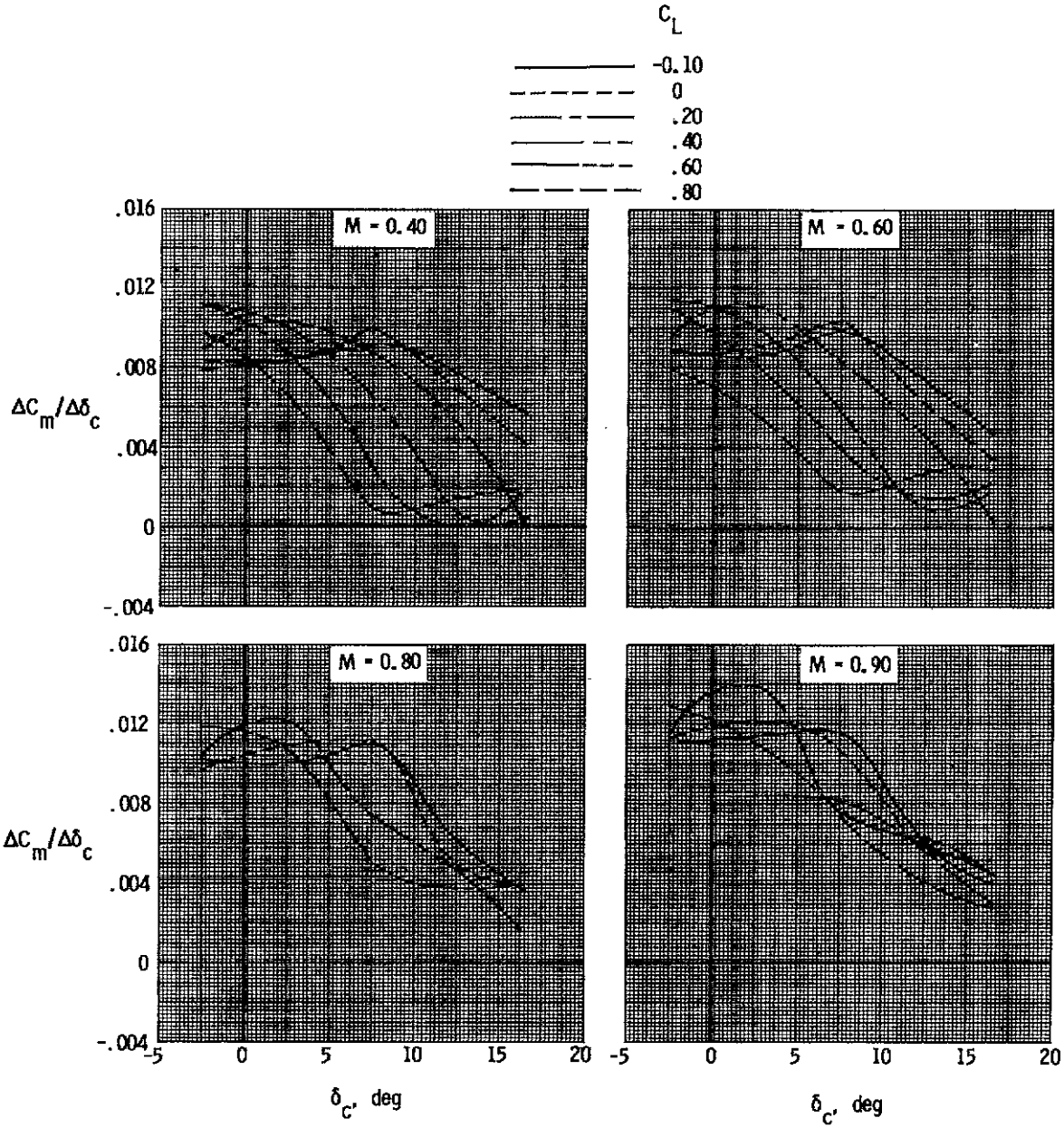

(d) $\Delta C_m/\Delta\delta_c$.

Figure 15.- Concluded.

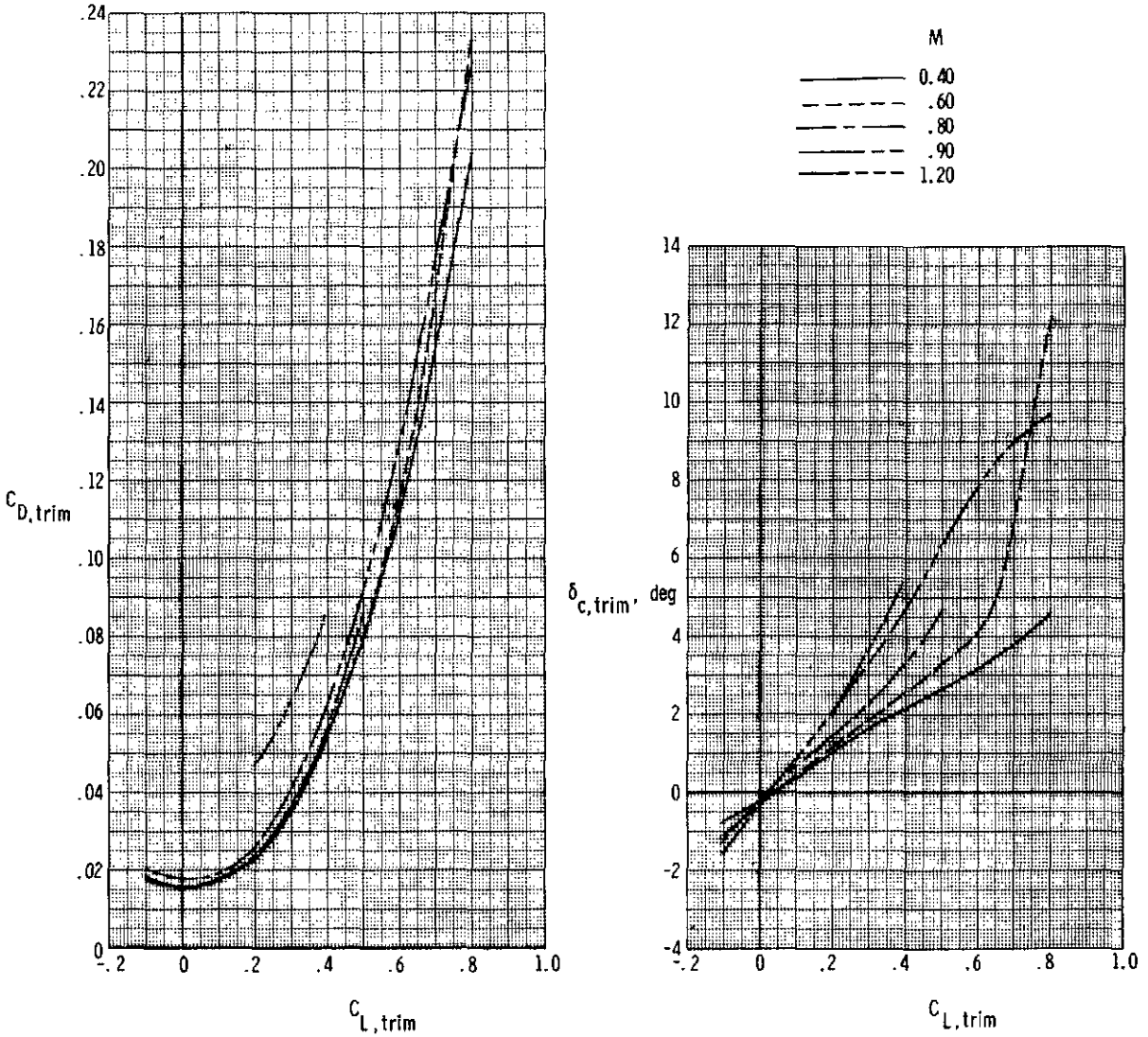

(a) $C_{D,trim}$ and $\delta_{c,trim}$.

Figure 16.- Trimmed model characteristics with canard as trimming surface. $\delta_{w,le} = \delta_{w,te} = 0^o/0^o$; $\delta_{c,le} = \delta_{c,te} = 0^o$; vertical tails and ventrals on.

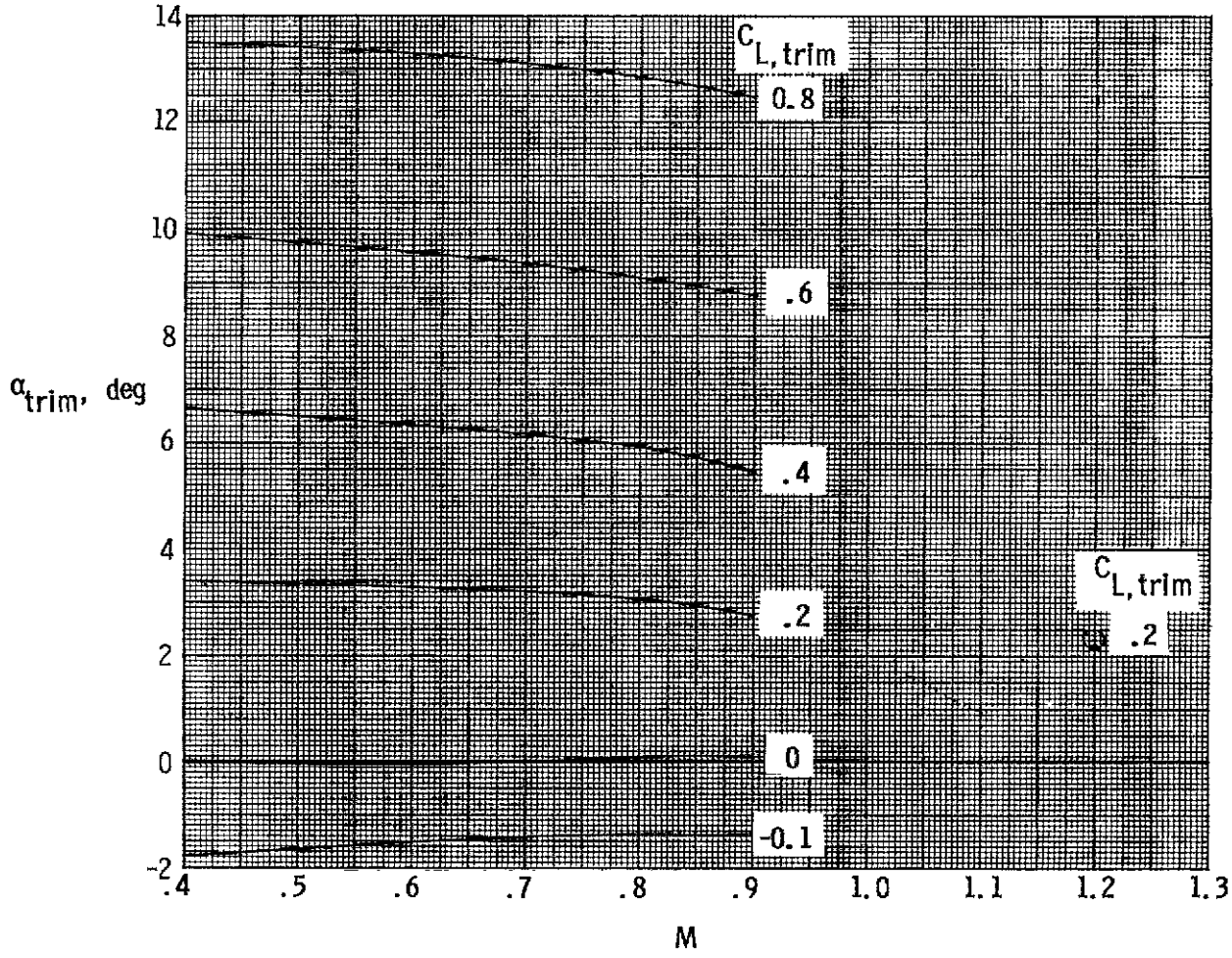

(b) α_{trim}.

Figure 16.- Continued.

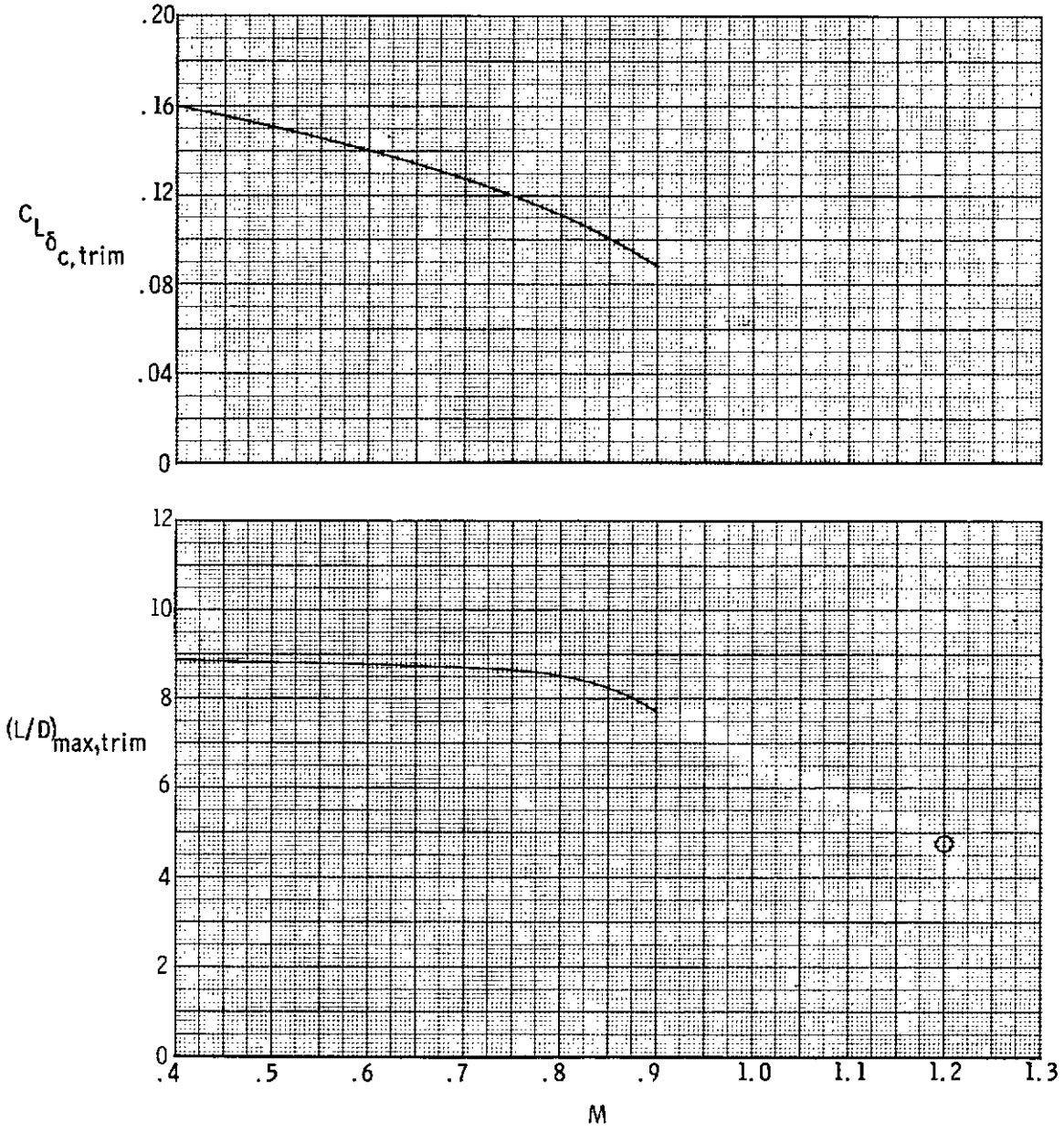

(c) $C_{L_{\delta_{c,trim}}}$ and $(L/D)_{max,trim}$.

Figure 16.- Concluded.

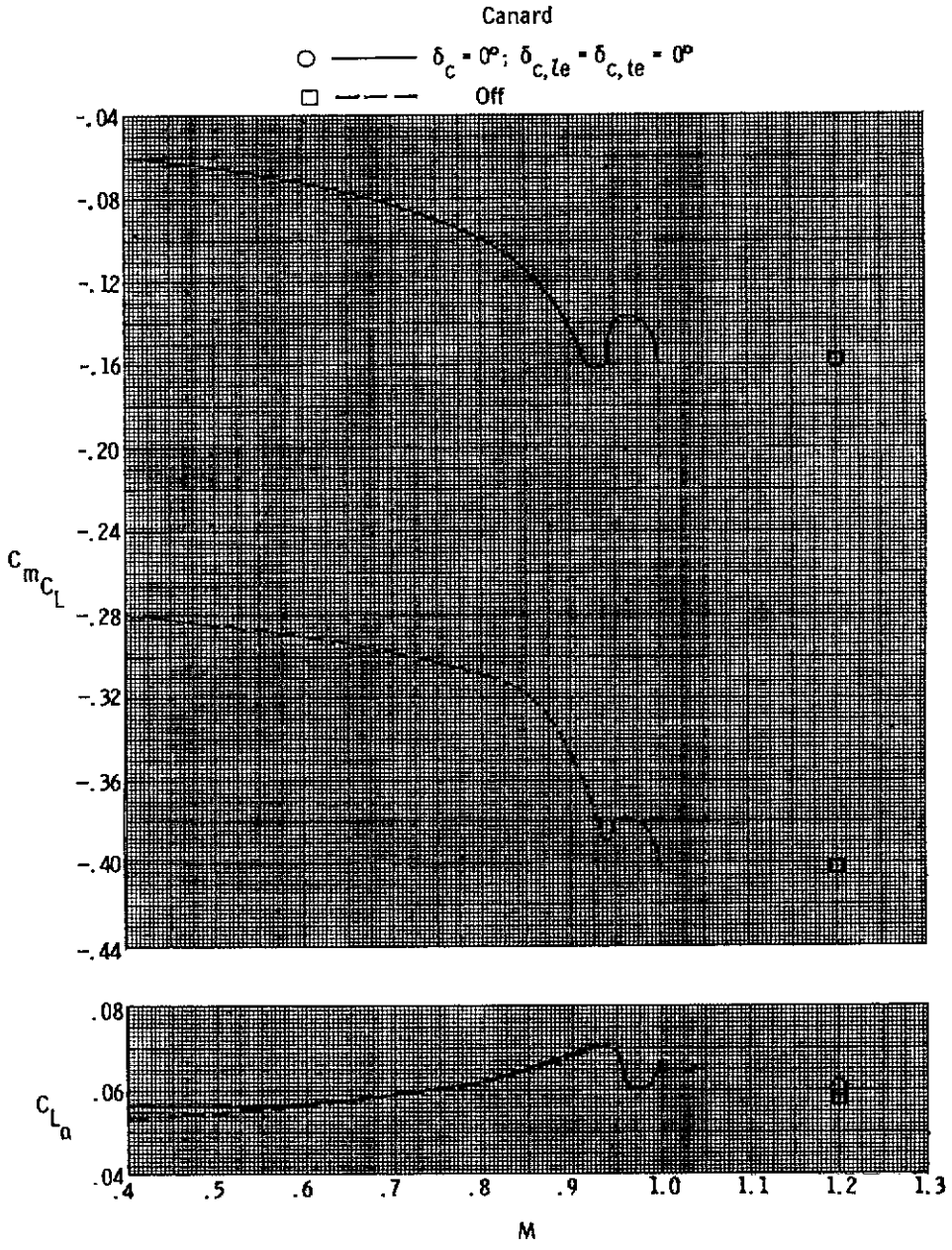

(a) Cm_{C_L} and C_{L_α} for $\delta_{w,te} = 0^o/0^o$.

Figure 17.- Effect of wing trailing-edge flap deflection on model longitudinal aerodynamic parameters with canard on and off. $\delta_{w,le} = 0^o/0^o$; vertical tails and ventrals on.

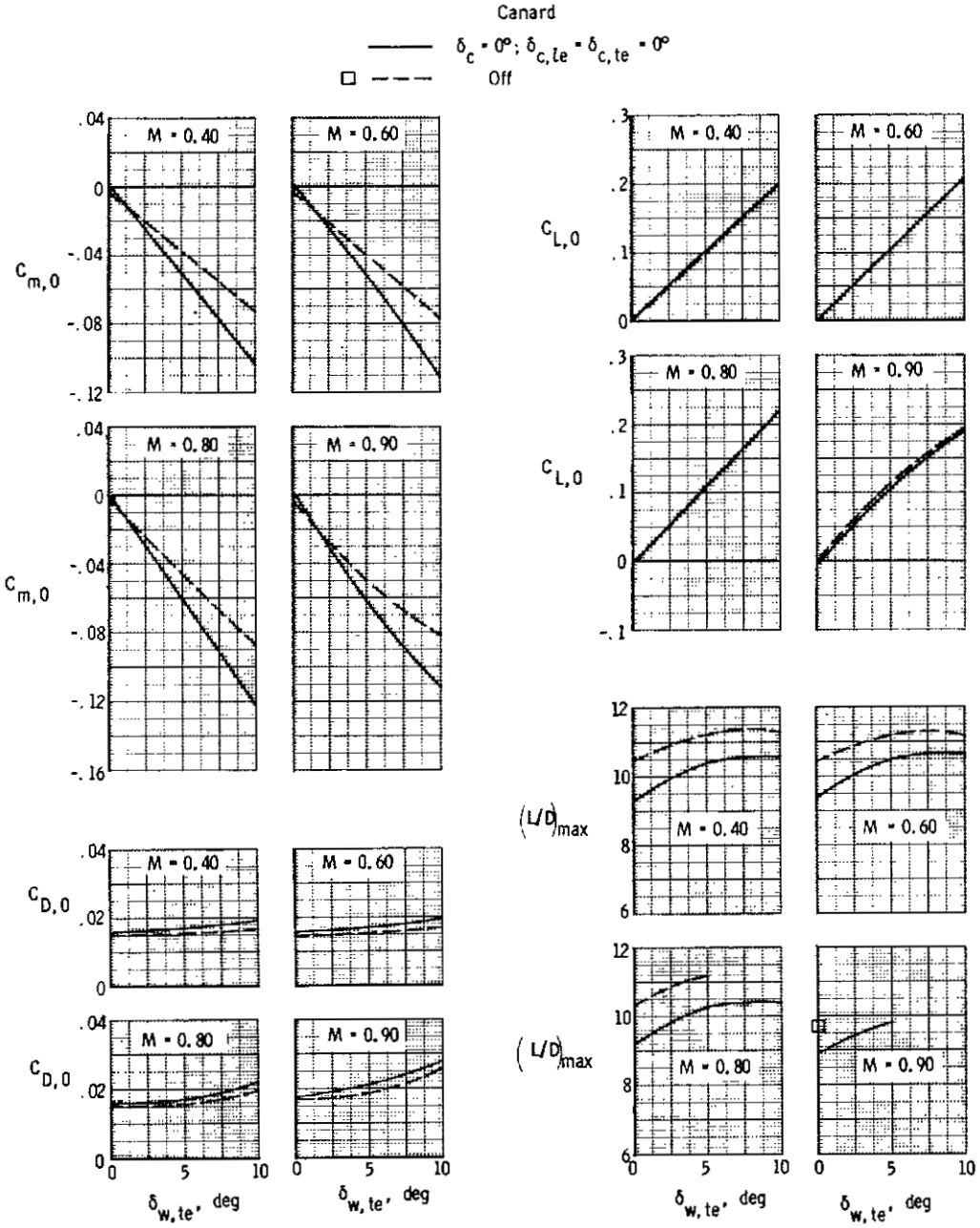

(b) $C_{m,0}$, $C_{L,0}$, $C_{D,0}$, and $(L/D)_{max}$.

Figure 17.- Continued.

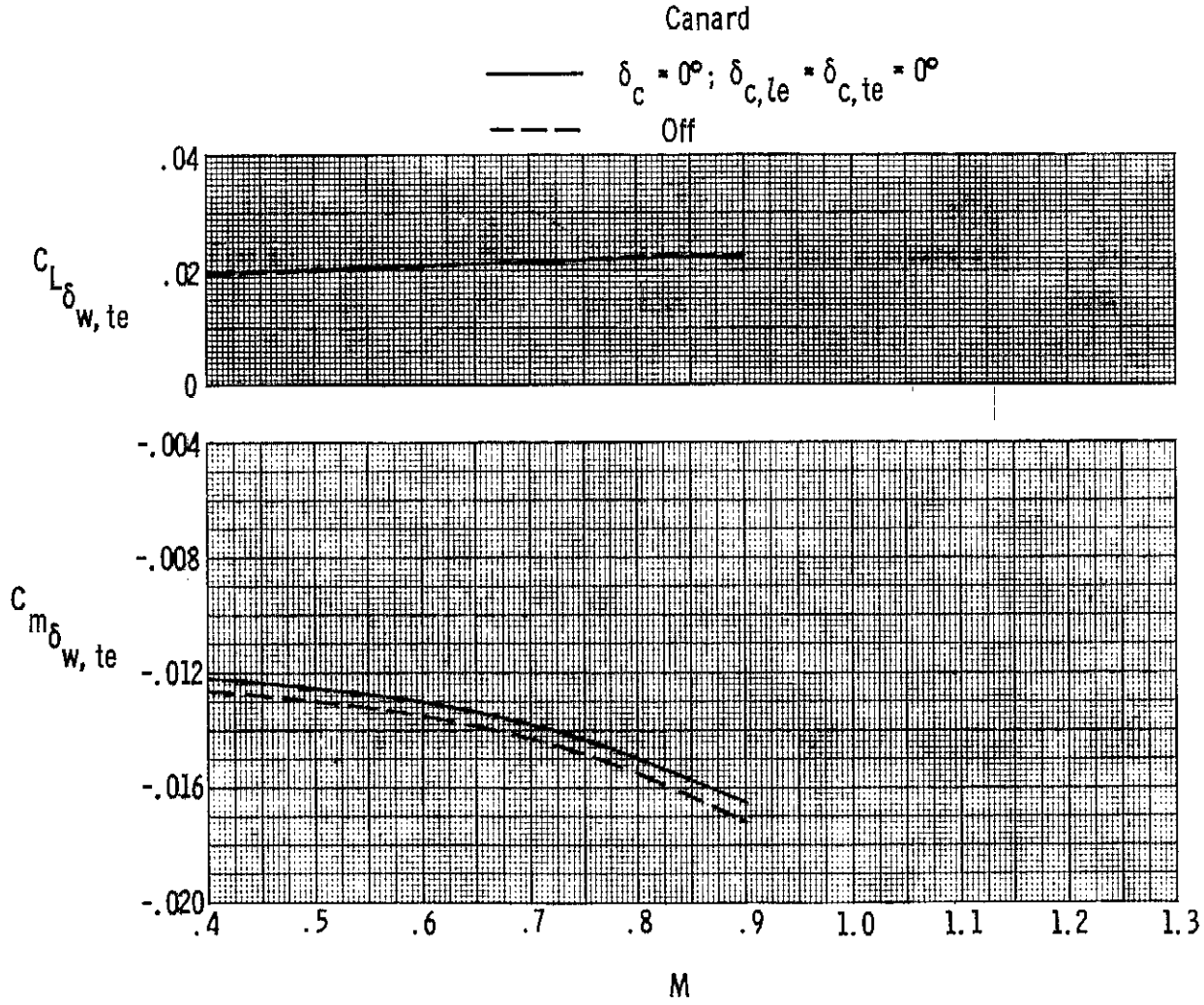

(c) $C_{L_{\delta_{w,te}}}$ and $C_{m_{\delta_{w,te}}}$.

Figure 17.- Concluded.

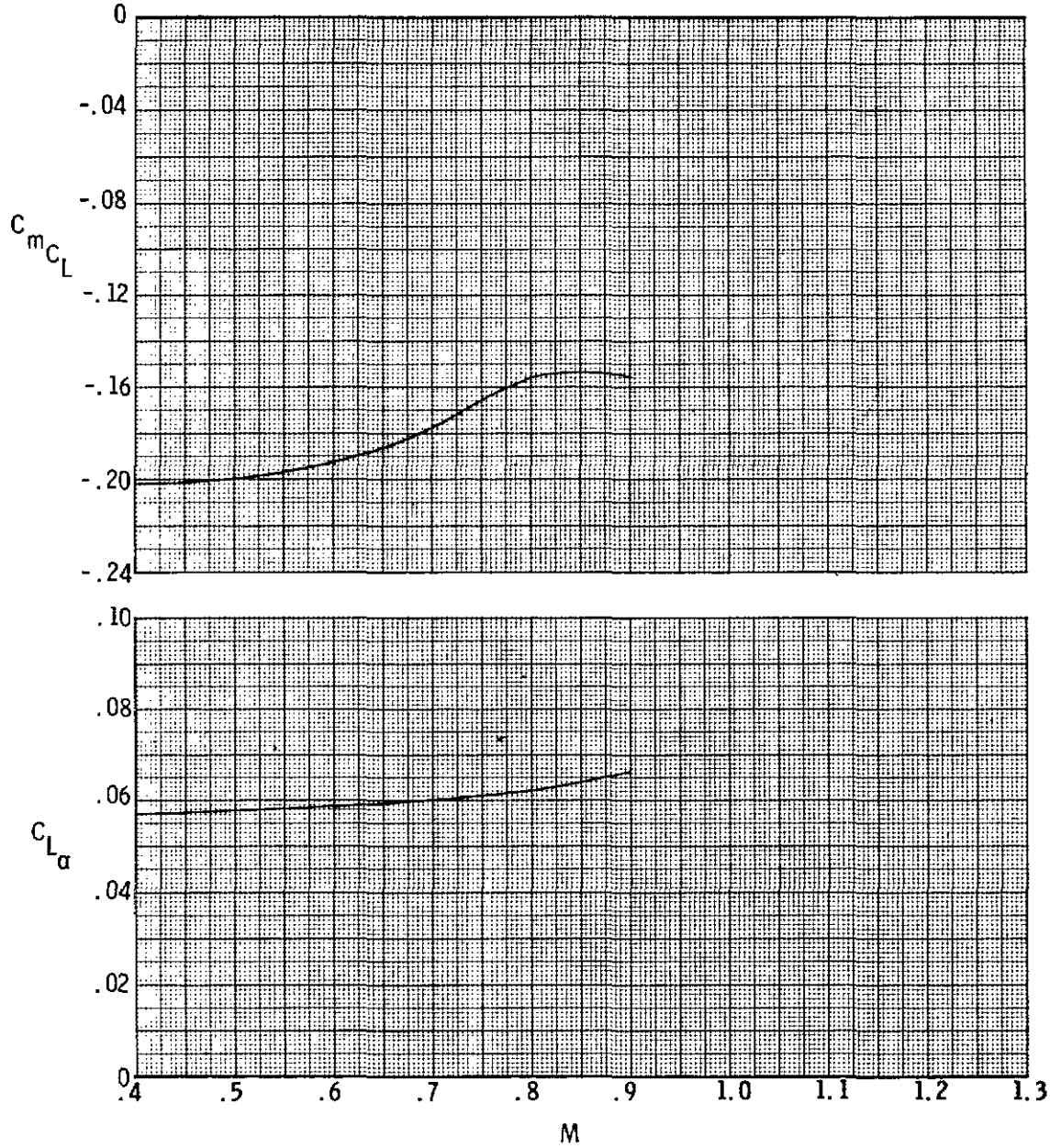

(a) $C_{m_{C_L}}$ and C_{L_α} for $\delta_{w,te} = 0^o/0^o$.

Figure 18.- Effect of wing trailing-edge flap deflection and free-stream Mach number on model longitudinal aerodynamic parameters with $\delta_c = 18^o$ and $\delta_{c,le} = \delta_{c,te} = 15^o$. $\delta_{w,le} = 0^o/5^o$; vertical tails and ventrals on.

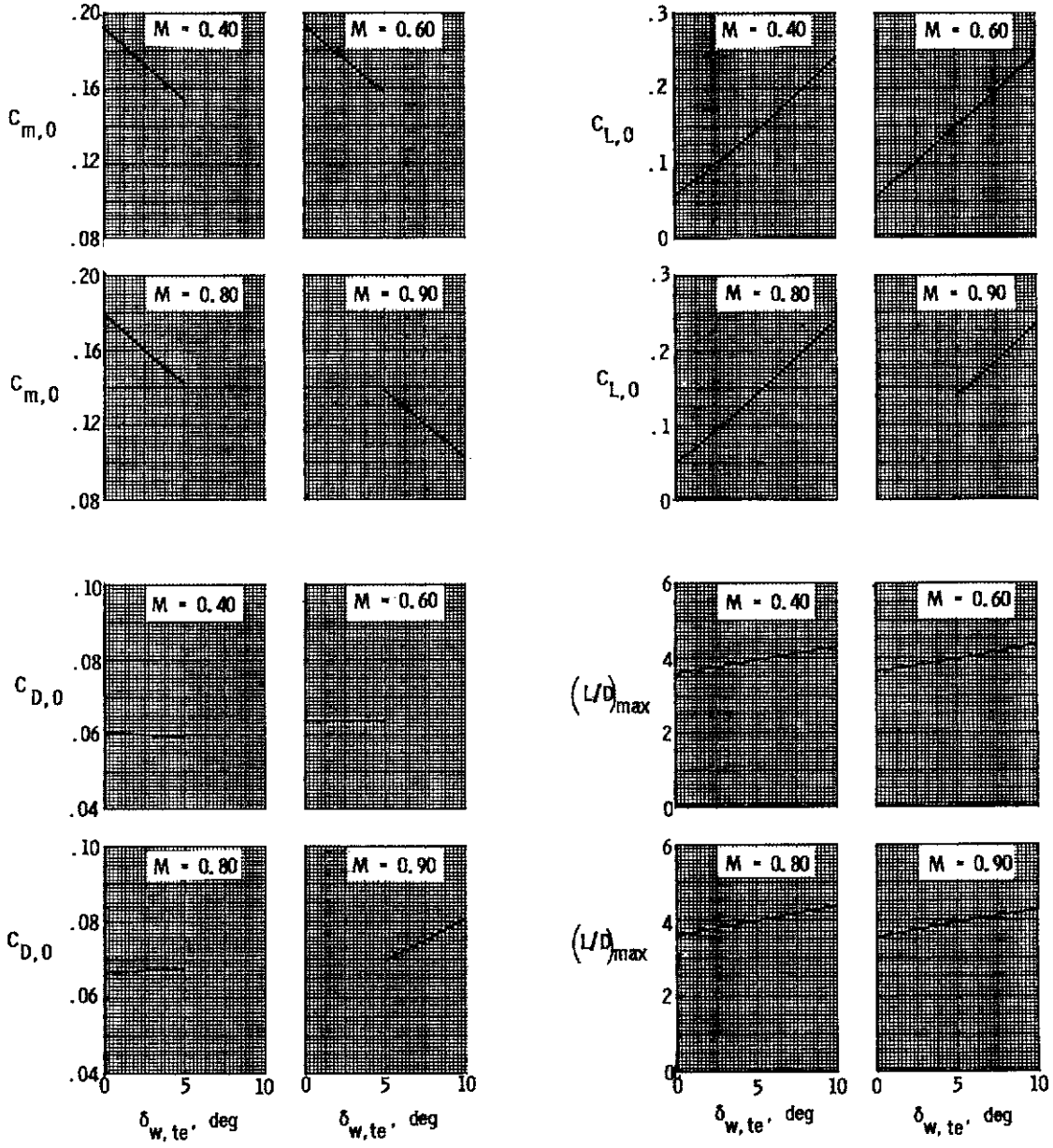

(b) $C_{m,0}$, $C_{L,0}$, $C_{D,0}$, and $(L/D)_{max}$.

Figure 18.- Continued.

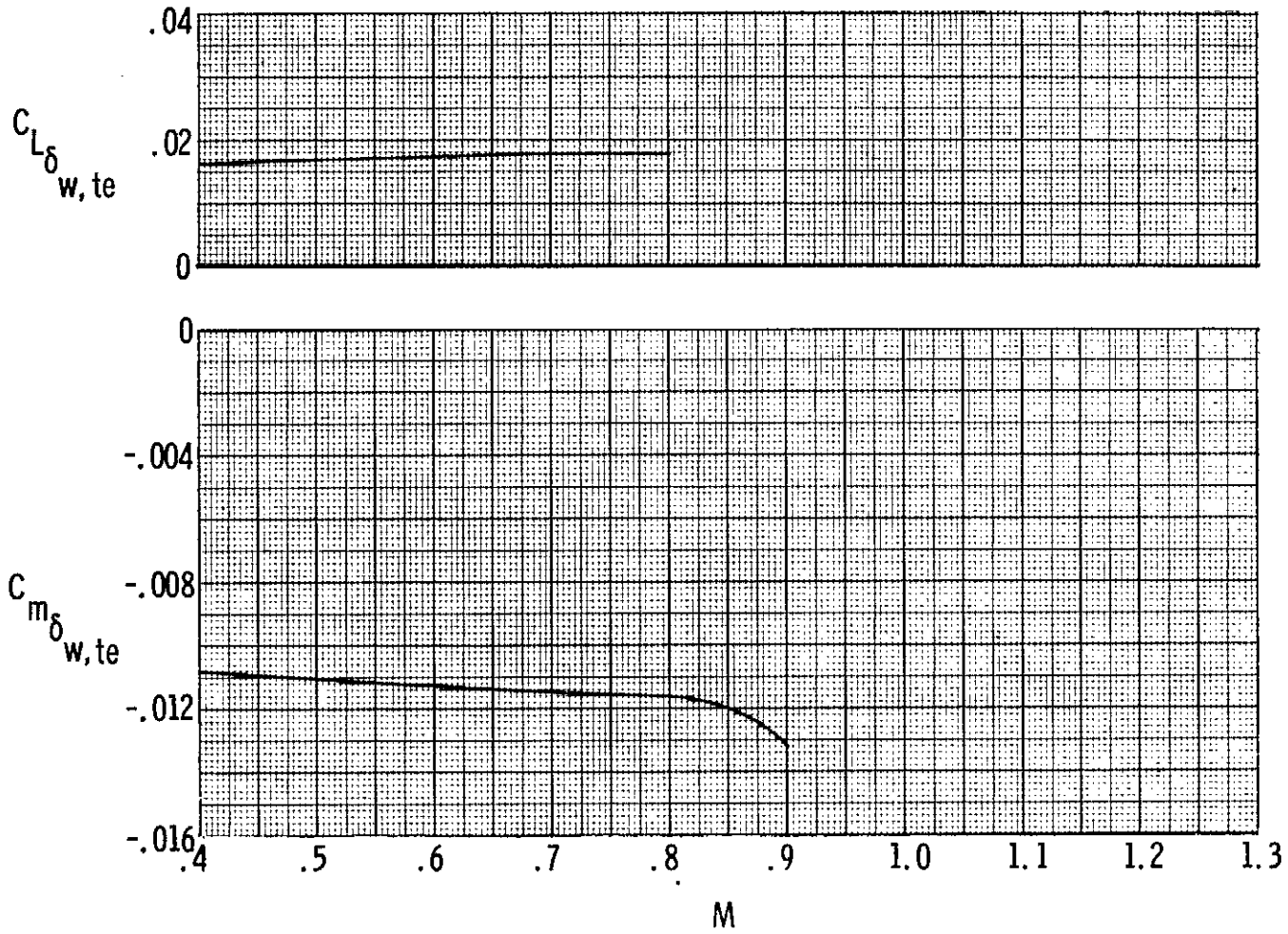

(c) $C_{L_{\delta_{w,te}}}$ and $C_{m_{\delta_{w,te}}}$.

Figure 18.- Concluded.

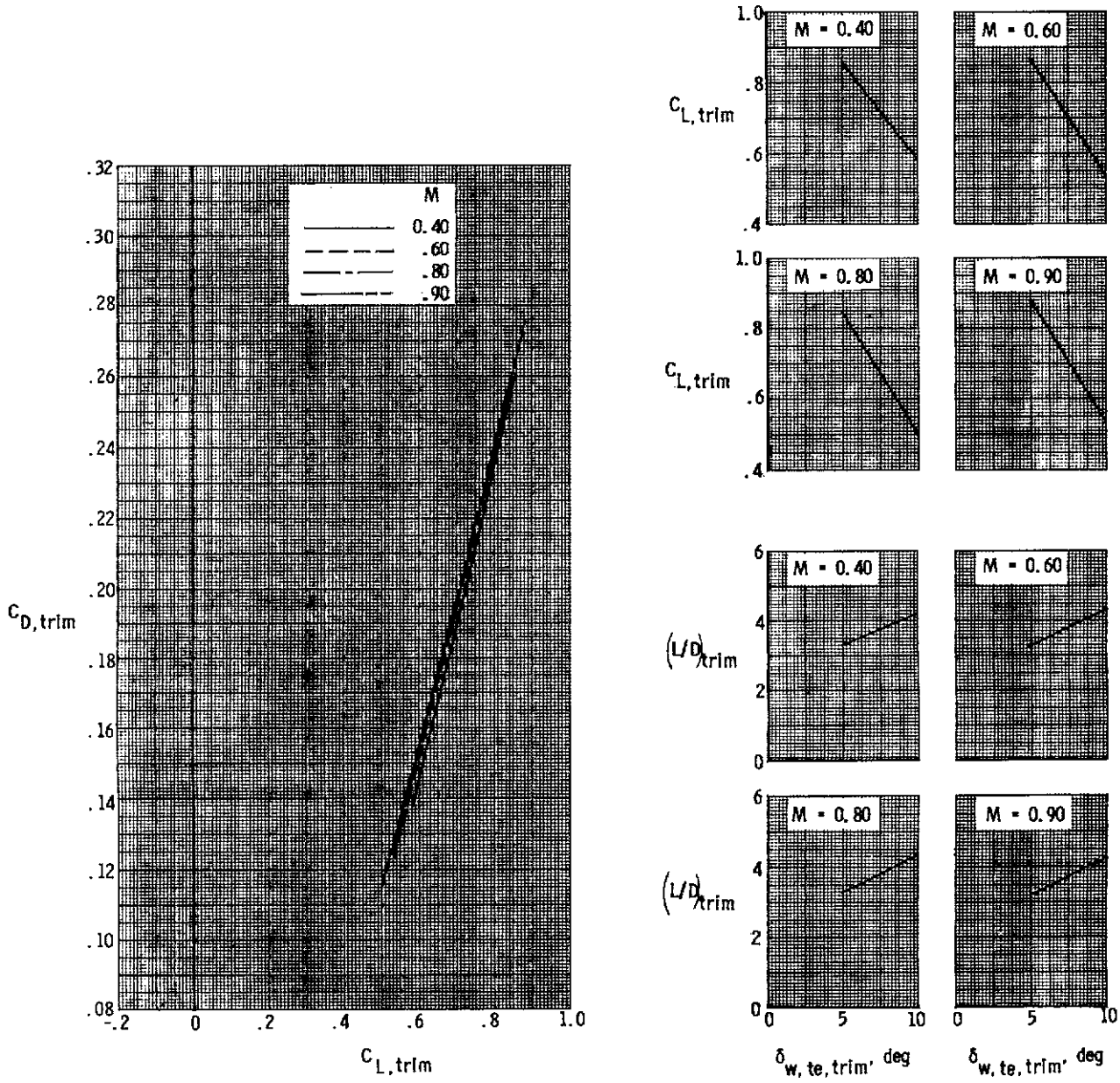

(a) $C_{D,trim}$, $C_{L,trim}$, and $(L/D)_{trim}$.

Figure 19.- Trimmed model characteristics with wing trailing-edge flaps as trimming surfaces. $\delta_{w,le} = 0^o/5^o$; $\delta_c = 18^o$; $\delta_{c,le} = \delta_{c,te} = 15^o$; vertical tails and ventrals on.

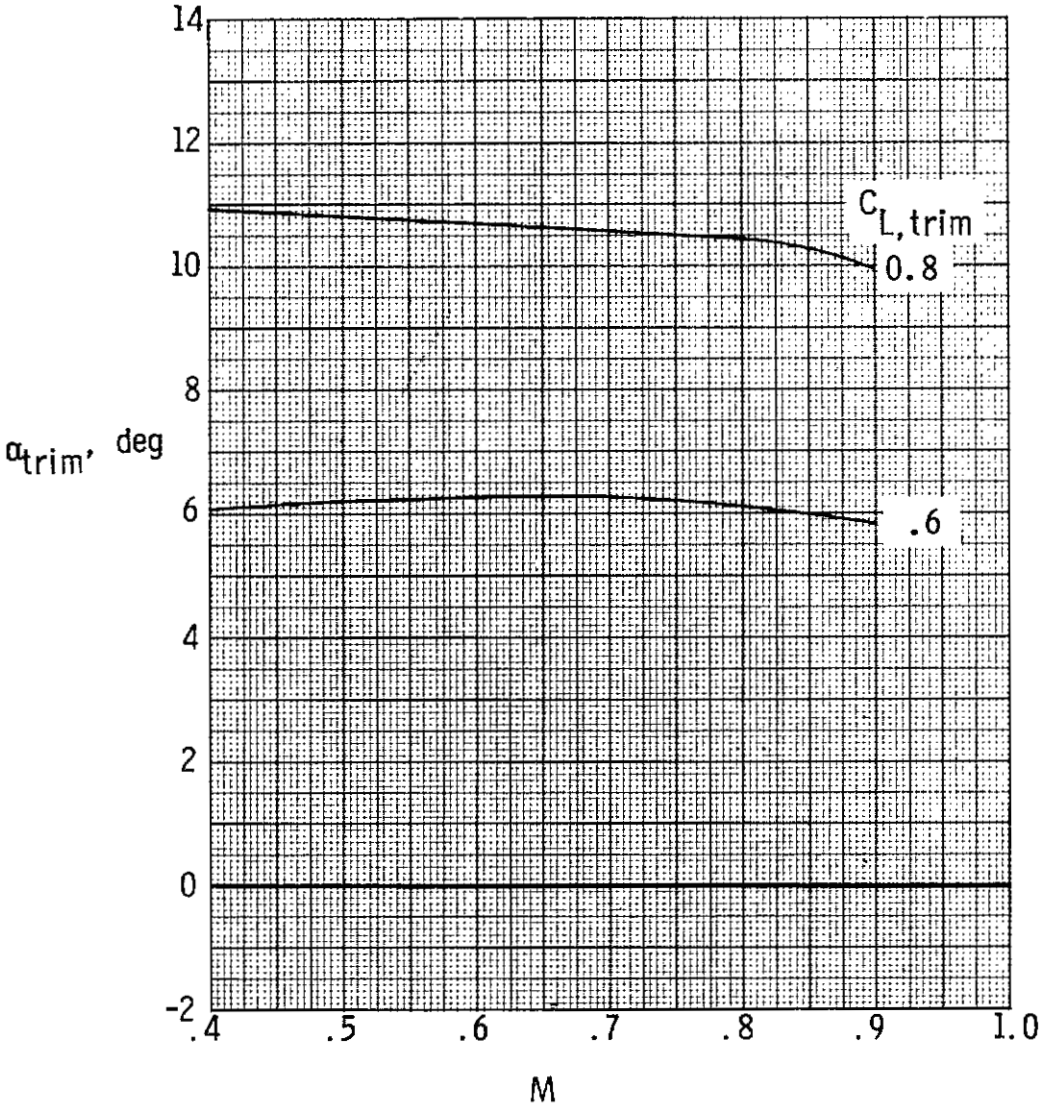

(b) α_{trim}.

Figure 19.- Concluded.

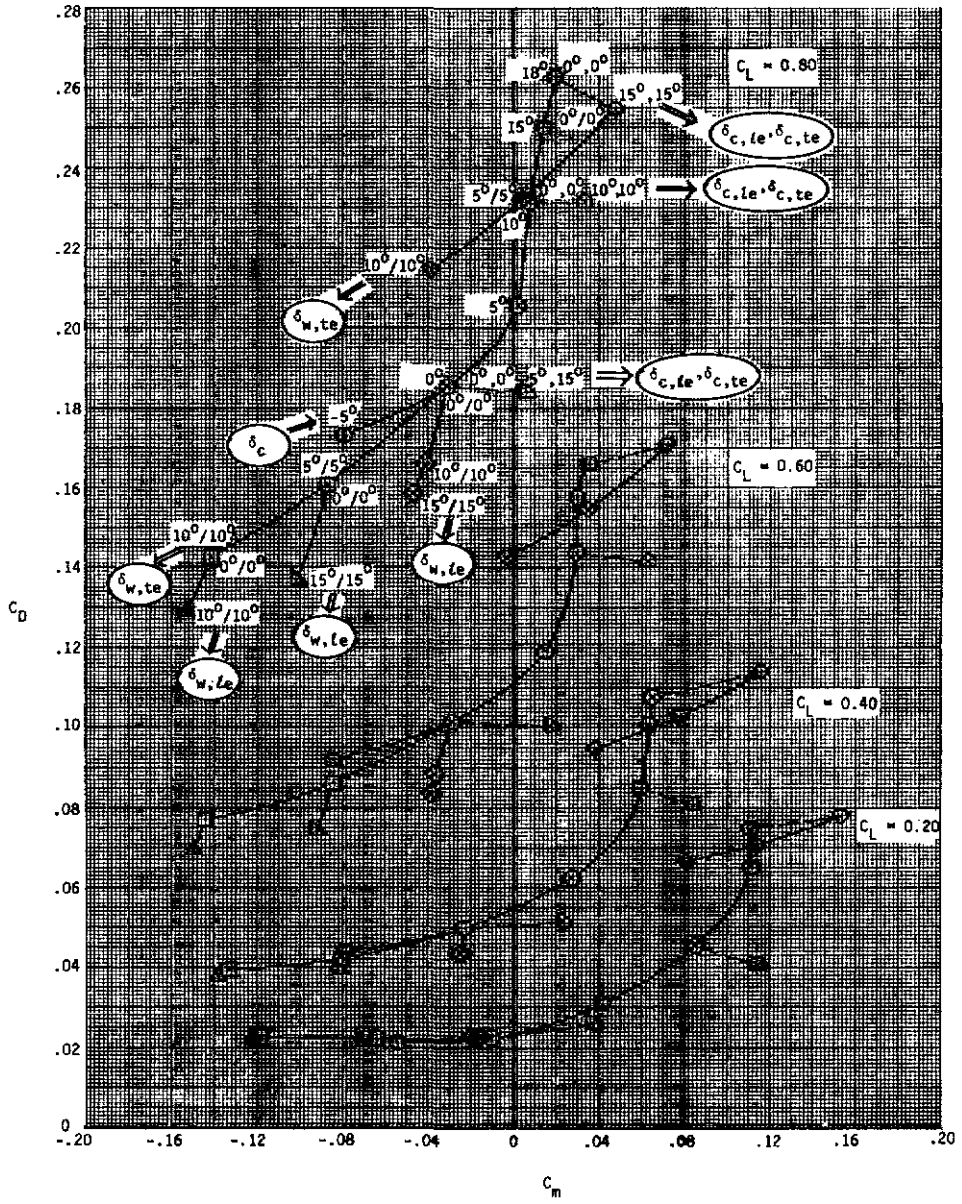

Figure 20.- Variation of drag coefficient with pitching-moment coefficient for all control variables (canard on) for constant values of lift coefficient at M = 0.40. (This figure is generated from crossplots of basic data; symbols indicate geometric control settings, not actual data points.)

1 Report No.	2. Government Accession No.	3. Recipient's Catalog No
NASA TP-1206		

4 Title and Subtitle	5. Report Date
LONGITUDINAL AERODYNAMIC CHARACTERISTICS OF A FIGHTER MODEL WITH A CLOSE-COUPLED CANARD AT MACH NUMBERS FROM 0.40 TO 1.20	July 1978
	6. Performing Organization Code
7 Author(s)	8. Performing Organization Report No.
Richard J. Re and Francis J. Capone	L-12081
	10. Work Unit No
9. Performing Organization Name and Address	505-11-23-02
NASA Langley Research Center Hampton, VA 23665	11 Contract or Grant No
	13. Type of Report and Period Covered
12. Sponsoring Agency Name and Address	Technical Paper
National Aeronautics and Space Administration Washington, DC 20546	14 Sponsoring Agency Code

15 Supplementary Notes

16. Abstract

An investigation of the longitudinal aerodynamic characteristics of a fighter model with a close-coupled canard mounted above the wing chord plane has been conducted. Model angle of attack was varied from -4° to 15°; canard incidence was varied from -5° to 18°; and selected canard and wing flap deflections were investigated.

The model could be trimmed by changing canard incidence for lift coefficients up to 0.80 at subsonic free-stream Mach numbers. By using the canard incidence for trim (with canard and wing flaps at 0°), maximum trimmed lift-drag ratios of about 8.8, 7.7, and 4.7 were obtained at free-stream Mach numbers of 0.40, 0.90, and 1.20, respectively. At a lift coefficient of 0.60, model trim angle of attack could be varied over an incremental range (nose-pointing capability) between 3.0° and 3.8°, depending on Mach number, by different combinations of control settings. At high lift coefficients, larger trimmed lift-drag ratios were obtained by using the deflection capability of the canard leading- and trailing-edge flaps before increasing canard incidence angle.

17. Key Words (Suggested by Author(s))

Direct lift
Close-coupled canard
Leading-edge flaps
Trailing-edge flaps
Canard

18. Distribution Statement

Unclassified – Unlimited

Subject Category 08

19 Security Classif. (of this report)	20 Security Classif. (of this page)	21. No. of Pages	22. Price*
Unclassified	Unclassified	78	$6.00

*For sale by the National Technical Information Service, Springfield, Virginia 22161

NASA-Langley, 1978

National Aeronautics and
Space Administration

Washington, D.C.
20546

Official Business
Use for Private Use, $300

THIRD-CLASS BULK RATE

Postage and Fees Paid
National Aeronautics and
Space Administration
NASA-451

U.S.MAIL

1 1 1U,A, 062378 S00903DS
DEPT OF THE AIR FORCE
AF WEAPONS LABORATORY
ATTN: TECHNICAL LIBRARY (SUL)
KIRTLAND AFB NM 87117

NASA

POSTMASTER: If Undeliverable (Section 158 Postal Manual) Do Not Return